AD-A181 924 FACTORS FOR MPD THRUSTORS(U) MASSACHUSETTS INST OF TECH 1/2
CAMBRIDGE SPACE SYSTEMS LAB M MARTINEZ-SANCHEZ
01 MAY 86 AFOSR-TR-87-0816 AFOSR-83-0035

UNCLASSIFIED F/G 21/3 NL

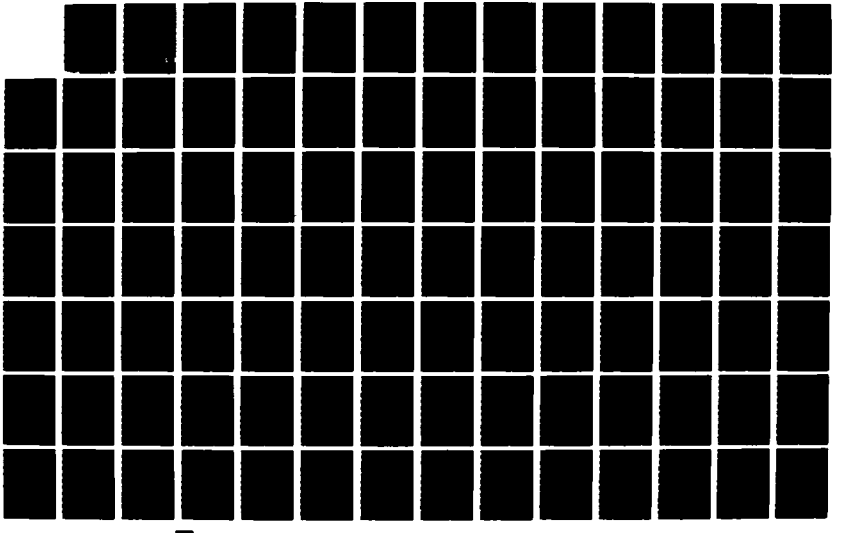

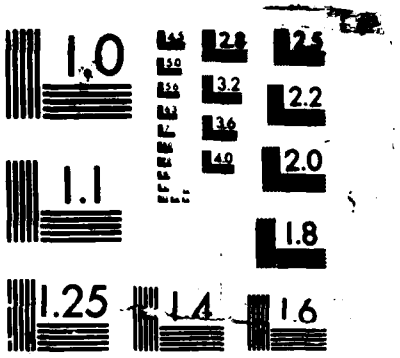

MICROCOPY RESOLUTION TEST CHART

AD-A181 924

5. MONITORING ORGANIZATION REPORT NUMBER(S)	AFOSR-TR- 87-0816
6a. NAME OF PERFORMING ORGANIZATION: Space Systems Laboratory, Mass. Institute of Technology	6b. OFFICE SYMBOL (If applicable):
7a. NAME OF MONITORING ORGANIZATION: AFOSR/NA	
6c. ADDRESS (City, State and ZIP Code): Bldg. 37-401, M.I.T. 77 Massachusetts Avenue, Cambridge, MA 02139	7b. ADDRESS (City, State and ZIP Code): Building 410, Bolling AFB DC 20332-6448
8a. NAME OF FUNDING/SPONSORING ORGANIZATION: AFOSR /NA	8b. OFFICE SYMBOL (If applicable):
9. PROCUREMENT INSTRUMENT IDENTIFICATION NUMBER: ~~Grant~~ #AFOSR-83-0035	
8c. ADDRESS (City, State and ZIP Code): Bolling Air Force Base, Washington, D.C. 20332	10. SOURCE OF FUNDING NOS.

PROGRAM ELEMENT NO.	PROJECT NO.	TASK NO.	WORK U NO.
61102F	2308	A1	

11. TITLE (Include Security Classification): Factors for MPD Thrustors (U)

12. PERSONAL AUTHOR(S): M. Martinez-Sanchez

13a. TYPE OF REPORT	13b. TIME COVERED	14. DATE OF REPORT (Yr., Mo., Day)	15. PAGE COUNT
Annual	FROM 12/15/83 TO 12/14/84	1986 May 1	150

16. SUPPLEMENTARY NOTATION

17 COSATI CODES			18. SUBJECT TERMS (Continue on reverse if necessary and identify by block number)
FIELD	GROUP	SUB. GR.	Electric Propulsion, MPD Thrusters

19. ABSTRACT (Continue on reverse if necessary and identify by block number)

The work reported here for the period 12/15/83 to 12/14/84 resulted in: (a) A generalization of the classical anode depletion theory of onset to conditions below onse giving insights as to anode drops and flow rearangement; (b) Analytical results describ the current concentration at cathode roots due to the Hall effect, and also the axial voltage distribution in a segmented thruster with suppressed axial current; (c) Complet of our study on local plasma stability, with the conclusion that damping, mostly due to heat conduction makes it unlikely that "onset" can be due to a local instability. Work was initiated on a theory of flow in contoured channels.

20. DISTRIBUTION/AVAILABILITY OF ABSTRACT	21. ABSTRACT SECURITY CLASSIFICATION
UNCLASSIFIED/UNLIMITED ☒ SAME AS RPT. ☒ OTIC USERS ☐	Unclassified

22a. NAME OF RESPONSIBLE INDIVIDUAL	22b. TELEPHONE NUMBER (Include Area Code)	22c. OFFICE SYMBOL
Julian M Tishkoff	(202)767-4935	AFOSR/NA

DESCRIPTIVE FIGURES FOR THIS
PROJECT

SCIENTIFIC APPROACH:

MODELING PLASMA DYNAMICS AND PHYSICS

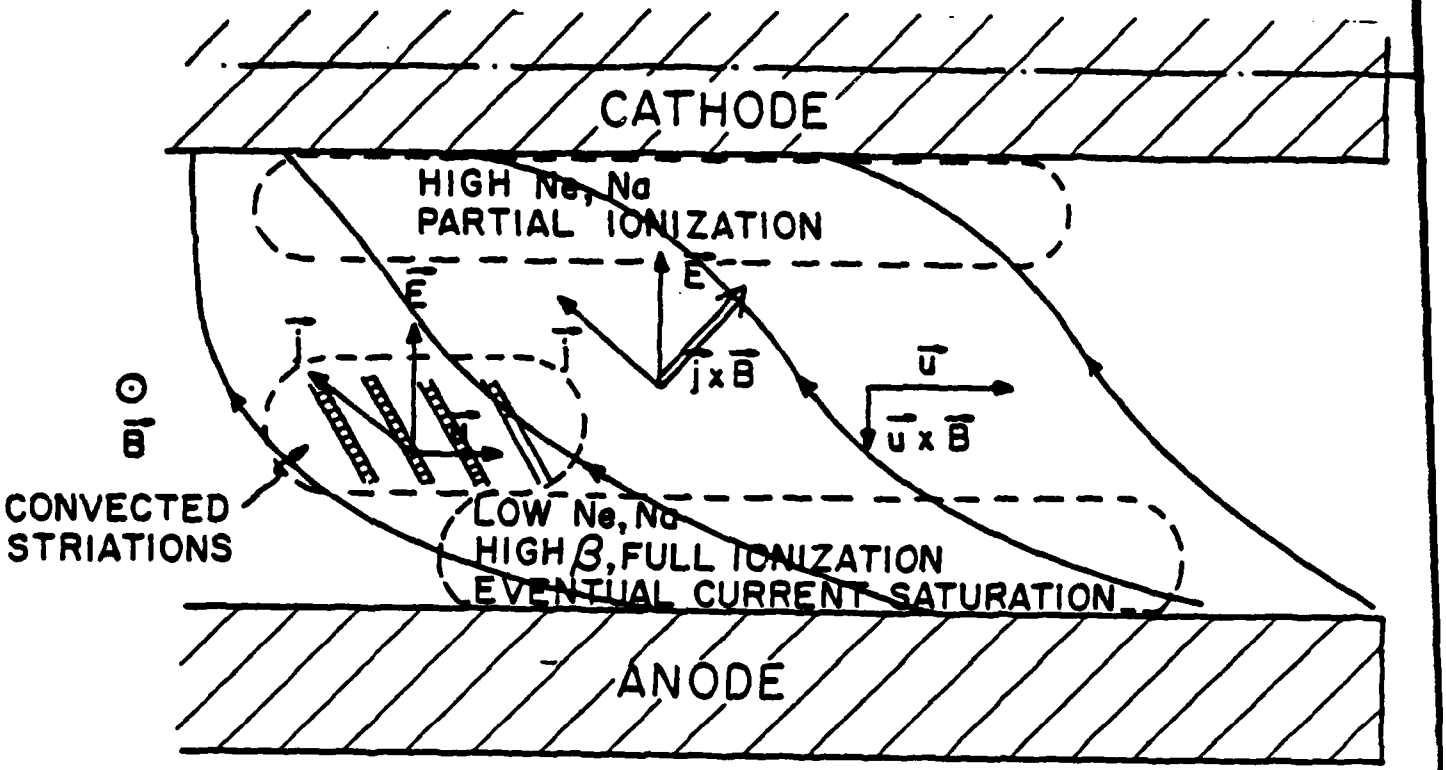

APPROACH:

(A) EXTEND CLASSICAL MODEL OF BAKSHT TO INCLUDE

- PARTIAL IONIZATION
- SELF-CONSISTENT T_e
- PRE-ONSET REGIME

(B) STUDY LOCAL STABILITY IN HIGH HALL PARAMETER, PARTIALLY IONIZED REGIONS

(C) CONCEIVE AND ANALYZE THRUSTER DESIGN VARIATIONS TO IMPROVE PERFORMANCE, DELAY ONSET

(D) DEFINE AND DESIGN SMALL EXPERIMENTAL THRUSTER TO VERIFY THEORY

EXPECTED ACCOMPLISHMENTS

ANALYTICAL/NUMERICAL PREDICTIONS OF CONFIGURATION EFFECTS:

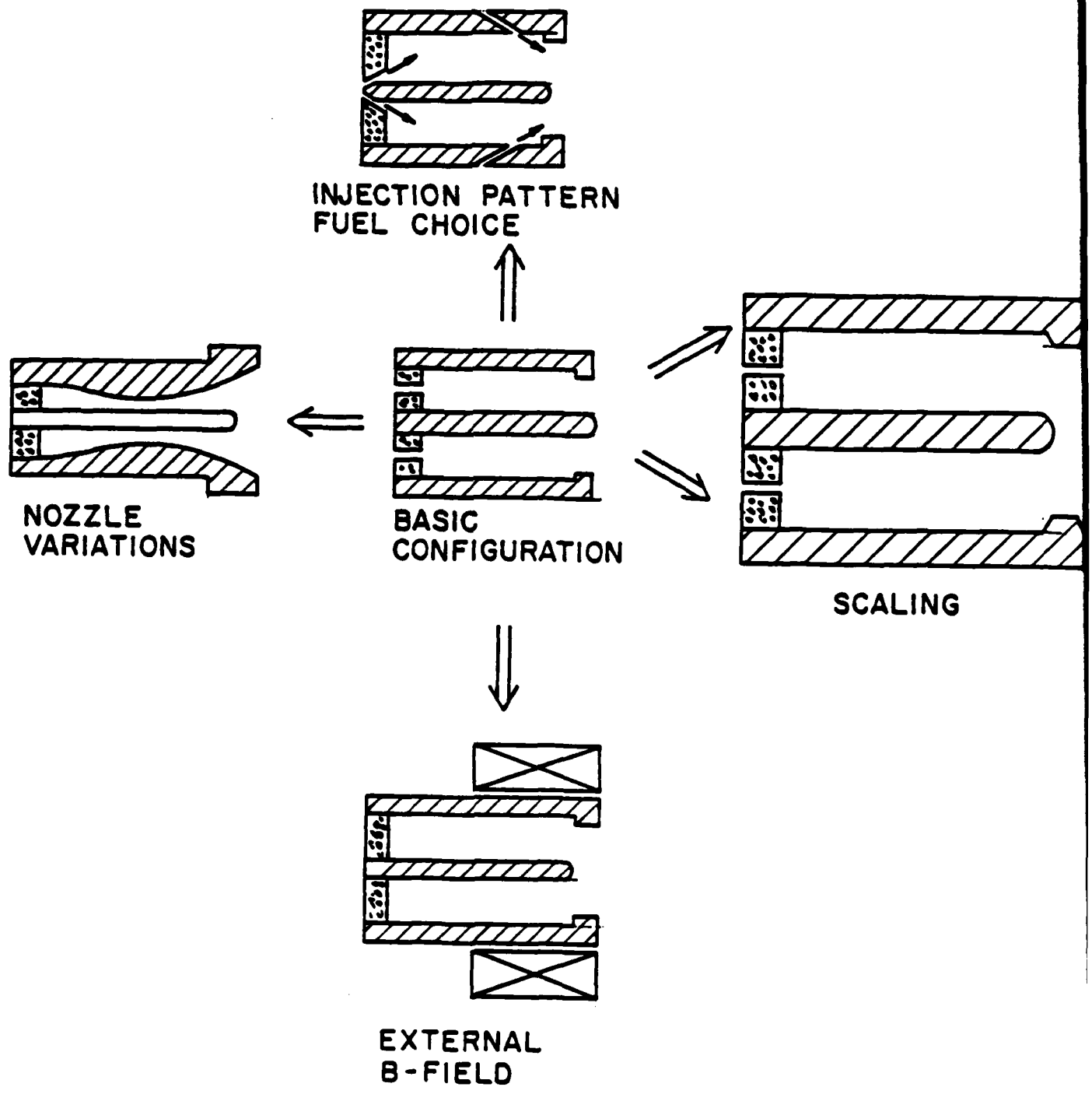

SECOND YEAR EFFORD DEVOTED TO

(A) EXTENDING ONSET THEORY

(B) STUDYING LOCAL EFFECTS

(C) COMPLETING STABILITY ANALYSIS

(D) INITIATING SHAPED CHANNEL ANALYSIS

1. Research Objectives

For the period Dec. 15, 1983 - Dec. 14, 1984, the proposed work plan included three tasks:

(a) To complete, develop and verify a quasi-two dimensional MPD channel model which was under development at proposal time. This model included many physical effects which had not been previously addressed (finite ionization kinetics, particle interdiffusion, etc.), and was specifically constructed in an attempt to verify and refine the onset predictions of Ref. 1.

(b) To conceive and analyze several design variations including axial fields, segmented electrode construction and contoured wall designs. This was to be done by and large analytically, with initiation of a numerical model development also contemplated.

(c) Definition and design of a small-scale experiment to test one of the above concepts, to be performed on an outside facility with support from MIT.

(d) To complete an ongoing study of the local stability of an MPD plasma, including both the partially ionized and the fully ionized range of operation, and assessing the effects of finite size, heat conduction, species diffusion and finite self-magnetic field effects.

The following section gives an overview of the work accomplished in each of these tasks, and makes reference to several Appendices, where more detailed results and discussions are contained.

2. Outline of Work Accomplished

The bulk of the work proposed under Task (a) above was in fact completed during the first year of the Grant, and reported in our 1st Yearly Report. The work showed the effects of geometrical parameters on degree of ionization, wall recombination losses, etc. One very important result was the fact that partial ionization had only a minor impact on the predicted "onset" current. We have used this result to justify the continued use of simplified full-ionization plasma models designed to illuminate other effects, such as those of a predominantly dynamic nature. It is clear, however, that any assessment of losses or efficiency must be based on more complete plasma formulations.

The original Baksht model (Ref. 1), as well as our own extension discussed above, were specifically confined to the "onset" condition. This was done by imposing a condition of vanishing plasma density at the anode wall. It is of interest to inquire about the approach to onset from below, since that may provide guidance as to how close to that limiting condition it is safe to operate, and, in addition, it should illuminate the physical events responsible for or triggered by the gradual depletion of the anode, such as the growth of the anode voltage drop. We report such an analysis in Appendix 1 to this Report. The conclusions are that:

(a) Onset symptoms are absent up to currents 90% of critical

(b) Anode drops remain close to those corresponding to the floating potential for the whole channel also up to about 90% of I^{*}.

(c) Anode plasma density decreases with current at about the same

rate as cathode density up to near Γ^*, then drops rapidly to near zero. The anode drop is negative, except very near onset.

In work related to Task (b) above, we undertook local analyses of various parts of a typical MPD thruster, in an effort to isolate and illuminate the dominant physical effects in each.

Near the inlet, where the flow speed is still low, the main component of the local electric field is purely ohmic, producing the strong local dissipation which leads to rapid ionization. One problem which has recurred in most channel designs is a strong current concentration at the cathode root, with erosion of both the cathode and the backplate. While one part of this has been shown in the previous analysis (App. 1) to be associated with the reduced uB back-emf in that region (and becomes especially strong at onset), we expect one additional component of current concentration at the cathode root due to the peculiarly skewed current pattern occurring in the presence of a finite Hall effect. To analyze this effect, we start in Appendix 2 by formulating a general tensor Ohm's law in a form which shows a clear division of the local field into the gradient of a generalized potential, plus a generalized back emf (these generalizations arise from the Hall and electron diffusion effects). This leads naturally to an induction equation, governing the magnetic field. We then particularize to small flow velocities, and show that the field B obeys $\nabla^2 B = 0$, despite the Hall parameter gradients occuring due to density gradients (which are themselves due to axial currents). It is also shown that in this region, and for a fully ionized plasma, electron

diffusion has the effect of reducing by a factor of 2 the effective value of the local Hall parameter. By making the additional simplification of taking a mean, constant Hall parameter, we are able to obtain analytical solutions for the current density distribution on the electrodes, including a singularity of the inverse factional-power type at the cathode root (and a similar zero at the anode root).

The identification of anode depletion, driven by axial currents, as the most likely trigger for onset, had led us to propose (Ref. 3) a segmented channel construction, with only two external terminals due to diagonal cross-connection, designed such as to cancel the axial currents by the establishment of appropriate axial electric fields.

There are many questions to be answered regarding this design, which, however, holds the potential for significantly delaying onset, and hence increasing thruster power and efficiency. In Appendix 3 we have provided a simplified analysis to show how, under conditions where axial current has indeed been suppressed, the transverse current and the voltage are distributed in the axial direction. This leads to the establishment of limitations for this type of thruster: essentially, the ratio of current to mass flow must be above a certain limit (shown to correspond to a Hall parameter of 0.6 for Argon), or else not enough voltage overlap develops between the anode and cathode walls to allow cross-connection. It is shown that thrusters with $\dot{m}$ less than about 2 g/sec can easily be designed to avoid this limitation, while still remaining below traditional onset limits (and, in addition, the new onset limit is now likely to be higher).

Work has also been initiated on a model of the effect of wall contouring on the distribution of current and other quantities. This model exploits the simplifications afforded by the high values of the typical magnetic Reynolds number based on length (5-10), and of the ratio of magnetic to gas pressure. Results are expected within the next reporting period.

The experimental work has been deferred pending acquisition of advanced instrumentation to be acquired under a parallel DoD Instrumentation Grant and completion of our contoured wall analysis. It is our intention to design a contoured channel for even current distribution (minimizing hot spots) and to conduct detailed diagnostic tests comparing its performance and flow and current patterns to theory and to conventional thrusters. This will also serve to assess the feasibility of a later segmented channel, as discussed above. Tests will be at an outside facility to be selected, using an MIT provided thruster and also MIT optical diagnostics and digital data acquisition equipment.

Finally, Appendix 4 gives a complete account of our investigations on the local stability of an MPD plasma, a part of which was advanced in our previous Report (Ref. 2). The new work consisted of a clarification of the types of potential instability modes depending on the operating regime, mainly the degree of ionization α. It was found that, up to $\alpha \simeq 0.9$ the predominant effect is the classical ionization instability, involving mainly variations in electron density, whereas very near $\alpha = 1$, a purely static mode involving mainly temperature

variations becomes predominant. Heat conduction stabilizes this mode for moderate Hall parameters, but this effect is weakened and eventually disappears at a critical value of this Hall parameter. This is qualitatively similar, but for a completely different reason, to the role played by the Hall parameter in catalyzing the ionization instability. For MPD conditions, it is concluded that striations with wavelenghts below some 3 cm will be well damped; since regions of near-complete ionization are unlikely to be much more than this size, the expectation is that the static mode will not become unstable. Again, this conclusion is similar to that reached earlier (Ref. 2) on the sense that the ionization mode is unlikely to be unstable due to the small spacial extent of high Hall parameter regions. Taken together, these results tend to discound the possibility of the onset phenomena being directly associated with bulk plasma instability, and to reinforce the anode depletion viewpoint.

3. Personnel Associated with the Research Effort

The research was led by Associate Prof. Manuel Martinez-Sanchez, with the cooperation of graduate Research Assistants D. Heimerdinger (Doctoral Candidate) and Tze-Wing Poon (Masters Candidate). A new Research Assistant, J. Marc Chanty joined the group towards the end of the period, and will be working on numerical MPD simulation.

1. Baksht, F.G., Moizhes, B.Ya and Rybakov, A.V., "Critical Regime of Plasma Accelerator", Zhurnal Tekhnicheskoi Fiziki, Vol. 43, pp. 2568-2573, Dec. 1973.

2. M. Martinez-Sanchez, "A Theoretical Study of Performance-Limiting Factors in MPD Thruster", Yearly Report on Grant AFOSR 83-0035.

3. M. Martinez-Sanchez, Proposal for Continuation of Grant AFOSR 83-0035, June 21, 1983.

Appendix 1

Quasi two-dimensional MPD flow theory - A generalization of the theory of Baksht, Moizhes and Rybakov to conditions below onset

Introduction

The simple theoretical treatment of MPD flow given in Ref. 1 is remarkably successful in predicting the basic trends and even the correct magnitudes of conditions at the onset of instability and erosion. Additionally, this provides a clear mechanistic description of the reasons for the observed "onset" phenomena, to be contrasted with the somewhat obscure arguments contained in alternative theories, such as those based on the "critical ionization velocity" or the "minimum voltage principle".

In this section we will present a theory that essentially accepts all of the simplifications introduced in Ref. 1 for the treatment of the flow, but removes the restriction as to the anode boundary conditions, so that the results can span a range of currents below that for which anode depletion occurs. This will provide additional insight on at least three aspects of the problem: (a) the variation of anode voltage drop with current, (b) the variation of overall transverse voltage with current, and (c) the progressive decrease of near-anode density as the critical (onset) condition is approached.

2. Formulation

The basic assumptions are as follows:

(a) Two-dimensional, rectangular, slender channel $(\frac{\partial}{\partial y} >> \frac{\partial}{\partial x})$

(b) Near full ionization ($n_e = n_i = n$, $n_n << n_e$)

(c) Constant temperature and conductivity

(d) Axial Lorentz force dominant over axial pressure gradient

(e) Transverse Lorentz force balanced by transverse pressure gradient (weak transverse flows)

In addition, we will impose anode boundary conditions similar to those applying to a Langmuir probe in contact with the local plasma density. This will relate anode voltage drop to local current density. Notice at this point that Ref. 1 used only a limiting form of this conditions, namely, that <u>at onset</u> the anode does not retard electrons (zero or positive anode drop). We will find that over most other operating conditions the anode drop is <u>negative</u>, i.e., the anode rejects a fraction of the random current in order not to exceed the current demands of the channel.

The geometry is depicted in Fig. 1, with B coming out of the plane of the paper.

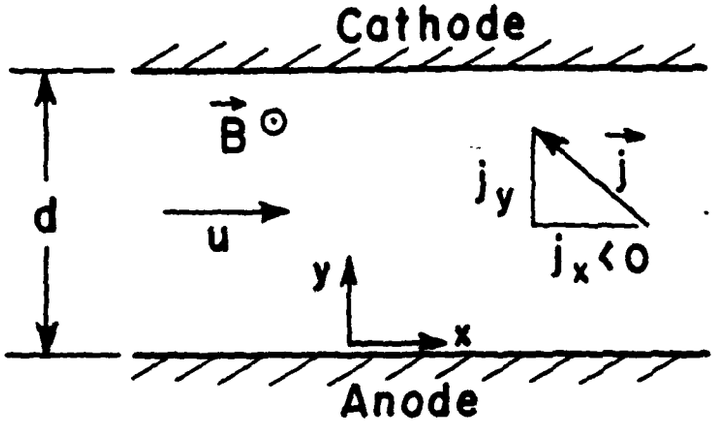

Fig. 1 Geometry for Analysis

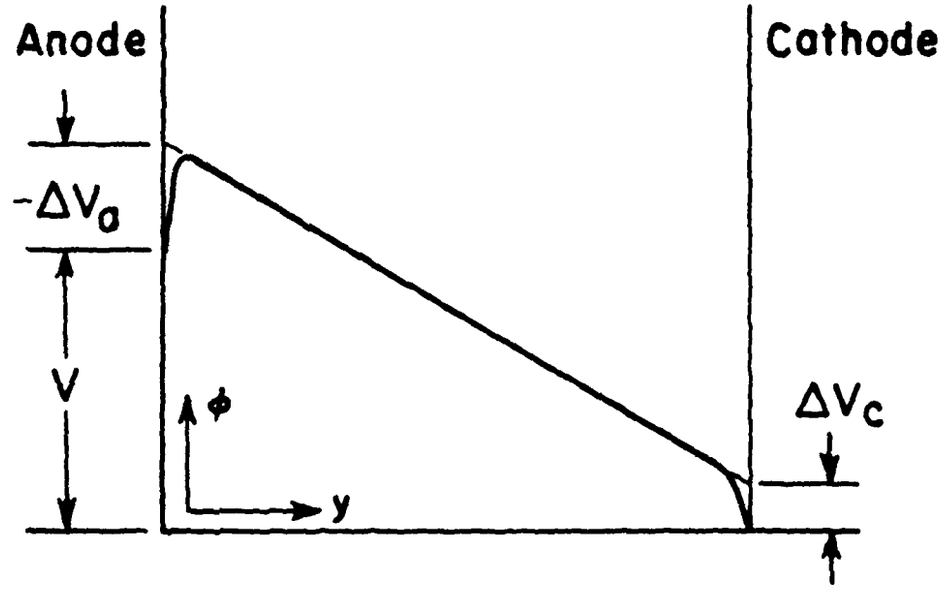

Fig. 2 Transverse Voltage Profile with $\Delta V_a < 0$

Two types of equations will be used: (a) axial balance equations for which transversally averaged quantities, ($\overline{\quad}$) will be used, and (b) transverse balance equations, in which axial derivatives will be neglected. The axial equations are

$$\text{Continuity:} \qquad m_i \bar{n} \bar{u} A = \dot{m} \tag{1}$$

$$\text{Momentum:} \qquad \frac{\dot{m}}{A} \frac{d\bar{u}}{dx} + \frac{d\bar{p}}{dx} = \bar{j}_y \bar{B} = -\frac{1}{\mu_0} \bar{B} \frac{d\bar{B}}{dx} \tag{2}$$

where m_i is the ion mass, $\dot{m}$ the mass flow and $A = D \times H$ is the cross-sectional area. In Eq. (2) we will neglect the $\frac{d\bar{p}}{dx}$ term compared to the $\bar{j}_y \bar{B}$ term from here on, and we have used Ampere's law to relate $\bar{j}_y$ to $\bar{B}$. An integration of Eq. (2) with the approximate initial condition $\bar{u} = 0$ gives

$$\frac{\dot{m}}{A} \bar{u} + \frac{\bar{B}^2}{2\mu_0} = \frac{B(o)^2}{2\mu_0} \tag{3}$$

where B(o), the initial magnetic field is related to I, the total channel current, through

$$I = \frac{H}{\mu_0} B(o) \tag{4}$$

The transverse momentum equation is

$$- j_z \bar{B} = \frac{\partial P}{\partial y} = 2kT \frac{\partial n}{\partial y} \qquad (5)$$

and, since $\frac{\partial}{\partial x} << \frac{\partial}{\partial y}$, the current conservation equation reduces to

$$\frac{\partial j_x}{\partial y} \simeq 0 \; ; \quad j_y \simeq \bar{j}_y(x) \qquad (6)$$

The tensor Ohm's law, including electron diffusion is

$$\sigma \left(\vec{E} + \vec{u} \times \vec{B} + \frac{kT}{e} \frac{\nabla n}{n}\right) = \vec{J} + \vec{J} \times \vec{\beta} \qquad (7)$$

so here $\vec{\beta} = \beta \frac{\vec{B}}{B}$, and β is the Hall parameter, which varies with plasma density as

$$\beta = \frac{\sigma}{en} B \qquad (8)$$

Solving Eq. (7) for the current components, and imposing the approximate condition $E_z \simeq 0$ (to be varified later), plus $\frac{\partial \ln n}{\partial x} \simeq 0$,

$$\frac{1 + \beta^2}{\sigma} j_z = - \left(Ey - uB + \frac{kT}{e} \frac{\partial \ln n}{\partial y}\right)\beta \qquad (9)$$

$$\frac{1 + \beta^2}{\sigma} j_y = Ey - uB + \frac{kT}{e} \frac{\partial \ln n}{\partial y} \qquad (10)$$

one of which can be replaced by

$$j_z = -\beta\, j_y \qquad (11)$$

Substituting Eq. (11) into Eq. (5), and using Eq. (8) for β, we obtain,

$$\frac{\sigma B^2}{en}\,\bar{j}_y = 2kT\,\frac{\partial n}{\partial y} \qquad (12)$$

which integrates to

$$n^2 = \frac{\sigma \bar{B}^2 \bar{j}_y}{ekT}\, y + \text{const.} \qquad (13)$$

In order to determine the constant in (13) we will impose the condition that the anode current density equals the difference between the arriving (retarded) electron current and the Bohm-limited arriving ion current. This presupposes a negative anode drop, i.e., a transverse voltage profile of the type shown in Fig. 2, and can be written as:

$$\bar{j}_y = en(o)\left[\frac{\bar{c}_e}{4}\, e^{\frac{e\Delta V_a}{kT}} - v_s\right] \qquad (14)$$

where $\bar{c}_e = \sqrt{8kT_e/(\pi m_e)}$ and $u_s = \sqrt{kT_e/m_i}$. For cases where ΔV_a turns out to be positive (only very near onset conditions), we will replace (14) by

$$\bar{j}_y = en(o)\frac{\bar{c}_a}{4} \tag{15}$$

and neglect the small retarded ion current. Both (14) and (15) can be written together as

$$\bar{j}_y = en(o)\,\frac{c^*}{4} \tag{16}$$

where c^* is a function of ΔV_s whose definition is obvious from Eqs. (14) and (15). Solving (16) for n(o), we can use this as an initial condition in Eq. (13), with the result

$$n(y) = \sqrt{(\frac{4\bar{j}_y}{ec^*})^2 + \frac{\sigma B^2 \bar{j}_x}{ekT}\,y} \tag{17}$$

For use in the axial equations, we need the transversally averaged density. This can be explicitly found from (17) as

$$\bar{n} = \frac{2}{3}\,\frac{ekT}{\sigma B^2 \bar{j}_y d}\,\{\,[\,(\frac{4\bar{j}_x}{ec^*})^2 + \frac{\sigma B^2 \bar{j}_x d}{ekT}]^{3/2} - (\frac{4\bar{j}_x}{ec^*})^3\,]\,\} \tag{18}$$

Turning now to the y-component of Ohm's law (Eq. 10), we notice first of all that

$$\frac{\beta^2}{\sigma}\,\bar{j}_y = \frac{\sigma B^2}{e^2 n^2}\,\bar{j}_y = 2\,\frac{kT}{e}\,\frac{\partial \ln n}{\partial y} \tag{19}$$

where we have made use of Eqs. (8) and (12). Eq. (10) then reduces to

$$E_y = -\frac{\partial \phi}{\partial y} = \frac{\bar{j}_x}{\sigma} + \bar{u}\,\bar{B} + \frac{kT}{e}\frac{\partial \ln n}{\partial y} \tag{20}$$

and, if the cathode potential is taken to be zero, we can integrate to obtain the voltage across the plasma core as (with reference to Fig. 2)

$$V - \Delta V_a - \Delta V_c = \left(\frac{\bar{j}_x}{\sigma} + \bar{u}\,\bar{B}\right) d + \frac{kT}{e} \ln \frac{n(d)}{n(o)} \tag{21}$$

or

$$V = \Delta V_a + \Delta V_c + \left(\frac{\bar{j}_x}{\sigma} + \bar{u}\,\bar{B}\right) + \frac{kT}{2e} \ln\left(1 + \frac{e}{16kT}\frac{\sigma B^2 c^{*2}}{\bar{j}_y} d\right) \tag{22}$$

Eqs. (1), (3), (16), (18) and (22) constitute at each $\bar{B}$ a set of five algebraic equations in the unknowns $\bar{n}$, $\bar{u}$, $\bar{j}_y$, $n(o)$ and ΔV_a (through c^*), provided ΔV_c is regarded as a given quantity (here taken to be independent of x), and provided B(o) (or I) <u>and</u> V are both specified. If this set can be solved for each value of $\bar{B}$ between $\bar{B}(o)$ and a value to be assigned to the channel end (we will take this to be zero, as in Ref. (1)), then the spacial variable x can be calculated through integration of Ampere's law:

$$x = \int_{\bar{B}}^{\bar{B}(o)} \frac{d\bar{B}}{\mu_o \bar{j}_y} \tag{23}$$

and, in particular, the full channel length is

$$L = \int_{o}^{\bar{B}(o)} \frac{d\bar{B}}{\mu_o \bar{j}_y} \tag{24}$$

More rationally, L would be a specified channel dimension, and only one of the electrical terminal properties (I or V) would be given. This will require a global iteration in which terminal values are tried until the proper length is achieved.

3. Method of Solution

From continuity and momentum:

$$\bar{u} = \frac{Hd}{2\dot{m}\mu_o} \left[\bar{B}(o)^2 - \bar{B}^2 \right] \tag{25}$$

and

$$\bar{n} = \frac{\dot{m}}{m_i A \bar{u}} \tag{26}$$

These expressions can be substituted into Eq. (18), resulting in a relationship linking $\bar{j}_y$ with $\bar{B}$ and ΔV_s (through c^2). Algebraic rearrangement yields a cubic equation for $\bar{j}_y$, which can be compacted to the form

$$\xi^3 + a\xi + b = 0 \tag{27}$$

where

$$a = 4\eta\left(1 - \frac{\eta}{3}\right) \tag{28}$$

$$b = -\left(1 + 2\eta + \frac{19}{3}\eta^2 + \frac{16}{27}\eta^3\right) \tag{29}$$

$$\eta = \frac{12\ kT\ \mu_0 \dot{m}^2}{\sigma\ m_i H^2 d^3 c^{*2}} \frac{1}{\bar{B}^2\left[\bar{B}(o)^2 - \bar{B}^2\right]} \tag{30}$$

and, after solution for ξ,

$$\bar{j}_y = \frac{eod}{48kT} c^{*2} \bar{B}^2 \left(\xi - 1 + \frac{2}{3}\eta\right) \tag{31}$$

Since $\eta > 0$, the cubic discriminant $\frac{b^2}{4} + \frac{a^3}{27}$ can be shown from (28) and (29) to be positive, which indicates a single real root for Eq. (27). This root is

$$\xi = \left[-\frac{b}{2} + \sqrt{\frac{b^2}{4} + \frac{a^3}{27}}\right]^{1/3} + \left[-\frac{b}{2} - \sqrt{\frac{b^2}{4} + \frac{a^3}{27}}\right]^{1/3} \tag{32}$$

The algorithm for solution now involves the following steps:

(1) Prescribe I, H, L, d, $\dot{m}$, ΔV_c

(2) Guess V

(3) Select values of $\bar{B}$ between $\bar{B}(o) = \mu_0 I/H$ and o

(4) At each $\bar{B}$, guess ΔV_s, calculate c^*

(5) Compute η, a, b and ξ, leading to $\bar{j}_y$

(6) Compute V from Eq. (21). If not right, modify ΔV, return to (4)

(7) When converged, update $\bar{B}$ by $\bar{B} \rightarrow \bar{B} - \Delta\bar{B}$, advance x by

$$\Delta x = -\frac{\Delta\bar{B}}{\mu_0 \bar{j}_y}$$

(8) Continue to $\bar{B} = 0$, obtain $L = x$ ($\bar{B} = 0$)

(9) If L not right, modify V, return to (2).

(10) Iterate to convergence.

4 Conditions for Onset

As I is increased at a fixed $\dot{m}$, it will be found that the increased cross-force $j_x B$ leads to a progressive reduction of density at the anode (n(o)), requiring a reduction of the retarding potential drop (a less negative ΔV_a) in order to satisfy the increased $\bar{j}_y$ demands (See Eq. (14)). An alternative is for j_y itself to be reduced, but, clearly, this cannot happen over the whole channel length, since the net I is increased; it may happen, however, over the central portion of the channel, where $\bar{u}\,\bar{B}$ nearly cancels the whole core field, but $\bar{u}\,\bar{B}$ is small at the channel ends, where either $\bar{u}$ or $\bar{B}$ are small. As a consequence, we obtain a progressive redistribution of current towards the two ends of the channel, with ΔV_a simultaneously becoming zero or positive over the center, and negative only over smaller and smaller sections near the ends. These sections have axial thicknesses of the order of the channel length divided by the magnetic Reynolds number based on length, and are therefore rather narrow. Thus, the eventual consequence is an inability for the channel as a whole to deliver the prescribed current, a steepening of V(I) and a saturation of I. Clearly, any further increase in current must imply a radically different conduction mechanism, most likely in the form of highly erosive vacuum arcs on the most loaded parts of the anode, so as to

provide extra mass through which the current may channel itself. This is the "onset" condition.

In terms of our model, we can obtain (following Ref. (1)) a simple condition for onset by noting that n(o) becomes then much smaller than $\bar{n}$ or n(d). In Eq. (17) this means that the first term inside the root is negligible, and then Eq. (18) simplifies to

$$\bar{n} = \simeq \frac{2}{3} \sqrt{\frac{\sigma \bar{B}^2 \bar{j}_x d}{ekT}} \tag{33}$$

Solving for $\bar{j}_y$ and using (25) and (26),

$$\bar{j} = 9 \frac{ekT\mu_0^2}{\sigma H^4 d^6} \frac{1}{m_i^2} \frac{1}{\bar{B}^2 [\bar{B}(o)^2 - \bar{B}^2]} \tag{34}$$

This explicit relationship between $\bar{j}_y$ and $\bar{B}$ can then be inserted into Eq. (24) and integrated. Rearranging the result we obtain:

$$\frac{I^7}{\dot{m}^4} m_i^2 = \frac{945}{8} \frac{ekT}{\sigma \mu_0^4} \frac{LH^3}{d^6} \tag{35}$$

For fixed channel dimensions, and ignoring the relatively weak variations of T and σ, this relationship has the form

$$\frac{I^{1.75}}{\dot{m}} \sqrt{m_i} = \text{const}$$

which is very close to the experimentally observed onset condition $\frac{I^2}{\dot{m}}\sqrt{m_i}$ = const. (and, incidentally, also to the similar expression obtained by equating the exit velocity to the Alfven critical ionization velocity).

As an example, we have used values close to those that would apply to a standard Princeton MPD thruster (with some uncertainty about the appropriate channel width d to be used for a coaxial geometry):

$H = 2\pi \times 5$ cm $L = 15$ cm $d = R_a - R_c = 8$ cm

$T = 30{,}000$ K $\sigma = 8000\ \Omega^{-1}/m$ (Argon).

For $\dot{m}$ = 6 g/sec, we then calculate an "onset" current of 14,900 Amp. This is somewhat lower, but of the same order as those measured experimentally (20-25 KA).

In performing numerical calculations using the more general (below onset) conditions, we have indeed observed current saturation at a I value corresponding very closely with that given by Eq. (35). These calculations are reported in the next section.

5. Sample Results Below Onset

To illustrate the features of MPD flows, we have obtained numerical results from the theory explained in Sections 2 and 3 for two examples, defined as follows:

Case A: Argon gas, $\dot{m}$ = 6 g/sec

T = 20,000 K $\quad \sigma = 8000\ \Omega^{-1}/m$

H = 31.4 cm $\quad$ d = 8 cm $\quad$ L = 11.2 cm

Case B: Argon Gas $\quad \dot{m} = 6$ g/sec

T = 20,000 K $\quad \sigma = 5000\ \Omega^{-1}/m$

H = 31.4 cm $\quad$ d = 5 cm $\quad$ L = 27.8 cm

The calculated onset current, from Eq. (35) is 13.6 KA in Case A and 23.03 KA in Case B, the difference being mostly due to the narrower gap (d) in Case B.

For Case A, Fig. 3 shows the axial distribution of the negative anode drops at three current levels, one of which is very near onset. Notice that for the given conditions the anode "floating potential" (i.e., the ΔV_a for which $j_y = 0$ according to Eq. (14) is -8.05 Volt. We see in fig. 3 that at 10 KA, and even at 12.5 KA, ΔV_a stays within 1 volt of this level, whereas, as we come very close to the onset current, ΔV_a rapidly approaches zero or even reverses sign (although this happens so near onset that calculations are difficult in that case). The same trend is even more clearly apparent for Case B, in Fig. 6. One can also notice the survival of the large negative anode drop (even near onset) in the channel-end regions. This is where the back emf $\bar{u}x\bar{B}$ is small, and the anode still has to keep up its barrier to counteract nearly the full interelectrode potential. The Magnetic Reynolds numbers based of the width of these regions (about 1cm in either case) is about 0.5, as was to be expected. The length-based magnetic Reynolds numbers are 7 and 14 for Cases A and B respectively.

Fig. 4 presents current density results for Case A. As shown, the

center region of the channel is relatively unaffected as the net current increases, since the corresponding channel voltage increase is being compensated by a similar increase in ΔV_s. On the other hand, the end regions are strongly affected, and, to a first approximation can be seen to collect all of the extra current as one approaches onset. The same trends can be seen in Fig. 7 for Case B. Of course, the current peak at the downstream end is to be interpreted as a "bottled-up" reflection of what normally would be a two-dimensional current distribution extending into the plume; we have forced it back into the channel by imposing $\bar{B} = 0$ at the exit plane.

Figs 5 and 8 (Cases A and B respectively) summarize the salient trends versus total current. Shown are:

(a) The total transverse voltage. Notice the similar shapes in both cases, with a sharp upturn as the onset current I^* is approached.

(b) The negative anode drop (at mid-channel), showing the constant value, close to floating potential, up to about 90% of I^*, followed by the rapid drop (or increase in + ΔV_s). Even if the absolute value of the computed ΔV_s may be unrealistic, due to the neglect of near-wall excess Ohmic losses, this trend should be observable at currents approaching I^*.

(c) The plasma densities at the anode and cathode walls (at mid-channel). Here one sees, first of all, the general reduction of n as current increases, which is due to the higher velocity produced and the constancy of $\dot{m}$ and A. But, more interestingly, Figs. 5 and 8 show

the dramatic departure of n_{ANODE} from $n_{CATHODE}$ as I approaches I^*, and, in fact, the approach of n_{ANODE} to zero at I^*. Due to this radical redistribution of mass, the near-cathode density actually stops falling with current in the regime near I^*.

6. Conclusions

The results presented above indicate several interesting facts:

(a) The symptoms of "onset" are largely absent up to some 90% of the onset current, which shows the desirability of operation fairly close to I^*.

(b) The anode drop should remain nearly constant along the channel length, except at currents near I^*. This indicates that simple models based on an "equipotential" anode should be acceptable for $I \leq 0.9\ I^*$.

(c) The rapid increase of ΔV_a predicted near onset should be observable by probing the plasma potential near the anode surface. This should constitute a strong verification of the line of modeling taken here and in Ref. 1.

(d) A similar comment applies to the near-anode density, whose rapid decrease with current near onset should be detectable spectroscopically or by means of probes. This has, in fact, been done, by Rudolph (Ref. 2).

1. Baksht, F.G., Moizhes, B. Ya. and Rybakov, A.V., "Critical Regime of a Plasma Accelerator", Zhurnal Tekhnickeskoi Fiziki, Vol. 43, pp 2568-2573, Dec. 1973.

2. Rudolph, L.K., Jahn, R.G. and Von Jaskowsky, W.F., "Onset Phenomena in Self-Field MPD Arcs". AIAA paper 78-653, April 1978.

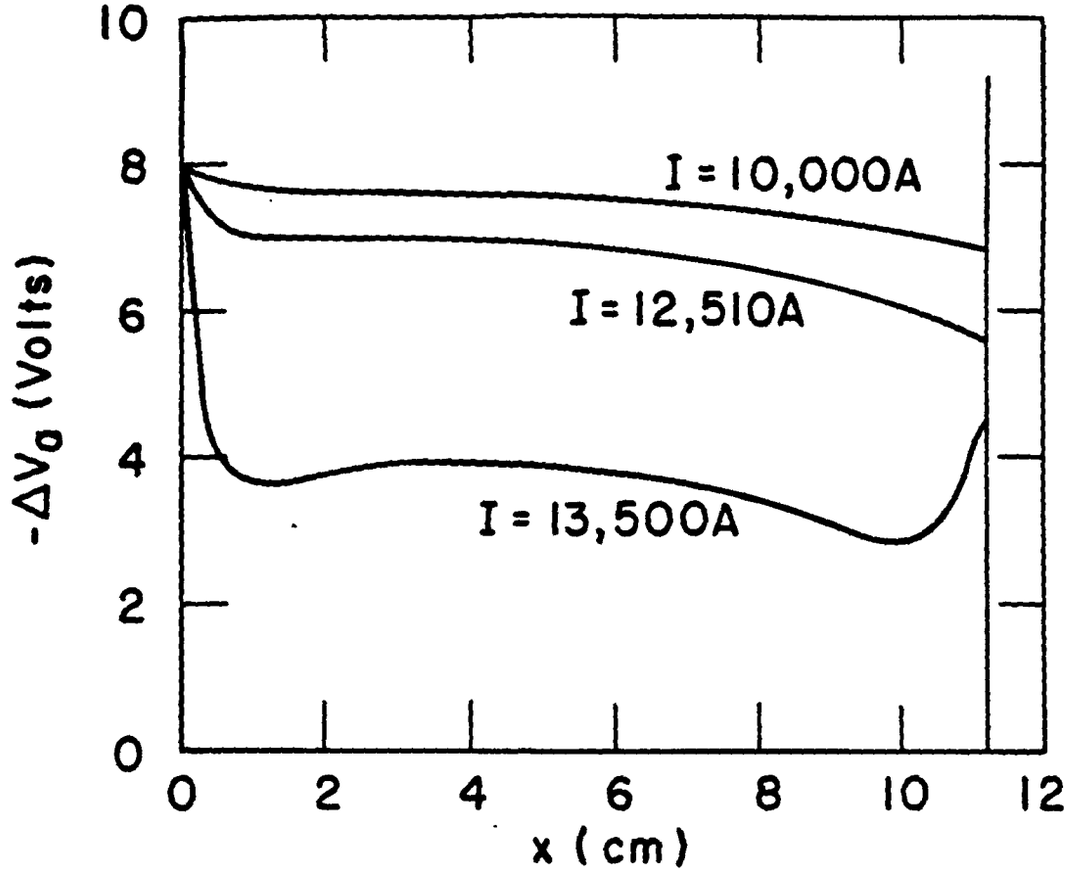

Fig. 3 ARGON, T = 20,000 K, σ = 8000 Ω -1/m, m = 6 g/sec
H = 31.4 cm d = 8 cm (I^* = 13,600 A)

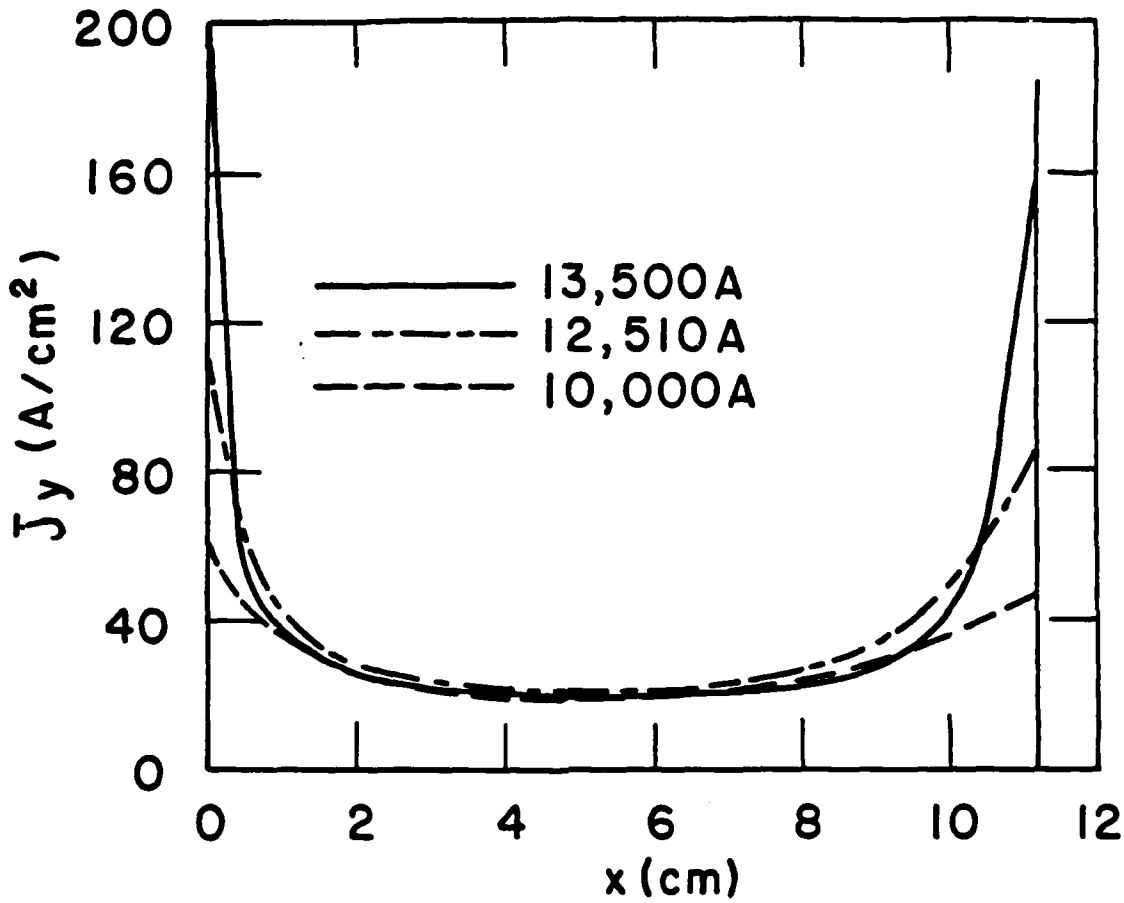

Fig. 4. ARGON, T = 20,000 K, σ = 8000 Ω -1/m m = 6 g/sec
H = 31.4 cm d = 8 cm (I^* = 13,600 A)

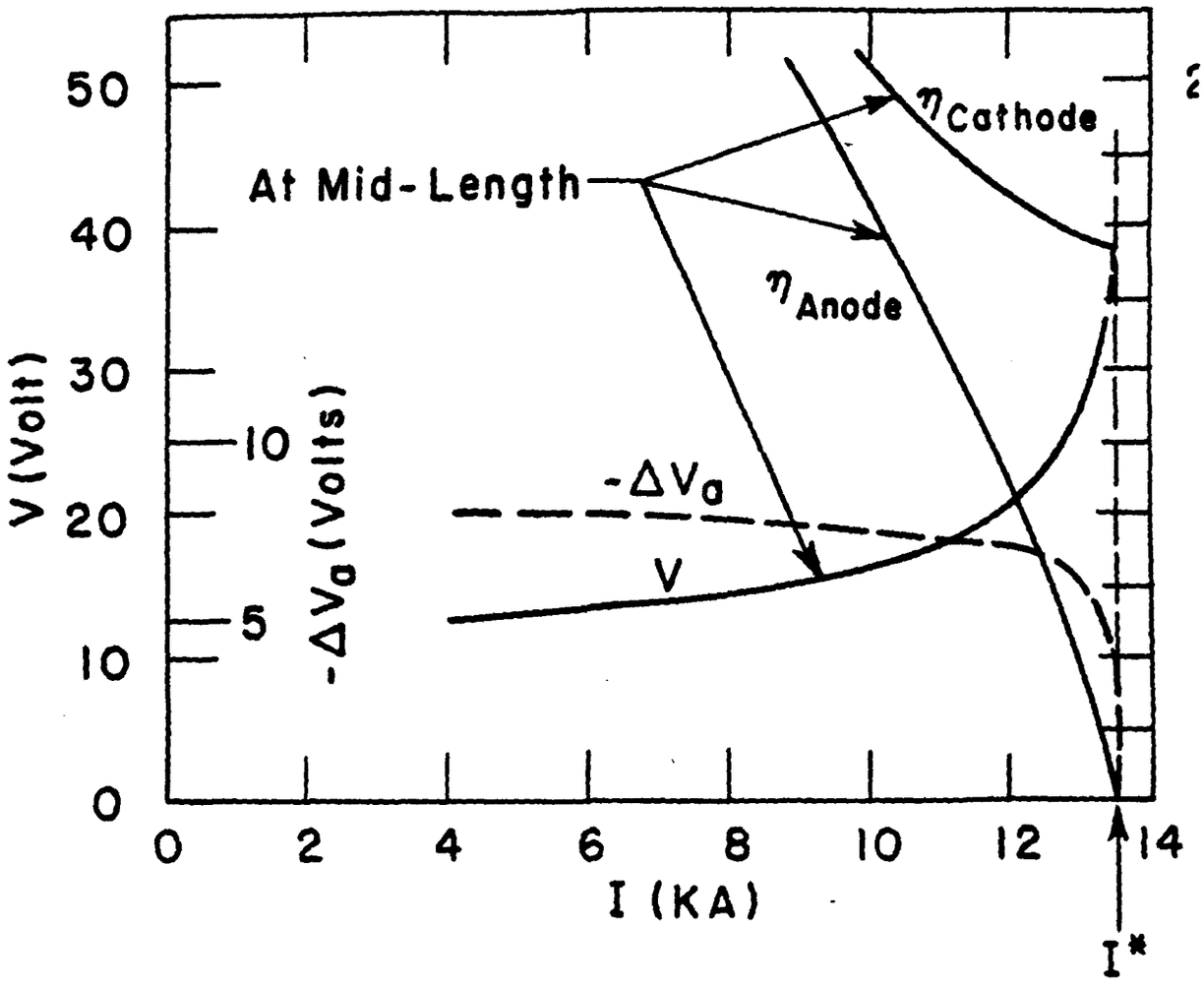

Fig. 5 ARGON, 6 g/sec

T = 20,000 K σ = 8,000 Ω -1/m ΔV_c = 20V

H = 31.4 cm d = 8 cm

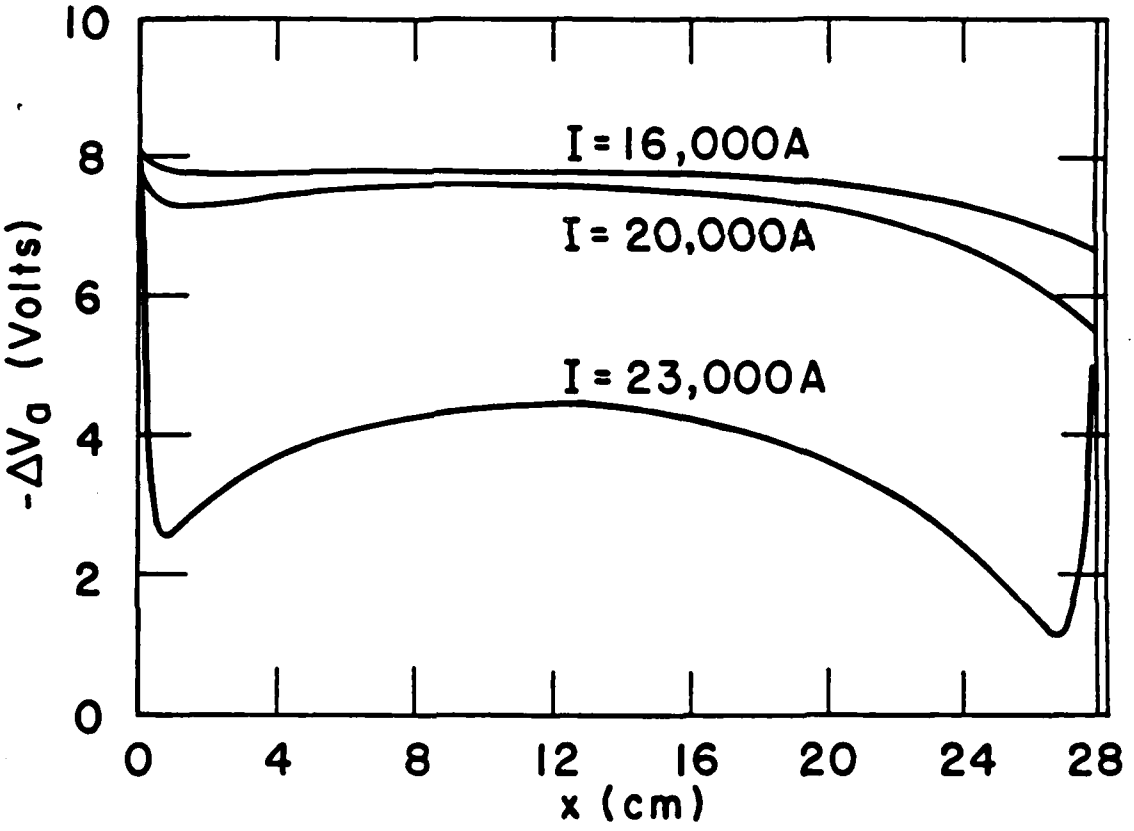

Fig. 6. ARGON, m = 6 g/sec T = 20,000 K σ = 5000 Ω -1/m
H = 31.4 cm d = 5 cm (I^* = 23,031 A)

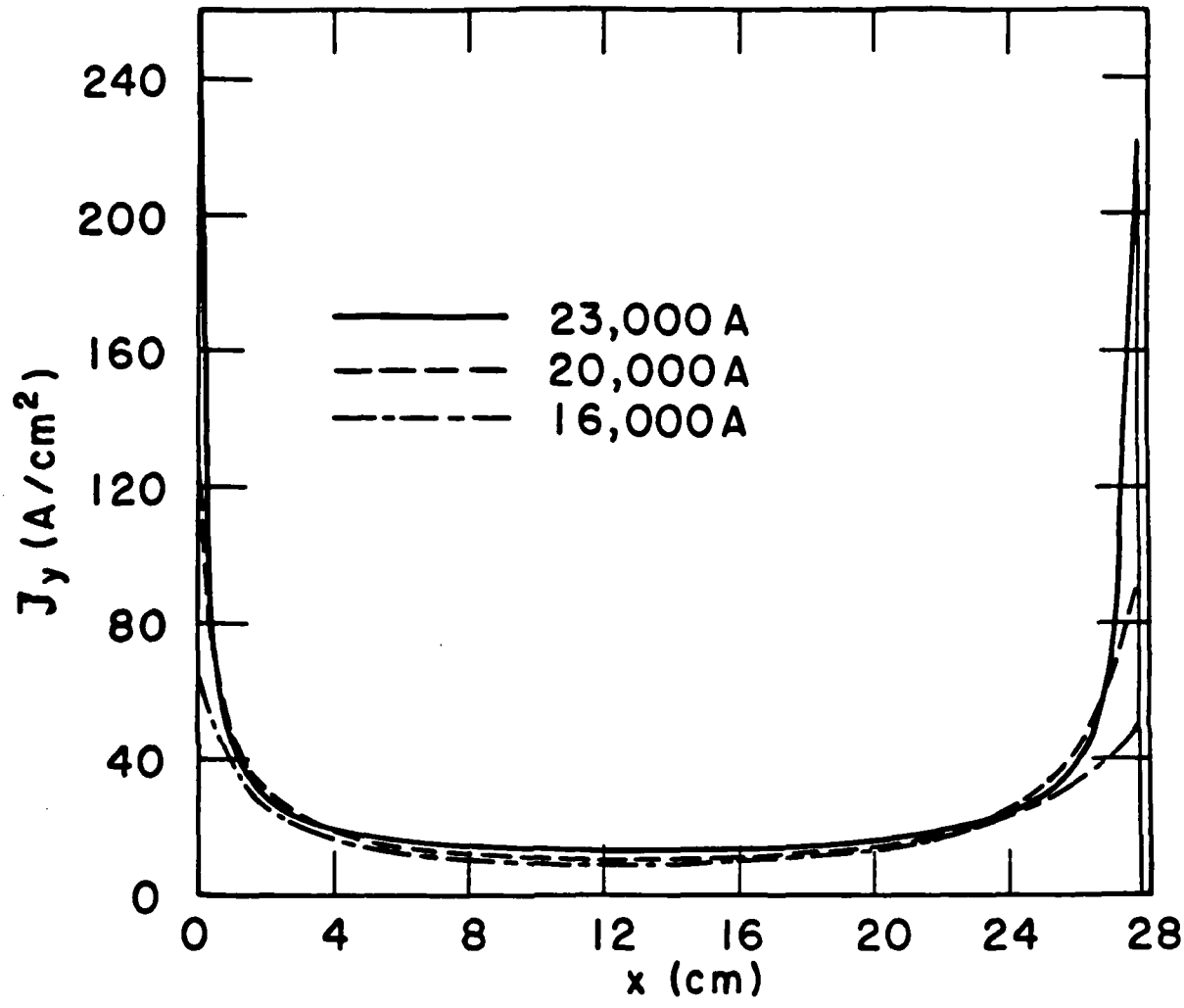

Fig. 7. ARGON, m = 6 g/sec T = 20,000 K σ = 5000 Ω -1/m
H = 31.4 cm d = 5 cm (I^* = 23,031 A)

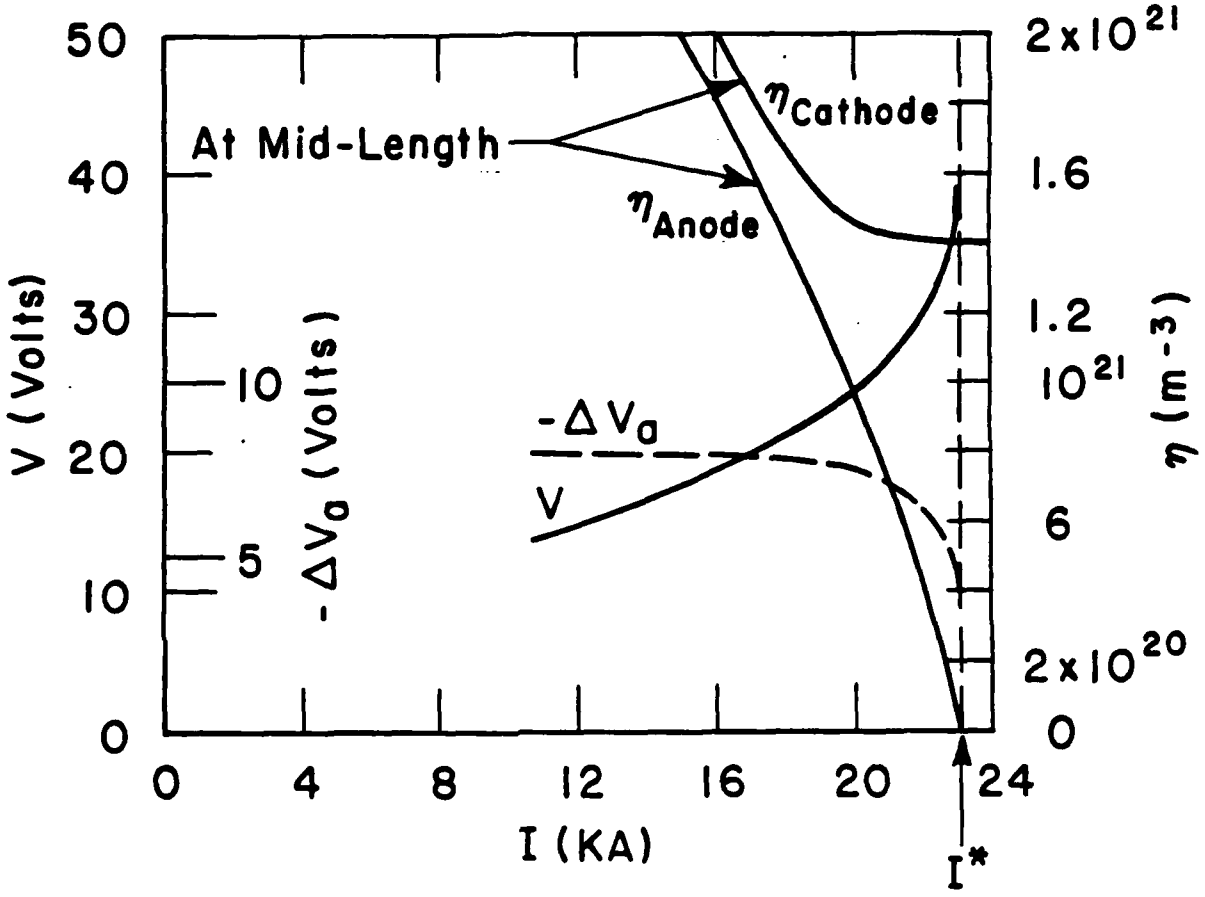

Fig. 8. ARGON, 6 g/sec

T = 20,000 K σ = 8,000 Ω -1/m ΔV_c = 20V

H = 31.4 cm d = 8 cm

Appendix 2

In this Appendix, a two-dimensional induction equation for MPD channels will be developed and used in a local description of the thruster entrance.

For this work, the plasma is modeled as a steady, fully ionized, single temperature gas characterized by a constant electrical conductivity, σ, and a Hall parameter, β, which is proportional to the magnetic induction B and inversely proportional to the gas density, ρ:

$$\sigma \simeq \text{Constant} \; ; \quad \beta \simeq c\,\frac{B}{\rho} \quad \left(c = \frac{\sigma m_i}{e}\right) \qquad (1)$$

where m_i is the ionic mass and e is the fundamental charge. The plasma is assumed to follow the ideal gas law, $P = 2n_i kT$, where $2n_i = n_e + n_i$ is the total number density, k is the Boltzmann constant, and T is the plasma temperature. Experimental data [1] and theory [2] have shown that the electron temperature varies slowly throughout most of the discharge except in the initial ionization region. Therefore the discharge is assumed to be isothermal. This approximation is also justifiable due to the large electron thermal conductivity and the excess available ionization and excitation energy found in the MPD, but it is ultimately just a convenient device to facilitate the analysis.

The generalized Ohm's law can be written as

$$\sigma\left(\vec{E}' + \frac{\nabla P_e}{en_i}\right) = \vec{J} + \vec{J} + \vec{\beta} \; ; \quad \vec{E}' = \vec{E} + \vec{u} \times \vec{B} \qquad (2)$$

where $\vec{\beta} = \beta\, \mathbf{E}/B$ and β is the Hall parameter, $\vec{u}$ is the mean mass velocity vector, $\mathbf{B}$ is the magnetic induction vector, $\mathbf{E}$ is the electric field and $\mathbf{J}$ is the current density.

We will also make use of the conservation equations for mass and momentum, as well as of Ampere's law and $\mathbf{E}$ - field irrotationality. For a two-dimensional geometry, with OZ perpendicular to the plane of the flow and OX along the channel axial direction, these are

$$\nabla \cdot \rho \vec{u} = 0 \tag{3}$$

$$\rho(\vec{u}\cdot\nabla)\vec{u} = -\nabla\left(p + \frac{B^2}{2\mu_0}\right) \tag{4}$$

$$\mathbf{J} = \nabla \times \frac{\mathbf{B}}{\mu_0} \quad ; \qquad \mathbf{B} = B\, \mathbf{I}_z \tag{5}$$

$$\nabla \times \mathbf{E} = 0 \tag{6}$$

In Eq. (4), the Lorentz force $\mathbf{J} \times \mathbf{B}$ has been converted to a magnetic pressure gradient $-\nabla(B^2/2\mu_0)$. An entirely similar transformation gives for the Hall field in Eq. (2).

$$\frac{1}{\sigma}\, \mathbf{J} \times \vec{\beta} = -\frac{1}{e n_i}\, \nabla\left(\frac{B^2}{2\mu_0}\right) \tag{7}$$

and using the momentum equation,

$$\frac{1}{\sigma}\, \mathbf{J} \times \vec{\beta} = \frac{1}{e n_i}\, [\, \rho(\vec{u}\cdot\nabla)\, \vec{u} + \nabla(2 n_i kT)] \tag{7b}$$

Substituting this into Ohm's law (Eq. (2))

$$\sigma(\vec{E}' + \frac{\nabla(n_i kT)}{en_i}) = \vec{J} + \frac{\sigma}{en_i}[\rho(\vec{u}\cdot\nabla)\vec{u} + 2\nabla(n_i kT)] \qquad (8)$$

It can be seen that the effect of the electron pressure gradient term in Ohm's law is to cancel 1/2 of the similar term appearing on the right hand side as a consequence of the Hall field (more generally, in a partially ionized gas, it would cancel the ∇P_e and leave the $\nabla(P_i + P_e)$ part). We can rewrite Eq. (8) as

$$\vec{J} = \sigma[\vec{E}' - \frac{m_i}{e}(\vec{u}\cdot\nabla)\vec{u} - \frac{kT}{e}\nabla \ln n_i] \qquad (9)$$

where the (-) sign in the $\nabla \ln n_i$ term is to be carefully noted.

It is useful to think of the whole bracketed term in Eq. (9) as the effective electric field. This field contains parts which are irrotational, plus others which are of the form $\vec{u} \times (\ )$. We can obtain this separation by noting that $(\vec{u}\cdot\nabla)\vec{u} = \nabla(u^2/2) + \vec{\omega} \times \vec{u}$, where $\vec{\omega}$ is the flow vorticity, $\vec{\omega} = \nabla \times \vec{u}$. Using also $\vec{E}' = -\nabla\phi + \vec{u} \times \vec{B}$ (ϕ = electric potential), we obtain

$$\vec{J} = \sigma[-\nabla(\phi + \frac{m_i u^2}{2e} + \frac{kT}{e} \ln n_i) + \vec{u} \times (\vec{B} + \frac{m_i}{e}\vec{\omega})] \qquad (10)$$

Notice here the grouping together of $\vec{B}$ and $\frac{m_i}{e}\vec{\omega}$, both of which are vectors along OZ. It is interesting that the ion gyro frequency Ω is eB/m_i, so that

$$\mathbf{B} + \frac{m_i}{e}\vec{\omega} = \frac{m_i}{e}(\vec{\Omega} + \vec{\omega}) \qquad (11)$$

Eq. (10) is a convenient point of departure for obtaining the induction equation. for this purpose we take the curl of both sides and use

$$\nabla \times \mathbf{J} = \frac{1}{\mu_0}\nabla \times \nabla \times \mathbf{B} = -\frac{1}{\mu_0}\nabla^2 \mathbf{B}$$

and

$$\nabla \times (\vec{u} \times \mathbf{B}) = \vec{u}(\nabla\cdot\mathbf{B}) + (\mathbf{B}\cdot\nabla)\vec{u} - (\vec{u}\cdot\nabla)\mathbf{B} - \mathbf{B}(\nabla\cdot\vec{u})$$
$$= -(\vec{u}\cdot\nabla)\mathbf{B} + \frac{\mathbf{B}}{\rho}\vec{u}\nabla\rho = -\rho(\vec{u}\cdot\nabla)(\frac{\mathbf{B}}{\rho})$$

with an entirely similar expression for $\nabla \times (\vec{u} \times \vec{\omega})$. Here we have used the two-dimensionality to cancel the term $(\mathbf{B}\cdot\nabla)\vec{u}$. With these substitutions, the induction equation is found as

$$\frac{\nabla^2 \mathbf{B}}{\sigma\mu_0} = \rho(\vec{u}\cdot\nabla)(\frac{\mathbf{B} + \frac{m_i}{e}\vec{\omega}}{\rho}) \qquad (12)$$

At high Magnetic Reynolds number ($R_m = \mu_0 \sigma u l$), Eq. (12) indicates that the quantity $\frac{1}{\rho}(B + \frac{m\omega}{e})$ is convective (conserved along a streamline). Alternatively, we may say that $\frac{\Omega + \omega}{\rho}$ is convective. Under some conditions $\frac{\omega}{\rho}$ itself may also be convective or constant, i.e., when the flow is uniform in a cross-section; in such cases, $\frac{B}{\rho}$ is a convective quantity too, and this property will be exploited in theoretical work now in preparation.

To conclude this section we note that an alternative form of the induction equation can be obtained by straightforward application of the curl operator to Eq. (2), with the result, in two dimensions,

$$\nabla^2 B + \left[\frac{\partial B}{\partial y}\frac{\partial \beta}{\partial x} - \frac{\partial B}{\partial x}\frac{\partial \beta}{\partial y} \right] = \mu_0 \sigma \rho (\vec{u}\cdot\nabla)\left(\frac{B}{\rho}\right) \qquad (13)$$

where the bracketed term is equivalent to the term $\sigma\mu_0 \rho(\vec{u}\cdot\nabla)(\frac{m_i \vec{\omega}}{e\rho})$ in Eq. (12), and indicates that whenever B and β (or B and n_i) are functionally related, such that the corresponding gradients are aligned, we will then have pure convection of vorticity (convective $\frac{\omega}{\rho}$).

2. The Inlet Region

The propellant is injected at low speed through the backplate of an MPD thruster. As long as (a) the momentum term in Eq. (4) is small compared to either the Lorentz force or the pressure gradient, and (b) the back emf, uB, remains small compared to the applied field, then the general Ohm's law (Eq. (10)) reduces to

$$J \simeq -\sigma \nabla(\phi + \frac{kT}{n_i} \ln n_i) \qquad (14)$$

while the momentum equation reduces, to first order, to

$$2 n_i kT + \frac{B^2}{2\mu_0} \simeq \text{const.} \qquad (15)$$

and (as can be seen by taking the curl of (14)), the induction equation

reduces to

$$\nabla^2 B = 0 \qquad (16)$$

Note that Eq. (16) does not necessarily imply a constant Hall parameter β. The reason the bracketed term in the more general form Eq. (13) is now absent is that, to order $\frac{\rho u^2}{B^2/2\mu_0}$, B and n_i are indeed functionally related (through the hydrostatic balance (15)). It is an interesting fact that the very simple law (16) for B is found to apply even in the presence of potentially large Hall parameter gradients.

Using Eq. (7b), Ohm's law (14) becomes

$$\vec{J} + \vec{J} \times (\frac{\vec{\beta}}{2}) \simeq \sigma \vec{E} \qquad (17)$$

indicating an effective Hall parameter reduced by 1/2 due to the electron diffusion effect.

There are several issues we would like to explore in connection with this inlet region:

(1) The corner singularites in B, i.e., current concentrations, due to the action of the Hall effect. This is similar to the known current concentration effect on the downstream edge of cathode segments in MHD channels, except that in the case of an accelerator ($uB < E_y$) the concentration will be at the <u>upstream</u> cathode edge.

(2) The redistribution of mass in response to the lateral $\vec{J} \times \vec{B}$ force as it develops away from the back plate (at the back plate

itself, $\mathbf{J} \times \mathbf{B}$ is purely axial, though).

(3) The ionization and heating effects associated with flow entrance.

Effects (2) and (3) are for now deferred, and we will concentrate on effect (1) above. For this purpose, Laplace's equation (Eq. 16) must be solved with appropriate boundary conditions. In formulating these boundary conditions, we will assume nonzero, but constant Hall parameter β. This is permissible because only the cathode corner is of interest, and the fact that the value of β or the anode wall may be different (higher) is of little significance, because very little current will in fact go to the upstream anode corner. In what follows we will implicitly assume a constant Hall parameter β of the order of (1/2) the value at the cathode corner.

For solution, this section of the MPD will be modeled as a constant area channel at a constant potential (Fig. 1). In the absence of strongly variable sheaths, the tangential electric field at the anode and the cathode is zero. Additionally, at axial distances far from the backplate, the axial electic field goes to zero and the transverse electric field goes to V/h. These assumptions lead to the boundary conditions for the channel

$$\text{at } (x,y) = (0,y)$$

$$j_x = \frac{1}{\mu_0} \frac{\partial B}{\partial y} = 0$$

$$\text{at } (x,y) = (x,0),(x,h)$$

$$\frac{\partial B}{\partial y} = \beta \frac{\partial B}{\partial x}$$

$$\text{at } (x,y) = (x \to \infty, y)$$

$$j_{x+e} = \sigma(1+\beta^2)^{-1}\left(\frac{V}{h} - uB\right)$$
$$j_{y,x+e} = \sigma(1+\beta^2)^{-1}\left(\frac{V}{h} - uB\right) \qquad (18)$$

where uB has been retained despite the inconsistency with the basic assumptions explained above, since this solution is then valid for a constant-velocity, constant β channel.

This is a well posed elliptic formulation that can be readily solved. In the complex representation, the complex variables are expressed as

$$z = x+iy$$
$$\hat{B} = B + i\Psi \qquad (19)$$

The complex magnetic field and the magnetic field in real coordinates can be connected through the definition of the complex derivative

$$\frac{d\hat{B}}{dz} = \frac{\partial B}{\partial x} - i\frac{\partial B}{\partial y} = \frac{d\hat{B}}{dw}\frac{dw}{dz} \qquad (20)$$

Equation(20) shows that the magnetic field gradient consists of two parts, one relating the original coordinate system (z) to a new mapped system (w) and another describing the variation of the complex field in the mapped system.

The mapping part of the solution can be facilitated by the Schwartz-Christoffel Transformation. This provides a simple mechanism for converting the semi-infinite region defined in the real (z-plane)

to the upper half of the complex (w-plane) bounded by the real axis (see Fig. 2)

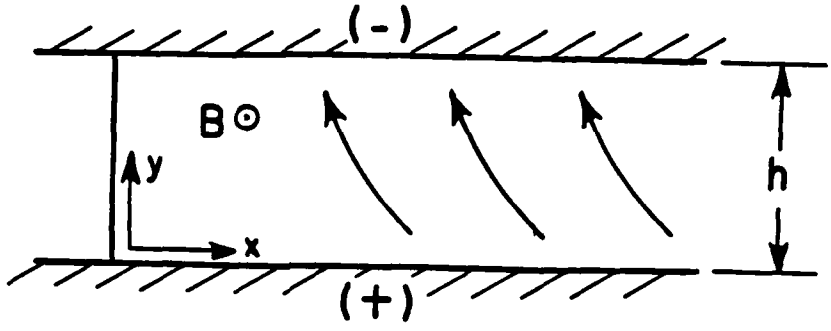

Fig. 1. Channel Geometry

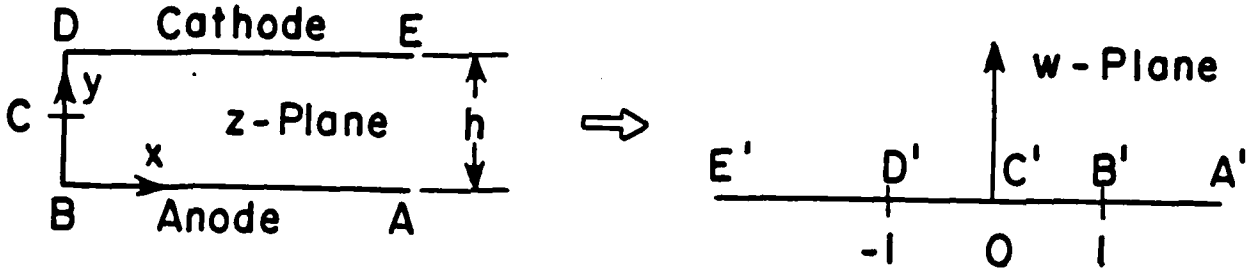

Fig. 2. Coordinate Transformation

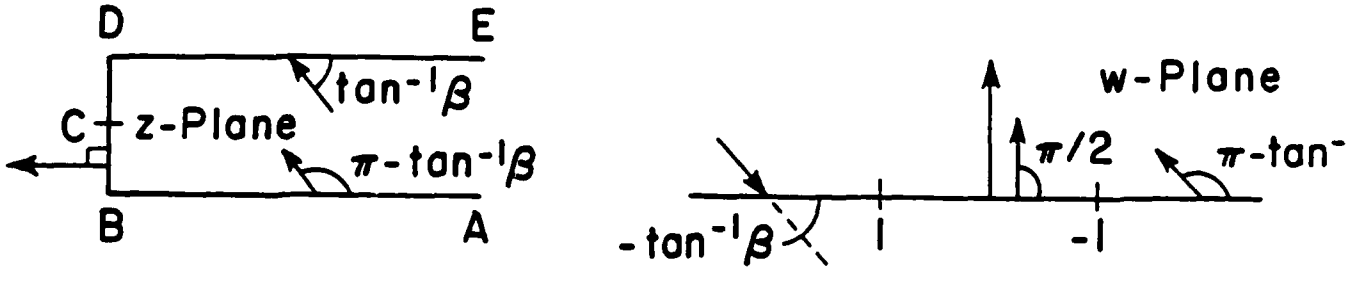

Fig. 3. Arguments of $\frac{d\hat{B}}{dz}$ and $\frac{d\hat{B}}{dw}$

This transformation is accomplished using the function

$$w = \cosh\left(\frac{\pi z}{h}\right) \tag{21}$$

Construction of an analytic function relating the complex magnetic field to the coordinate system in the w-plane requires mapping the boundary conditions from the z-plane to the w-plane. In the z-plane, the boundary conditions on $\frac{d\hat{B}}{dz}$ can be obtained readily from Eqs. (18) and (20):

$$\text{Anode and Cathode:} \quad \text{Arg}\left(\frac{d\hat{B}}{dz}\right) = \text{Arg}(1 - i\beta) = \pi - \tan^{-1}\beta$$

$$\text{Backplate:} \quad \text{Arg}\left(\frac{d\hat{B}}{dz}\right) = \pi$$

the mapping (21) subtracts o on the anode, $\frac{\pi}{2}$ on the backwall and π on the cathode, leaving the $\frac{d\hat{B}}{dw}$ arguments shown in Fig. 3, which can be mathematically expressed as

$$\begin{aligned}
&\text{along A'B'} \;:\; \arg\left(\frac{d\hat{B}}{dw}\right) = \pi - \tan^{-1}\beta \\
&\text{along D'B'} \;:\; \arg\left(\frac{d\hat{B}}{dw}\right) = \frac{\pi}{2} \\
&\text{along E'D'} \;:\; \arg\left(\frac{d\hat{B}}{dw}\right) = -\tan^{-1}\beta
\end{aligned} \tag{22}$$

If the analytic function

$$\frac{d\hat{B}}{dw} = \hat{K}(w - 1)^{\alpha}(w + 1)^{\gamma} \qquad (23)$$

is selected with $\hat{K}$ being a complex constant, the coefficients α and γ and the argument of $\hat{K}$ can be related in order to satisfy (22), and are and found to be equal to

$$\alpha = -\frac{1}{2} + \frac{\tan^{-1}\beta}{\pi} \qquad (24)$$

$$\gamma = -1 - \alpha = -\frac{1}{2} - \frac{\tan^{-1}\beta}{\pi} \qquad (25)$$

$$\arg(\hat{K}) = \pi(\tfrac{1}{2} - \alpha) \qquad (26)$$

Using Eq. 20 it can then be shown that

$$\frac{d\hat{B}}{dz} = \frac{\pi}{h}\,|\hat{K}|\; e^{i(\pi-\tan^{-1}\beta)}\; (\tanh\frac{\pi z}{2h})^{(\frac{2}{\pi}\tan^{-1}\beta)} \qquad (27)$$

Solving for the real and imaginary parts of Eq. (27), and referring to Eq. (20), the partial derivatives of the magnetic induction can be derived as follows

$$\frac{\partial B}{\partial x} = -\frac{\pi}{h}|\hat{K}|\left[\frac{\cosh(\frac{\pi x}{h})-\cos(\frac{\pi y}{h})}{\cosh(\frac{\pi x}{h})+\cos(\frac{\pi y}{h})}\right]^{\frac{\tan^{-1}\beta}{\pi}} \cos[(\tan^{-1}\beta)(1 - \frac{2}{\pi}\tan^{-1}\left[\frac{\sin(\frac{\pi y}{h})}{\sinh(\frac{\pi x}{h})}\right])]$$

$$\frac{\partial B}{\partial y} = -\frac{\pi}{h}|\hat{K}|\left[\frac{\cosh(\frac{\pi x}{h})-\cos(\frac{\pi y}{h})}{\cosh(\frac{\pi x}{h})+\cos(\frac{\pi y}{h})}\right]^{\frac{\tan^{-1}\beta}{\pi}} \sin[(\tan^{-1}\beta)(1 - \frac{2}{\pi}\tan^{-1}\left[\frac{\sin(\frac{\pi y}{h})}{\sinh(\frac{\pi x}{h})}\right])] \tag{28}$$

For $x \to \infty$, the constant $|\hat{K}|$ can be calculated from the boundary conditions, Eq. (18), and is found to be

$$|\hat{K}| = \frac{\mu_0 \sigma h}{\pi}(1 + \beta^2)^{-1/2}(\frac{V}{h} - uB) \tag{29}$$

The above results show that a closed form solution for B may not be possible; however, these results are exact expressions for the components of the current density vector. At the insulator backplate,

$$j_x = 0$$

$$j_y = \sigma(1 + \beta^2)^{-1/2}(\frac{V}{h} - uB)[\tan(\frac{\pi y}{h})]^{(\frac{2\tan^{-1}\beta}{\pi})} \tag{30}$$

The distribution of j_y along the backplate can be seen in Fig. 4. The anticipated singular region is seen at the cathode root. Similarly, along the anode (y=0)

$$j_x = -\beta\sigma(1 + \beta^2)^{-1}(\frac{V}{h} - uB)[\tanh(\frac{\pi x}{2h})]^{(\frac{2\tan^{-1}\beta}{\pi})}$$

$$j_y = \sigma(1 + \beta^2)^{-1}(\frac{V}{h} - uB)[\tanh(\frac{\pi x}{2h})]^{(\frac{2\tan^{-1}\beta}{\pi})} \tag{31}$$

and along the cathode (y=h)

$$j_x = -\beta\sigma(1+\beta^2)^{-1}\left(\frac{V}{h} - uB\right)\left[\coth\left(\frac{\pi x}{2h}\right)\right]^{\left(\frac{2\tan^{-1}\beta}{\pi}\right)}$$

$$j_y = \sigma(1+\beta^2)^{-1}\left(\frac{V}{h} - uB\right)\left[\coth\left(\frac{\pi x}{2h}\right)\right]^{\left(\frac{2\tan^{-1}\beta}{\pi}\right)} \qquad (32)$$

The distribution of current at the anode and the cathode is diagrammed in Figs. 5 and 6.

It has been shown that a very simple model of the entrance region of the MPD can be constructed that has a limited range of validity but demonstrates the singular nature of the channel current distribution.

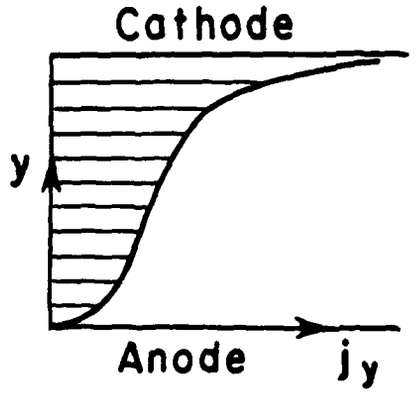

Fig. 4.

Distribution of transverse current density on the face of the Backplate

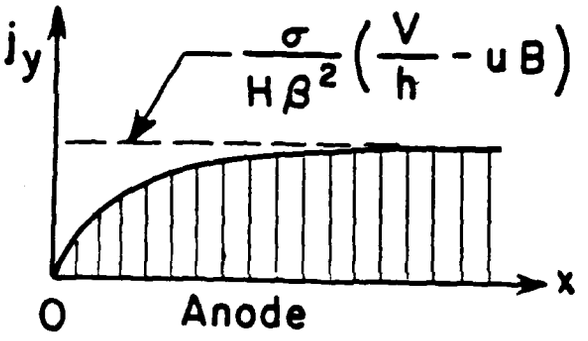

Fig. 5.

Distribution of transverse current density along the anode wall

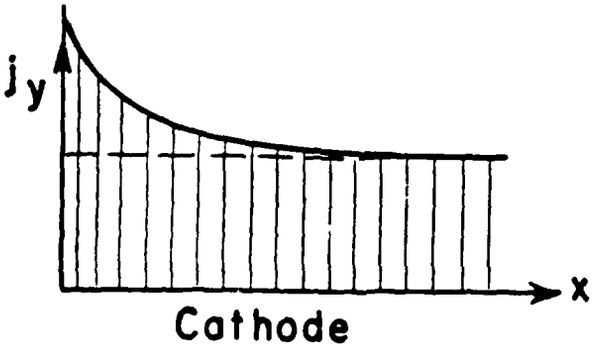

Fig. 6.

Same as Fig. 7, along the cathode wall

References

1. Turchi, P.J., "The Cathode Region of a Quasi-Steady Magnetoplasma-dynamic Arcjet," Ph.D. thesis, September 1970, Princeton University, Princeton, New Jersey.

2. Heimerdinger, D., "An Approximate Two-Dimensional Analysis of an MPD Thruster," SM Thesis, Massachusetts Institute of Technology, Cambridge, MA, 1984.

Appendix 3

Simultaneous Hall and Magnetic Convection Effects

Consider a rectangular channel (Fig. 1) of length L, height W and depth H, with infinitely segmented electrode walls and bounded by electrical insulators at

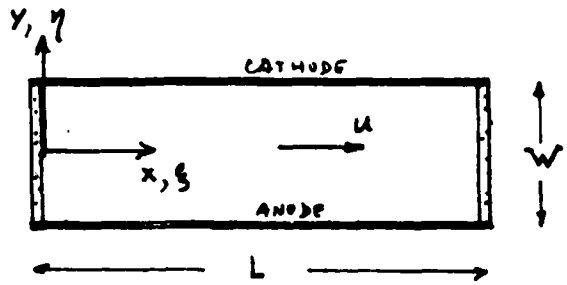

FIG. 1. RECTANGULAR CHANNEL SCHEMATIC

its ends. A fluid of constant conductivity σ and Hall parameter β is assumed to flow in the channel at a constant velocity u. We define as a reference non-dimensional quantity the Magnetic Reynolds number

$$R = \mu_o \sigma u L \tag{1}$$

where $\mu_o = 4\pi \times 10^{-7}$ (MKS units) We also normalize distance as

$$\xi = \frac{x}{L} \quad , \quad \eta = \frac{y}{L} \quad , \quad w = \frac{W}{L} \tag{2}$$

If we impose the design condition that the current vector $\vec{j}$ be everywhere transverse ($j_x \equiv 0$), it can be shown that the

j_y component and the potential ϕ with respect to the cathode tip are given by

$$j_y = \sigma B_o u \frac{e^{R\xi}}{e^R - 1} \tag{3}$$

and

$$\phi = \frac{u B_o L}{1 - e^{-R}} \left[\frac{w}{2} - \eta + \frac{\beta}{R} (1 - e^{-R(1-\xi)}) \right] \tag{4}$$

where B_o is the magnetic field at $x = 0$, related to the total current I by

$$I = \frac{H}{\mu_o} B_o \tag{5}$$

Eq. 3 shows that, if $R \gg 1$, most current will concentrate in the last 1/R fraction of the channel length.

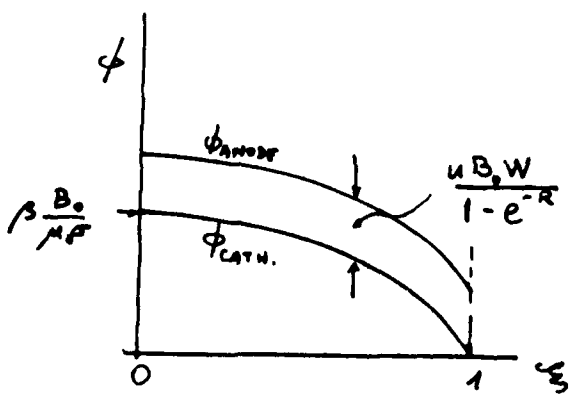

FIG. 2. ANODE AND CATHODE VOLTAGES FOR $\pm ER_0$ AXIAL CURRENTS

If there is substantial overlap between the anode and cathode voltages (Fig. 2), i.e., if

$$\beta >> \frac{Rw}{1 - e^{-R}} = \frac{\mu_o \sigma u W}{1 - e^{-R}} \qquad (6)$$

then the required voltage distribution could be approximated using a single external supply by externally interconnecting points on the anode and cathode which must be at equal potentials. This is schematized in Figs. 3 and 4, where a six-segment construction would result. The dotted lines in Fig. 4 indicate external shorting wires. Notice the total channel current is $I = 6\ I_{ext.}$, where I_{ext} is the power supply current, while the external voltage V_{ex} is $6(V_y + \Delta V_a + \Delta V_c)$, where V_y is the channel voltage, and ΔV_a and ΔV_c are the near-electrode voltage drops. The fractional voltage drop is the same as in a direct connection, since both the plasma and and the electrode drops are multiplied six times.

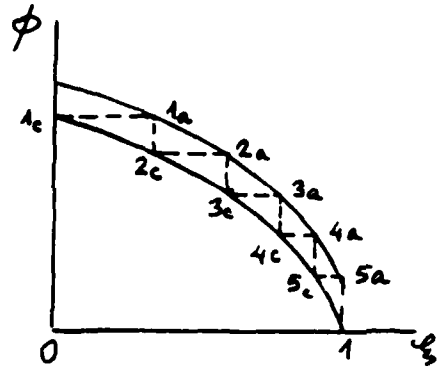

FIG. 3. POINTS 1A-1C, 2A-2C, ETC. CAN BE SHORTED EXTERNALLY

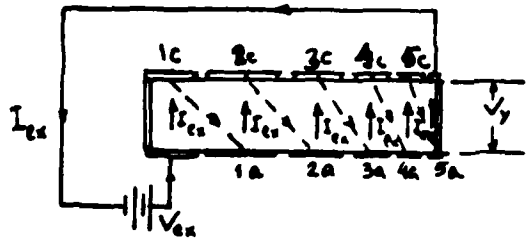

FIG 4. CROSS-CONNECTION SCHEMATIC FOR FIG. A3

Scaling and Numerical Estimates.

The Hall parameter β can be estimated as follows:

$$\beta = \frac{\sigma}{en_e} B \simeq \frac{\mu_o m_i}{e} \sigma u W \frac{I}{\dot{m}} \tag{7}$$

where full ionization has been assumed, and B_o has been used for B, since the magnetic field tends to fall mostly near the exit. Condition (6) becomes

$$\frac{I}{\dot{m}} >> \frac{(e/m_i)}{1 - e^{-R}} \tag{8}$$

For Argon, assuming $e^{-R} << 1$, this is

$$\frac{I}{\dot{m}} >> 2.4 \frac{KA}{(g/sec)} \tag{9}$$

This can be compared to an "onset" criterion; for Argon, an approximate condition for stability is

$$\frac{I^2}{\dot{m}} \lesssim 82 \frac{(KA)^2}{(g/sec)} \tag{10}$$

Assuming σ = 4000 mho/m, u = 6000 m/sec, W = 2 cm, Eq.(7) gives

$$\beta \simeq 0.25 \frac{I}{\dot{m}} \frac{(KA)}{(g/sec)} \tag{11}$$

Fig. 5 shows conditions (9) and (10) together with some constant-β lines. It can be seen from this figure that sufficient overlap exists for $\dot{m}$ below some 2 g/sec, even if the ordinary onset condition is not exceeded (of course, segmentation is intended as a means to exceed that condition). Incidentally, for the same conditions, $R \simeq 30\ L(m.)$, so that for $L \gtrsim 7$ cm the assumption $e^{-R} \ll 1$ is justified.

This analysis shows that axial current can be suppressed by appropriate voltage distributions on the electrode walls, and that such distributions can be approximated by cross-connected segmentation, using still a single power supply. It also shows, however, that the bunching up of current at the channel exit will persist if $R \gg 1$; for an open channel end, this would manifest itself as current lines "ballooning" into the plume.

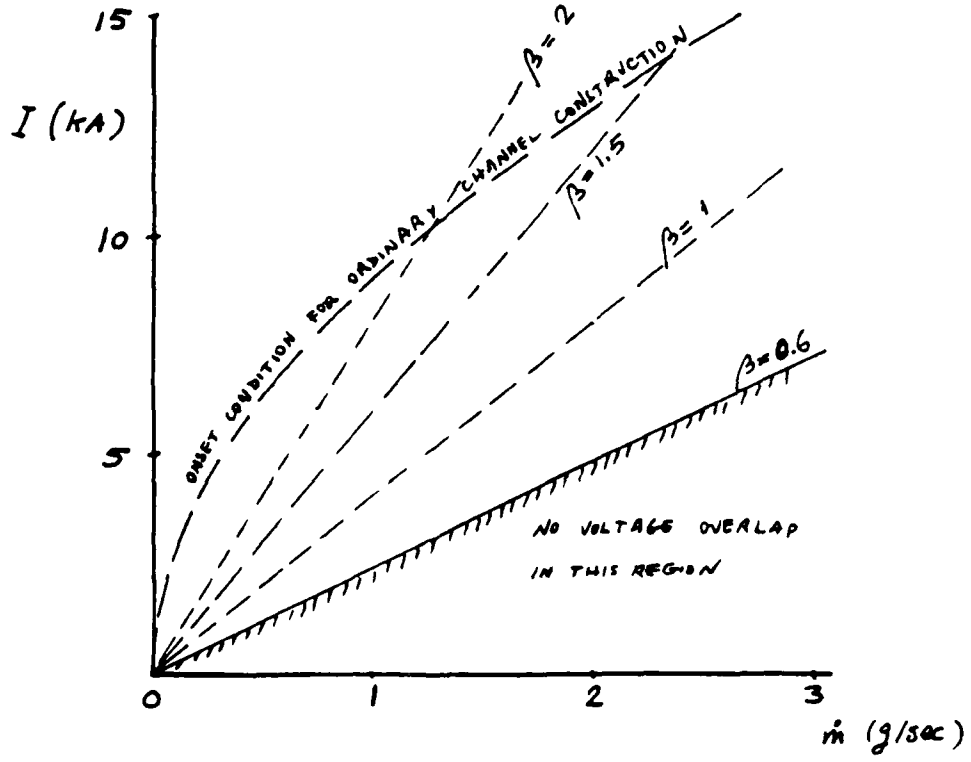

FIG. 5. CONDITIONS FOR ARGON MPD CHANNEL
THE NUMBER OF SEGMENTS IN A DIAGONALLY CONNECTED CONSTRUCTION WOULD BE ROUGHLY $1+\beta/0.6$.

APPENDIX 4

TABLE OF CONTENTS

LIST OF FIGURES

LIST OF TABLE

NOMENCLATURE

$\vec{B}$	Magnetic induction
$\vec{E}$	Electric field
e	Electron charge
h	Plank constant
$\vec{J}$	Current density
$\bar{\kappa}$	Thermal conductivity
k	Wave number
k	Boltzmann constant
n_e	Electron number density
n_i	Positive ion number density
n_n	Neutral number density
T_e	Electron temperature
T_i	Positive ion temperature
T_g	Neutral particle temperature
t	Time
$\vec{v}_e$	Electron velocity
$\vec{v}_i$	Positive ion velocity
x	Coordinate
y	Corrdinate

Greek:

β	Hall parameter
μ_e	Electron mobility
σ	Electric conductivity

CHAPTER I INTRODUCTION

High specific impulse with moderate thrust density and relative operational simplicity are the main features of the quasi-steady electromagnetic plasma accelerators (Magnetoplasmadynamics MPD Thrusters). In previous research, various schemes of application of external magnetic field and geometric variations were tested. [1] One particular concept which uses coaxial geometry, high current, flow rate in millisecond pulses and no external magnetic field [2,3], however, is the prime interest in this country. Considerable progress has been made in the design, operation and diagnosis of these thrusters. Still, two areas must be progressed and developed in order to bring these features of the thruster into functional reality. They are (i) to increase efficiency [4] and (ii) to increase lifetime [5] of the accelerator. In the last decade, many test data regarding the operation limitations of the accelerator have been accumulated. Most of them are on the self-field, coaxial type [6,7] mentioned above. (Figure 1.1, 1.2 & 1.3) Important efforts have also been made in the research of its lifetime. Not much data, however, has been collected. More efforts are now underway [8].

Regarding the performance limitation analysis, one-dimensional flow models [9] have provided hints about improvements of geometrical contouring, but the essentially two-dimensional phenomena at onset of fluctuations, which affects the attainable efficiency [10], cannot be addressed by these analysis. Some theories [11] attempt to correlate the onset phenomena by invoking the "Alfven" limiting velocity in a dimensional manner. Highly simplified two-dimensional theories have also been developed, [12] but geometrical shape of the thruster still remains to be the deciding factor.

A physically illuminating analysis by Baksht, et al [13] postulated that the side force, resulting from axial Hall current, reduces the near-anode plasma density. Then, current saturation will be reached when the whole anode has positive electric potential relative to the plasma. Therefore, other phenomena must occur if higher current is demanded.

Other phenomena accompanying current satuation are full ionization & high Hall parameter near the anode, and partial ionization but high electron & neutral number density near the cathode. These microscopic properties suggest that the analysis of local instability (microscopic instability) might provide answers for the global onset situation. Since the Hall parameter and electron density play a major role in local stability. More understanding regarding those parameters is needed.

Therefore, this thesis will discuss the local instability of the plasma inside the coaxial accelerator. In particular, a small disturbance's propagation through the plasma of uniform background will be the focus of our attention. Instabilities resulting from ionization and field variations will also be discussed in the later chapters.

CHAPTER II PROPAGATION OF DISTURBANCES THROUGH THE PLASMA WITH PARTIAL IONIZATION. CONSTANT TEMPERATURE & CONSTANT INDUCED MAGNETIC FIELD

2.1 INTRODUCTION

Global parameters such as electron temperature, density are important as premises for the formulation of our local analysis since they determine the background properties. Before starting, we must have some knowledge regarding the global situation.

Baksht, et al [13] analyzed the onset phenomena for a simple slender channel geometry by assuming constant temperature and full ionization throughout the plasma. The constant temperature approximation is substantiated by the measurements made by K. Rudolph [10] and P.J. Turchi [14], but full ionization can only be reached in some particular regions of the thruster.

Based on other measurements regarding the electron density and temperature, the plasma is at a density level one to two orders of magnitude below the Saha equilibrium density.[1] Therefore, bulk recombination is very unlikely to compete with the diffusion of charged particles to the wall of the thruster. (recombination can only occur at the wall)

---

[1] See appendix I

Radiation recombination is certainly present, but the process is slow in comparison with diffusion. It might have some effects on the local stability, but in this chapter, our prime interest is to set up a simple model, so we can investigate the basic response to small disturbances created inside the plasma. Also, because of its comparison with particle diffusion rate, we can safely ignore radiation recombination here.

Induced magnetic field is actually varying with time and space, as stated by Maxwell's equations. These variations are first assumed to be slow and negligible in the dimensions of interest, so it is assumed here that magnetic field is constant. The effect of varying magnetic field will be discuss in the next chapter.

So, our first model for analysis should follow the guidelines of the classical glow discharge theory of Schottky, [15] where bulk electron collision ionization is mainly balanced by ambipolar diffusion. The net gain of electron in ionization process is caused only by disturbances. In the global energy balance, all energy obtained by the plasma from external sources (by means of Joule heating) should be balanced by losses due to particle collisions.

2.2 CALCULATIONS

2.2.1 ASSUMPTIONS

From the global picture of the plasma mentioned above, we can extract some assumptions, and proceed with our analysis accordingly.

1. Constant temperature throughout the plasma.
2. Plasma is partially ionized but no net gain of electrons by the ionization process. (No steady-state ion densities time variations)
3. Constant magnetic field. (no space & time variations)
4. Positive ion and neutral possess the same value of temperature, which remains constant but differs from the electron temperature.

2.2.2 GOVERNING EQUATIONS

For the plasma of interest, the electrons have very rapid motion relative to the ions and neutrals(heavy species), simply because the mass of the electron is substantially smaller than that of the heavy species. Also, the energy transfer by electrons, by whatever means, is faster than any other species. So it is appropriate to consider the energy balance of the electrons only.

The energy input to the electron by Joule heating (J^2 / σ) is balanced on average by the collisional losses between the electrons and ions. (at moderate ionization fractions, electron-ion collisions are much more frequent than electron-neutral collisions) However, in the area where disturbances occur, the excess energy given by

the imbalance process will fuel the ionization process. Thus, the energy equation becomes,

$$eV_c \frac{\partial n_e}{\partial t} = \frac{J^2}{\sigma} - 3\frac{m_e}{m_g} n_e \nu_e K(T_e - T_g) \tag{2.1}$$

where $\nu_e = e/m_e\mu_e$ is the collision frequency between the electrons and ions. And $\mu_e = \beta/B$ is the mobility, β is the Hall parameter.

Electron temperature is much higher than the positive ion and neutral temperature because of its rapid random motion, so $T_e - T_g = T_e$

After rearranging the energy equation, it yields,

$$\frac{J^2}{\sigma} - 3\frac{KT_e}{m_g}\frac{\sigma B^2}{\beta^2} = eV_c \frac{\partial n_e}{\partial t} \tag{2.2}$$

Also, the momentum changes of the electrons are governed by Ohm's Law. (electron momentum equation)

$$\sigma\vec{E} = \vec{J} + \vec{J} \times \vec{\beta} \tag{2.3}$$

Since constant magnetic field is assumed, Maxwell's equations, which govern the electromagnetic relations of the charged particles, reduce to the form,

$$\nabla \times \vec{E} = 0 \tag{2.4}$$

$$\nabla \cdot \vec{J} = 0 \tag{2.5}$$

2.2.3 CALCULATION PROCESS

Before we rearrange the equations, let us set up the coordinate system. The disturbances are assumed to be of a plane wave form propagating at any random direction. We fix our coordinates as follow: (Figure (2.1)) The angle is the angle between the direction of the propagation of the disturbances, and the steady state (background) current flowing direction.

By applying the two Maxwell's equations (2.4, 2.5), we deduced that,

$$J_x = \text{Constant}$$

$$E_y = \text{Constant}$$

(there is no variations along the wave front, i.e $\partial/\partial y = 0$)

Let us denote the quantities in the background state by the bracket < >. For example, the current density to the zero'th order will be represented by < J >.

From the assumptions mentioned above, we also found that there is no background time variations, i.e. $\partial/\partial t\,(\langle n_e \rangle) = 0$. Since electron temperature and magnetic field are assumed constant, every quantity related to these two parameters carries the same value as the background situation. One of those quantities is conductivity of the plasma. In the regime which we are interested in, the collision process is dominated by Cloumb collisions. The conductivity under this condition is almost only a function of electron temperature, as appeared in the Spitzer formula,

$$\sigma = 0.0153 \frac{T_e^{3/2}}{\ln \Lambda}$$

$$\Lambda = \frac{d_D}{P_0}$$

$$d_D = 69 \sqrt{\frac{T_e}{n_e}}$$

$$P_0 = 2.1 \times 10^{-10} \left(\frac{3000}{T_e}\right)$$

We approximate Λ as a constant for our analysis; taking $\ln \Lambda = 6$, we obtain

$$\sigma = 2.55 \times 10^{-3}\ T_e^{1.5} \qquad (2.6)$$

The disturbances are assumed to be small in magnitude in comparison with the background quantities. We therefore can write,

$$J = \langle J \rangle + \delta J$$

(J has two components, J_x & J_y)

$$\beta = \langle \beta \rangle + \delta\beta$$

$$\mu_e = \langle \mu_e \rangle + \delta\mu_e$$

$\delta\beta$ is the first order variation (perturbed variation), and so

$$\frac{\delta\beta}{\langle\beta\rangle} << 1$$

After all these substitutions have been made in the governing equations (2.2, 2.3, 2.4 and 2.5), and the zero'th order terms cancelled out, we obtain the first order perturbation equation

$$\frac{\partial}{\partial t}(\delta\beta) = -3\frac{\omega_B^2 B}{V_i \sigma}\left[2 + \langle\beta\rangle \cdot \cdot \cdot 2\theta\right]\delta\beta \qquad (2.7)$$

where $\bar{s}^2 = KT_e/m_g$ is the square of the isothermal speed of sound in the ionized gas (also called the Bohn velocity).

V_i is the voltage (energy) required for the ionization process for a particular substance. (Argon, for example)

2.3 RESULTS

To solve the differential equation, we assume,

$$\delta\beta = \beta_0 e^{-\alpha t} \tag{2.8}$$

where

$$\alpha = \frac{3\nu_e^2 B}{\nu_i \omega} \left[2 + \langle\beta\rangle \sin\theta\right]$$

If α is positive, the disturbances will die out as time progresses, in other words, it will not propagate through the whole plasma, and so the system will be stable. The deciding factor in α is

$$2 + \langle\beta\rangle \sin\theta \tag{2.9}$$

The variations of this factor due to the changes of the current angle and the value of the Hall parameter are plotted in figure (2.2) and figure (2.3).

2.4 CONCLUSIONS

If the direction of the wave vector (direction of the propagation of the disturbances) falls between the direction of the current flow and electric field, stability occurs. It is also known that high Hall parameter means that the current flow direction is further deviated from the electric field vector, and this occurs at relatively low electron density in the case of constant induced magnetic field.

In figure (2.4), the situation falls into the stability category. In the high Hall parameter region, current density is higher than the two adjacent regions. As a result, energy deposition by means of Joule heating (J^2 / σ) will increase, and consequently the ionization rate will go up. More electrons will then fill the originally low density regions, thus, the discrepancy will ease. Uniform background can then be preserved. In our calculations, the angles of current flow which fell into this regime (0° to 90°; 180° to 270°) did exhibit stability at any value of the Hall parameter.

Conversely, in the case of figure (2.5), Joule heating in the originally low density regions will decrease. The discrepancy of electron density will then be magnified, and so the uniform background would be destroyed. As proved by our analysis, the directions of current flow which had the angle between 90° to 180°, 270° to 360° relative to the wave vector were the unstable region.

Another conclusion from the stability condition (equation 2.9)

$$\{ 2 + < \beta > \mathrm{SIN}(2\theta) \} > 0$$

is that the threshold value of the Hall parameter is 2 (corresponding to the worst orientation, $\theta = 135^{\circ}$). It serves as a reference point. The value of $<\beta>$ is considered to be high if it has a value greater than two, to be low otherwise.

In the "Barrel" luminous region of the MPD Arcjet observed by K. Rudolph [10] at the onset of fluctuations, the Hall parameter did exceed 2. (it reached 10 in that region) This suggested that local instability could have an effect on the phenomena of the onset of fluctuations. However, more refined analysis (to be presented later) indicates that heat conduction should provide some damping in the regime of interest.

CHAPTER III PROPAGATION OF DISTURBANCES WITH PARTIAL IONIZATION, CONSTANT TEMPERATURE BUT VARYING MAGNETIC FIELD

3.1 INTRODUCTION

In chapter two, we proved that local instabilities could contribute some effects to the global onset phenomena. The imbalance between the Joule heating and the collisional losses by the electrons will cause instability. But there are other mechanisms which can cause instabilities or stabilize the existing problem. So in this chapter, we will explore the effects of the wavelength dependence in wave propagation.

We neglected the variations of induced magnetic field in last chapter for simplicity. But in some cases, their associations with the growth of instabilities might be important. Specifically, a space varying magnetic field might not be able to penetrate through the whole plasma, since the "skin effect" will act as a damping force against the penetration. This will cause a wavelength dependent damping, where certain disturbances, whose wavelengths are of the order of some characteristic values associated with the skin depth with growth time, will die out preferentially. Since the normal size of the MPD device's dimension is of the order of 10^{-1} to 10^{-2} meters, the disturbances of interest to us must be of this order.

As stated earlier, the magnetic field is actually varying with time and space, as expressed in Maxwell's equations. So we will keep every assumption the same as in chapter II except the magnetic field. Thus we can analyze the effects of the wavelength damping.

3.2 CALCULATIONS

3.2.1 ASSUMPTIONS

We maintain every assumption in chapter two except that the magnetic field has time and space dependence.

1. Constant temperature throughout the plasma.
2. Plasma is partially ionized but no net gain of electrons or positive ions by the ionization process. (No time variations in ions densities)
3. Ions and neutrals possess the same value of temperature, which remains constant.
4. The magnetic field has space and time dependence.

3.2.2 GOVERNING EQUATIONS

We start off with the same energy equation as in chapter two, where excess energy obtained by the imbalance between Joule heating and collisional losses fuels the ionization process.

$$eV_i \frac{\partial n_e}{\partial t} = \frac{J^2}{\sigma} - 3 \frac{m_e}{m_a} \mu_e n_e k (T_e - T_g) \qquad (3.1)$$

The temperature difference between the electrons and heavy species is still assumed to be large compared to the gas temperature. Thus,

$$T_e - T_g = T_e$$

Substituting the proper expressions relating to n_e , ν_e and μ_e, we get

$$V_i \frac{\partial}{\partial x}(\mu_e) = 3\nu_B^2 - \frac{\mu_e}{\sigma} J^2 \qquad (3.2)$$

ν_B^2 (Bohm velocity) is the square of the isothermal speed of sound in ionized gases.

The electron momentum equation is

$$\sigma \vec{E} = \vec{J} + \vec{J} \times \vec{B} \qquad (3.3)$$

With proper substitutions, it yields

$$\sigma \vec{E} = \vec{J} + \vec{J} \times (\mu_e \vec{B}) \qquad (3.4)$$

Maxwell's equations which govern the electromagnetic effects between the charged particles are,

$$\nabla \times \vec{E} = - \frac{\partial}{\partial t} \vec{B} \qquad (3.5)$$

$$\nabla \cdot \vec{B} = 0 \tag{3.6}$$

$$\nabla \times \vec{B} = \mu_0 \vec{J} \tag{3.7}$$

3.2.3 CALCULATION PROCESS

Since our interest is the wavelength dependence of the propagation of disturbances, a plane wave form dependence of these quantities is assumed.

$$\delta u = \bar{u} e^{i[\omega t - \vec{k} \cdot \vec{x}]} \tag{3.8}$$

where $\bar{u}$ is constant with respect to time and space coordinates. represents the quantity of interest.

The coordinate system is the same as in chapter II, where the wave is propagating along the x-axis. The angle θ is defined as the angle between the background current flow and the wave vector(direction of propagation). The magnetic field vector will be perpendicular to the x-y plane. (Figure (2.1))

Then,

$$\frac{\partial}{\partial t}\delta u = i\omega u \tag{3.9}$$

$$\frac{\partial}{\partial x}\delta u = -i k u \tag{3.10}$$

Small disturbances are still assumed to exist. Every perturbed quantity is tiny when compared to the background state. For example:

$$\delta \hat{n}_e = \frac{\delta \mu_e}{\langle \mu_e \rangle} \ll 1$$

As in last chapter, there is no variations along the wave front, therefore, $\frac{\partial u}{\partial y} = 0$ for whatever quantity u represents.

Rearranging the Maxwell's equation (3.6, 3.7), we get

$$J_x = \text{Constant}$$

Again, every quantity in the background state is constant ($\frac{\partial}{\partial t}\langle n_e \rangle = 0$, $\frac{\partial}{\partial x}\langle \cdot \rangle = 0$, etc.) except the magnetic field, as appeared

in the Maxwell's equation (3.7)

$$\nabla \times \vec{B} = \mu_0 \langle \vec{j} \rangle$$

The magnetic field's background state variation in space equals to the average current flow density at that state; however, this needs not concern us, because gradients of < B > do not appear in the formulation.

$$\mu_0 \langle j \rangle \sin\theta = -\frac{\partial}{\partial x} \langle B \rangle$$

In this model, our first order variables are $\delta\mu_e$, δB , δE_y . Other variables such as δJ_y , etc., are just dependent variables of the three mentioned above.

Before we proceed any further, let us define some non-dimensional quantities in order to simplify the analysis.

The non-dimensional frequency will be defined,

$$\Omega = \omega \tau^*$$

$$\tau^* = \frac{\sigma \langle B \rangle^2}{\mu_0 \langle j \rangle^2} \qquad (3.11)$$

where τ^* can be interpreted as the time for Ohmic dissipation to generate an energy density equal to the magnetic energy density.

The non-dimensional wave number,

$$\psi = \frac{\lambda^*}{\lambda}$$

$$\lambda^* = \frac{2\pi_1 \langle B \rangle}{\mu_0 \langle j \rangle}$$

$$= \frac{K \langle B \rangle}{\mu_0 \langle j \rangle} \lambda \qquad (3.12)$$

$$\left(K = \frac{2\pi}{\lambda} \right)$$

where λ^* is the characteristic macroscopic variation length for B, such that a cyclic change of B with λ^* as the wavelength and with amplitude < B > would generate currents with amplitude < J >. The non-dimensional wave number ψ can also be interpreted as the inverse of the magnetic Renold's number.

Finally, the parameter measuring the energy invested in the ionization process,

$$\gamma_i = \frac{V_i \mu_o J}{\langle B \rangle} \tag{3.13}$$

can be interpreted as the ratio of ionization potential to Ohmic voltage.

μ_o is the magnetic permeability of free space. $\mu_o = 4 \times 10^{-7}$ in SI units.

From the y-direction component of the electron momentum equation, we get,

$$\delta J_y = \sigma \delta E_y - \langle \mu_e \rangle \langle B \rangle \delta J_x$$

$$+ \langle \mu_e \rangle \langle B \rangle \frac{\nu_{en}}{\omega_{ce}} \delta J_z \tag{3.14}$$

After the zero'th order terms of the energy equation are cancelled out, we find

$$V_i \langle \mu_e \rangle \frac{\partial}{\partial x} \delta \hat{\mu}_e = -2 \langle \mu_e \rangle \frac{\nu_{en}}{\omega_{ce}} \delta J_z$$

$$- 2 \frac{\langle \mu_e \rangle^2}{\sigma} \frac{\nu_{en}}{\omega_{ce}} \delta J_z \tag{3.15}$$

$\delta\hat{\mu}_e = \delta\mu_e / \langle\mu_e\rangle$ is the non-dimensional quantity for μ_e.

Combining it with equations (3.8) (3.9) (3.10) (3.11) (3.13) and (3.14), we get,

$$\left\{ i\Omega - \frac{\langle\beta\rangle^2}{\gamma_i}\sin\theta - \frac{2\langle\beta\rangle}{\gamma_i} \right\} \delta\hat{\mu}_e$$

$$+ \frac{2\langle\beta\rangle}{\gamma_i}\sin\theta\sqrt{1+\langle\beta\rangle^2}\,\delta\hat{E}_y \qquad (3.16)$$

$$+ \frac{\langle\beta\rangle^2}{\gamma_i}\sin\theta\,\delta\hat{B} = 0$$

Substituting the proper expressions into equation (3.7), it yields

$$\langle\beta\rangle\cos\theta\,\delta\hat{\mu}_e + \sqrt{1+\langle\beta\rangle^2}\,\delta\hat{E}_y \qquad (3.17)$$

$$+ \left[i\langle\beta\rangle\cos\theta - (\quad) \right]\delta\hat{B} = 0$$

From Maxwell's equation (3.5),

$$+ \psi\sqrt{1+\langle\beta\rangle^2}\,\delta\hat{E}_y - (\quad)\delta\hat{B} = 0 \qquad (3.18)$$

Now, the final form of our governing equations are

$$A(i,j) \begin{Bmatrix} \delta\dot{\mu}_c \\ \delta\dot{E}_i \\ \delta\dot{E} \end{Bmatrix} = 0$$

where

$$A(1,1) = i\Omega + \frac{\langle\beta\rangle^2}{\gamma_i}\sin 2\theta + \frac{\partial\langle\beta\rangle}{\gamma_i}$$

$$A(1,2) = \frac{\partial\langle\beta\rangle}{\gamma_i}\sin\theta\sqrt{1+\langle\beta\rangle^2}$$

$$A(1,3) = \frac{\langle\beta\rangle^2}{\gamma_i}\sin 2\theta$$

$$A(2,1) = \langle\beta\rangle\cos\theta$$

$$A(2,2) = \sqrt{1+\langle\beta\rangle^2}$$

$$A(2,3) = \langle\beta\rangle\cos\xi - i\psi$$

$$A(3,1) = 0$$

$$A(3,2) = i\psi\sqrt{1+\langle\mu\rangle^2}$$

$$A(3,3) = -i\Omega$$

For a non trivial problem, the determinant of the coefficient must equal to zero. In the determinant, Ω is treated as variable, while the rest is considered as input parameter.

Since plane wave dependence of the disturbances is assumed,

$$\delta u = e^{i(\omega t - kx)}$$

$$= e^{i\{\Omega\frac{t}{\tau} - \frac{x}{L}\}}$$

(τ , L are constants.)

We notice that the disturbances will exhibit unstable behavior if the imaginary part of Ω is negative. (ψ is assumed to be real)

Expanding the determinant into a quadratic form, we get,

$$\Omega^2 - i\Omega\left\{\frac{2\langle\beta\rangle}{\gamma_i} + i\psi\langle\beta\rangle\cos\theta + \psi^2\right\}$$

$$- i\psi\frac{\langle\beta\rangle}{\gamma_i}\left\{2\langle\beta\rangle\cos\theta - i\psi(2+\langle\beta^2\rangle\sin 2\theta)\right\} \tag{3.19}$$

Our prime interest here will be the imaginary part of the unknown Ω .

Looking into the equation in more detail, let us first establish the relationship between the oscillating part (Ω real) and the damping part (Ω imaginary). By separating the equation into real and imaginary part and setting them both equal to zero, we find

$$\Omega_R^2 - \Omega_I^2 + \Omega_R\psi\langle\beta\rangle\cos\theta$$

$$+ \Omega_I\left(\frac{2\langle\beta\rangle}{\gamma_i} + \psi^2\right) - \psi^2\frac{\langle\beta\rangle}{\gamma_i}(2+\langle\beta^2\rangle\sin^2\theta) = 0 \tag{3.20}$$

$$2\Omega_R\Omega_I + \Omega_I\psi\langle\beta\rangle\cos\theta$$

$$- \Omega_R\left(\frac{2\langle\beta\rangle}{\gamma_i} + \psi^2\right) - \psi\frac{2\langle\beta^2\rangle}{\gamma_i}\sin\theta = 0 \tag{3.21}$$

Rearranging equation (3.21), it yields

$$\Omega_R = \Psi \langle\beta\rangle \cos\theta \; \frac{\frac{2\langle\beta\rangle}{r_c} - \Omega_I}{2\Omega_I - \frac{2\langle\beta\rangle}{r_c} - \Psi^2} \tag{3.22}$$

We focus our interest on the worst orientations regarding stability (the magnitude of Ω_R imag is the lowest), so, by differentiating the equation with respect to θ and setting the derivative $\partial/\partial\theta(\Omega_I) = 0$, we find the angles of the worst orientations to be given by

$$\tan 2\theta = -\frac{2}{r_c} \frac{\left\{2\Omega_I - \frac{2\langle\beta\rangle}{r_c} - \Psi^2\right\}^{\frac{1}{2}}}{\left(\frac{2\langle\beta\rangle}{r_c} - \Omega_I(\Omega_I - \Psi^2)\right)} \tag{3.23}$$

We further specify our point of interest to be the threshold situation where the plasma is in neutral stability (zero growth rate for the disturbances), i.e $\Omega_I = 0$. So, the worst orientations and the relation between the oscillating part and damping part are

$$\tan 2\theta = \frac{\left(\Psi^2 + \frac{2\langle\beta\rangle}{r_c}\right)^{\frac{1}{2}}}{\langle\beta\rangle \Psi^2} \tag{3.24}$$

$$\Omega_R = -\psi \langle\beta\rangle \cos\theta \; \frac{\frac{2\langle\beta\rangle}{\gamma_i}}{\psi^2 + \frac{2\langle\beta\rangle}{\gamma_i}} \qquad (3.25)$$

From equation (3.24), we see that { COT (2 θ) } tends to zero both at short wavelengths ($\psi >> 1$) and long wavelength ($\psi << 1$). At the value $\psi = \sqrt{2\langle\beta\rangle/\gamma_i}$ (of order of unity in cases of interest), { COT (2 θ) } peaks at

$$[\ \mathrm{COT}\ (\ 2\ \theta\ )\ ]_{max} = \gamma_i\ /\ 8 \cong 0.2$$

Since, as will be seen, the range of ψ in the cases of interest is from about 7 to 700, it can be concluded that { COT (2 θ) = 0 } is a good approximation for maximum growth. This gives $\theta = 135^\circ$; the alternative choice $\theta = 45^\circ$ leads to minimum growth. Details of the variation of θ_{worst} for the range of wavelengths from 1 mm to 0.1 m are given in figure (3.1).

Now, combining equations, we get a relation between the non-dimensional wave number and the Hall parameter.

$$\left(\frac{\gamma_i}{\langle\beta\rangle}\psi^2\right)^2 - 4\left(\frac{\gamma_i\langle\beta\rangle}{\langle\beta\rangle^2 - 4}\right)\left(\frac{\gamma_i}{\langle\beta\rangle}\psi^2\right) + 4 = 0 \qquad (3.26)$$

We can see that at both limits where ψ is zero or approaching infinity (both extremely short and long waves), the value of the critical Hall parameter is 2. The long wavelength region ($\psi << 0$) is one where the disturbances have wavelengths larger than the distance λ^* required for the current to build up the existing background magnetic field. Thus, for a self-field device, this region is of dubious physical significance. The opposite limit ($\psi >> 1$, short wavelength) can be interpreted as follow: the penetration distance in a time t for a current disturbance in a plasma of conductivity σ is

$$\delta \sim \sqrt{\frac{t}{\mu_0 \sigma}}$$

In our case, t for unstable growth must be of the order of

$$\frac{J / \sigma}{\epsilon J}$$

In terms of our dimensionless factors, the growth $K_\delta = 2\pi \delta / \lambda$ is found to be

$$k_\delta = \sqrt{\frac{\quad}{\quad}}$$

Thus, when this growth is larger (and hence $< \beta > \longrightarrow 2$, as implied by equation (3.26)), the penetration (diffusion) distance of the disturbances is much greater than the propagation wavelength. This means that magnetic field disturbances

will be minimal, which is the limit postlated in our earlier simple analysis. Details are plotted in figure (3.2) for various values of γ_c .

3.3 RESULTS

First, let us state the typical background situation for the analysis.

Electron Temp.	T	= 20,000	K
Magnetic field	B	= 0.075	T
Current Density	J	= 5×10^5	Amp/m^2
Ionization potential	V_i	= 15.8	Volt.
Electric conductivity	σ	= 7212.	A^2/m^2V

So, the relations between those non-dimensional and real quantities will be,

$$\sigma = 0.1291 \times 10^{-3} \omega$$

$$\gamma_i = 1.9094$$

$$\Psi = 0.75 / \lambda$$

The wavelength of the wave is of the order of 1 mm to 0.1 m, since the dimension of the typical MPD devices are of the same order. Ψ will be 75 for λ being 1 cm, and so the range of Ψ is from 7 to 750.

Also, the value of γ_i is in the range of 1 to 3. As appeared in equation (3.13), it depends on the conductivity σ, magnetic field B and the ionization potential V_i. Examining the typical substances being used to generate the plasma, V_i does not exceed 20. In order to achieve higher value of γ_i, either higher

conductivity or lower magnetic field is required. But for the case of the self-field MPD devices, the value of B is related to the current density. Also, because the plasma is in Coloumb collision dominated regime, the conductivity depends upon the electron temperature and thus can be related to the current density. In other words, the parameter γ_i is a function of current density.

$$\gamma_i = f (< J >)$$

Since the onset phenomena limit the allowable current density, γ_i ranges only from 1 to 3 for the existing operation regime.

So, the only relevant region of figure (3.2) is for ψ^* greater than 49 and γ_i ranging from 1 to 3, i.e the flat part of the graph where the critical Hall parameter is nearly 2. We find that damping due to magnetic field variations does happen, but it just falls out of the range of the operating regime of the MPD devices currently being used. Details of the variations of ω_r vs. ω_{imag} with various $< \beta >$ is plotted in figure (3.3).

Looking at equation (3.22)

$$\Omega_R = \frac{\frac{2 < \beta >}{\gamma_i} - \omega_r^2}{\omega_r^2 - \frac{2 < \beta >}{\gamma_i} - \psi^*}$$

$$(\omega_{imag} \longrightarrow 0)$$

We can see quite easily that Ω_R approaches zero for both limiting cases where ψ approaches zero or infinity. This agrees with our finding in chapter two where there is only damping part in the propagation of disturbacnes when we return to the simple case described in chapter II. For the values of λ in the range from 1 mm to 0.1 m. Ω_R is plotted vs. wavelength in figure (3.4) It is growing with the wavelength in that region. Looking back to our numerical expressions regarding the real quantities, we find that the range of the oscillating part of the propagation can be up to 727 Hz.

In figure (3.5). Ω imaginary is plotted vs. the current angle θ with various values of ψ in the case of the wavelength being 6.28 centimeter It is apparent that $\theta = 135^\circ$ is the most unstable orientation for all ψ values in this case. As the wavelength gets larger, the worst orientation becomes less than 135° and 315° (Equation 3.23) But the deviation is small, and $\theta = 135^\circ$ for the worst orientation angle is still an acceptable assumption.

3.4 CONCLUSIONS

From the figures, we found that $< \beta > = 2$ is still the threshold value for stability at the worst orientations for the wavelength from 1 mm to 1 cm.

The variations of the magnetic field has little effect on the overall stability picture. In the existing operation regime of the typical MPD device, the magnetic field variations appear to the plasma as a short wave effect. It penetrates throughout the whole region quite easily, and is viewed as constant inside the plasma, because the "skin-effect" is no longer effective against the penetration. So the assumption of a constant magnetic field throughout the whole plasma stated in previous chapter is valid and sound.

Also, the result indicates that the type of instability is still the same as that in chapter two, where it is caused by the imbalance between the energy input (Joule heating) to the plasma and the collisional losses by the electrons. The rate of growth of the instability is less in the long wavelength case, but the reduction is not enough to reach stability. For the typical MPD devices, whose dimensions are of the order of centimeters or less, wavelength damping appears to be insignificant. In the next chapter, we will examine the effects of ionization non-equilibrium and heat conduction on the stability picture.

AD-A181 924 FACTORS FOR MPD THRUSTORS(U) MASSACHUSETTS INST OF TECH 2/2
CAMBRIDGE SPACE SYSTEMS LAB M MARTINEZ-SANCHEZ
01 MAY 86 AFOSR-TR-87-0816 AFOSR-83-0035

UNCLASSIFIED F/G 21/3 NL

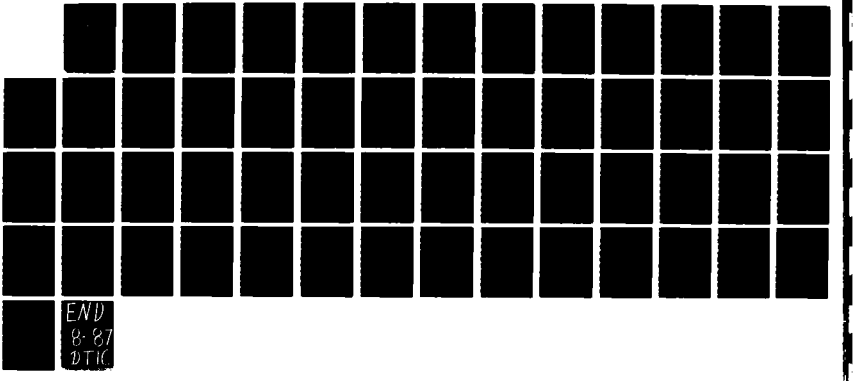

END
8-87
DTIC

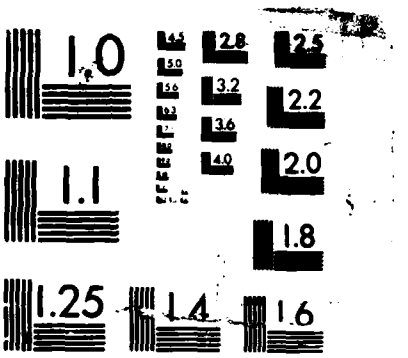

MICROCOPY RESOLUTION TEST CHART

CHAPTER IV PROPAGATION OF DISTURBANCES THROUGH THE PLASMA OF IONIZATION NON-EQUILIBRIUM WITH VARYING ELECTRON TEMPERATURE BUT CONSTANT MAGNETIC FIELD

4.1 INTRODUCTION

In the last two chapters, we examined the effects caused by the electron density variation by looking at the partially ionized regime of the plasma. We found that instability occurs when the energy transfer between the Joule heating and electron collisional losses is not in balance. The magnetic field variation was found to help stabilize the situation but it is insufficient in the regime of interest.

Now, we will turn to the situation of ionizaton non-equilibrium. In other words, the kinetics of the electrons, rather than the electron energy equation will determine the ionization rate(Appendix I). The excess electron-ion pairs will diffuse away and recombine as neutrals at the boundry.

Also, instability of the type mentioned in the last chapter does not appear near full ionization, since electron density can no longer vary. Now, by allowing the electron temperature to vary, instabilities might occur at or near the area where full ionization is reached.

Also, the effect of heat conduction in the plasma might play a major role in the overall stability picture. In previous chapters we found that the imbalance of energy transfer causes instability. But if heat conduction occurs within the plasma,

this imbalance might be eliminated, and thus the type of instability discovered in the last chapters might not appear.

So in this chapter, we will explore the effects of the ionization non-equilibrium, varying electron temperature, and heat conduction within the plasma.

4.2 CALCULATIONS

4.2.1 ASSUMPTIONS

As shown in last chapter, the effect of the variations of the magnetic field is insignificant in the regime of our interest. Thus, we will return to the assumption that the magnetic field remains constant. (No space and time variations)

The positive ion and neutral temperatures are still taken to be constant. As stated in previous chapters, the heavy species is considered as immobile when compared with the electron due to their enormous mass. Compared to the electron temperature variation, the other species' temperatures exhibit only smallar variations. Therefore, it is only necessary to consider the electrons in the number conservation, momentum and energy balances.

So, our assumptions will be,

1. The magnetic field is constant. (No space and time variations)
2. The positive ion temperature and neutral temperature are the same and remain constant.
3. In the background state, the net gain in electron density by the ionization process will be balanced by the ambipolar diffusion to the wall.
4. The heavy species number density (ion density plus neutral density) is constant.

4.2.2 GOVERNING EQUATIONS

The excess energy, which will fuel the ionization process and transfer away by means of heat conduction, is the difference between the Joule heating and the collisional losses by the electrons. So the energy equation will be,

$$\frac{\partial}{\partial t}\left[n_e\left(eV_i + \tfrac{3}{2}kT_e\right)\right] + \nabla\cdot\left[n_e\vec{v}_e\left(eV_i + \tfrac{3}{2}kT_e\right)\right]$$

$$+\nabla\cdot\vec{q}_e = \frac{J^2}{\sigma} - 3\frac{m_e}{m_i}n_e\nu_e k(T_e - T_g) \qquad (4.1)$$

where $T_e - T_g \approx T_e$; $\nu_e = \frac{e n_e}{m_e \sigma}$

The convective term can be expressed as

$$\nabla\cdot(n_e\vec{v}_e) = \dot{n}_e - \frac{\partial n_e}{\partial t}$$

($\dot{n}_e$ will be stated in equation (4.8))

The heat conduction term is expressed by,

$$\nabla\cdot\vec{q}_e = \frac{d}{dx}\left[-\overline{\kappa}\frac{dT_e}{dx}\right] \qquad (4.2)$$

where the thermal conductivity[2] is

$$\bar{\alpha} = \frac{75}{32} \frac{(4\pi\varepsilon_0)^2}{\sqrt{\pi}\, m_e} \frac{K(kT_e)^{3/2}}{e^3 \ln\Lambda} \left(\frac{1}{1+\beta^2}\right) \tag{4.3}$$

$$= \frac{137.983\,(T_e \times 10^{-3})^{5/2}}{1+\beta^2}$$

The electron momentum equation is,

$$\vec{J} + \vec{J} \times \vec{\beta} = \sigma \vec{E} \tag{4.4}$$

where $\vec{\beta} = \mu_e \vec{B}$; $\mu_e = \frac{\sigma}{e n_e}$

The plasma is still assumed to be in Couloumb collision dominated regime, so the conductivity is given by the Spitzer-Harm formula,

$$\sigma = \frac{0.0152}{\ln\Lambda} T_e^{3/2} \tag{4.5}$$

---

[2] Sutton & Sheman, *Engineering Magnetohydrodynamics*, pp 202

where

$$\Lambda = \frac{d_f}{D_o}$$

$$d_D = 69 \sqrt{\frac{T_e}{n_e}}$$

$$D_o = 2.1 \times 10^{-9} \left(\frac{3000}{T_e}\right)$$

Because $\ln\Lambda$ appears as a weak function of electron temperature and density, we, as in previous chapters, assume the value of Ln Λ = 6.

Maxwell's equations are:

$$\nabla \times \vec{E} = 0 \tag{4.6}$$

$$\nabla \cdot \vec{J} = 0 \tag{4.7}$$

These two equations lead to the conclusion that E_y and J_x are constants, in the orientation stated in previous chapters.

The rate of change of electron density is governed by the kinetics of electron and appeared as,

$$\dot{n}_e = R_i n_e \left(n_n \frac{n_e^{*2}}{n_n^*} - n_e^2 \right) \tag{4.8}$$

where

$$\frac{n_e^{+2}}{n_n} = S = 2\left(\frac{2\pi m_e kT_e}{h^2}\right)^{3/2} e^{-\frac{e\psi_i}{kT_e}}$$

is the Saha's equation. And according to the Bates' law,

$$R_i = 1.09 \times 10^{-20}\ T_e^{-9/2}$$

The convective term of electron density variation is the ambipolar diffusion to the wall,

$$\frac{D_a}{R^2} = \frac{\dot{n}_{e(conv)}}{n_e} \qquad (4.9)$$

where R is the "effective distance" regarding the ambipolar diffusion process.

To relate R to real dimension, let us model the plasma in the following way: It is confined in a one dimensional space with length H. At the middle of the chamber, there is no electron density gradient by reason of symmetry. Also, electron density at the wall (H/2 ; -H/2) is zero.

Thus, the boundry conditions are:

$$n_e = 0 \quad \text{at } y = H/2 \text{ ; } y = -H/2$$

$$\frac{\partial n_e}{\partial y} = 0 \quad \text{at} \quad y = 0$$

The diffusion equation is:

$$\frac{d}{dy}\left(-D_a \frac{dn_e}{dy}\right) = \dot{n}_{e(conv)} \tag{4.10}$$

Apply the boundry conditions and we find,

$$n_e = \frac{\dot{n}_{e(conv)}}{8D_a} H^2 - \frac{\dot{n}_{e(conv)}}{2D_a} y^2 \tag{4.11}$$

The only region of interest for the analysis of this chapter is the middle region of the model, since electron density is diffusing away in all directions. So,

$$n_{e(o)} = \frac{\dot{n}_{e(conv)}}{8D_a} H^2 = \frac{\dot{n}_{e(conv)}}{D_a} R^2$$

and

$$H = \sqrt{8}\, R \tag{4.12}$$

To find the expression for the diffusivity, we consider the ambipolar momentum balance in a slab geometry similar to that used for the heat diffusion calculation:

$$K(T_e + T_g)\frac{\partial n_e}{\partial y} = -\frac{m_i}{2e} Q_{in} \bar{C}_{in} (n_e + n_n)\, e\, n_i V_{iy} \tag{4.13}$$

and so

$$n_e V_{ij} = -\left[\frac{2k(T_e + T_i)}{\rho Q_{in} \bar{C}_{in}}\right] \frac{\partial n_e}{\partial y} \qquad (4.14)$$

D_a, the diffusivity, is the quantity in the square bracket,

$$D_a = \frac{2k(T_e + T_i)}{\rho Q_{in} \bar{C}_{in}} \qquad (4.15)$$

where

$$\bar{C}_{in} = \sqrt{\frac{8}{\pi} \frac{kT_i}{\mu_{in}}}$$

$$\mu_{in} = \frac{m_i}{2} = \frac{m_{in}}{2}.$$

μ_{in} is the reduced mass for the positive ion-neutral system, C_{in} is the effective collisional speed of positive ions with neutrals, and Q_{in} is the collisional cross-section between the positive ions and neutrals. For Argon, Q_{in} can be represented by the empirical formula[3]

$$Q_{in} = 2.9953 \times 10^{-18} \; T_g^{-0.2}$$

(Q_{in} is in SI unit and T_g is in K)

---

[3] W.H. Cramer, *Journal of Chemical Physics*, Vol. 30, pp 641-642

Note that the ambipolar diffusion rate is determined by the positive ion-neutral collisions rate, despite the fact that we only consider the electron balance in mass conservation, momentum and energy.

The electron conservation equation is then,

$$\frac{\partial}{\partial t} n_e + D_a \frac{n_e}{R^2} = R_i n_e \left(n_n \frac{n_e^{*2}}{n_n^*} - n_e^2 \right) \qquad (4.16)$$

The electron production rate, which depends on electron temperature and on the departure from Saha conditions (as the plasma is assumed in ionization non-equilibrium), will equal the time variation of the electron density plus the electron flux diffused away by means of ambipolar diffusion.

4.2.3 CALCULATION PROCESS

The coordinate system is still defined as before, where angle ϑ is the angle between the wave propagation vector and the average current vector. (Fig. 2.1) Also, a plane wave dependence of the disturbances is assumed,

$$\hat{u} = \frac{\delta u}{\langle u \rangle} = \bar{u}\, e^{i(\omega t + \tau_{\alpha})}$$

The disturbances will exhibit unstable behavior if the imaginary part of ω is negative. (τ_d is real)

Now, let us define some non-dimensional parameters before we arrange the governing equations.

$$\tau_e = \frac{\frac{3}{2}\langle T_e \rangle}{eV_i} \tag{4.17}$$

is the ratio between the thermal energy of the electrons to the energy required for the ionization process.

$$\mathfrak{L} = \frac{\langle D_a \rangle \langle n_e \rangle}{R^2} \tag{4.18}$$

is the rate of electron loss by means of ambipolar diffusion. (It has a dimensional unit of $sec^{-1}m^{-3}$)

$$\alpha = \frac{3}{2}(1+\bar{\tau}_e) \tag{4.19}$$

And finally,

$$\alpha = \frac{\langle n_e \rangle}{n_H} \tag{4.20}$$

the degree of ionization. ($n_H = n_e + n_n$ is the heavy species density)

Applying the perturbation treatment (same as those in chapter three) to the separate terms of the energy equation (4.1), we find the following terms to be:

Time variation term:

$$\frac{\partial}{\partial t}\left[\left(e\vec{V}_i + \frac{5}{2}k\vec{T}_e\right)n_e\right] = i\omega\langle n_e\rangle\left(e\vec{V}_i + \frac{5}{2}k\langle T_e\rangle\right)\hat{n}_e + i\omega\langle n_e\rangle\frac{5}{2}k\langle T_e\rangle\hat{\delta}_e$$

Convective term:

$$\nabla\cdot\left[n_e\vec{v}_e\left(e\vec{V}_i + \frac{5}{2}kT_e\right)\right] = \left\{e\vec{V}_i(1+Z_e)\left[\left(\alpha-\frac{1}{2}\right)\mathcal{D} + \alpha\langle R_i\rangle\langle n_e\rangle\right] + \frac{5}{2}\alpha\langle T_e\rangle\mathcal{D} + i\vec{k}\cdot\frac{5}{2}k\langle T_e\rangle\frac{\vec{V}_e}{r_0}\right\}\hat{\delta}_e + \left\{e\vec{V}_i(1+Z_e)\left[\frac{1}{2} - \langle R_i\rangle\langle n_e\rangle\langle\tau\rangle - 2\langle R_i\rangle\langle n_e\rangle^2\right] - i\omega\langle n_e\rangle e\vec{V}_i(1+Z_e)\right\}\hat{\delta n}_e$$

Heat conduction term:

$$\nabla \cdot \vec{q}_e = \frac{137.983 \, (\langle T_e \rangle / 10^5)^{5/2}}{1 + \langle \beta \rangle^2} \langle T_e \rangle k_1^2 \, \delta \hat{T}_e$$

Joule heating term:

$$\frac{J^2}{\sigma} = -\frac{3}{2} \cos\alpha\theta \, [illegible] \, \delta\hat{T}_e - \frac{\langle J \rangle^2}{\langle \sigma \rangle} \langle \beta \rangle \sin\alpha\theta \, \delta \hat{n}_e$$

Collisional loss term:

$$E_e = -\frac{1}{2} \langle E_e \rangle \, \delta \hat{T}_e + \alpha \langle E_e \rangle \, \delta \hat{n}_e$$

And the energy equation becomes:

$$\Big\{ [illegible] \langle n_e \rangle \tau_e \, [illegible] + e V_i (1 + \zeta_e) \big[([illegible] - \tfrac{3}{2}) E_y + [illegible] \big]$$

$$+ e V_i \, [illegible] + [illegible] \, \tau_e \, [illegible] \cos\theta + \frac{137.983 \, (\langle T_e \rangle / [illegible])^{5/2} \langle T_e \rangle}{1 + \langle \beta \rangle^2} k_1^2 \qquad (4.21)$$

$$+ \frac{3}{2} \cos\alpha\theta \, [illegible] - \frac{1}{2} \langle E_e \rangle \Big\} \, \delta \hat{T}_e$$

$$+ \Big\{ e V_i (1 + \zeta_e) \big[E_y - [illegible] \langle n_e \rangle^2 \langle \sigma \rangle - \alpha \langle [illegible] \rangle \langle n_e \rangle [illegible] \big]$$

$$+ \frac{\langle J \rangle^2}{\langle \sigma \rangle} \langle \beta \rangle \sin\alpha\theta + \alpha \langle E_e \rangle \Big\} \, \delta \hat{n}_e = 0$$

Rearranging the mass conservation equation, we get:

Convective term:

$$\frac{Da\, n_e}{R^2} = \mathfrak{L}\,(s\hat{u}_e + S\hat{u}_e)$$

Time dependent term:

$$\frac{\partial n_e}{\partial t} = i\omega \langle n_e \rangle S\hat{n}_e$$

Total growth rate:

$$n_e = \left[\mathfrak{D}\left(\mathfrak{A} - \frac{3}{2}\right) + \mathfrak{A}\langle R_1\rangle\langle n_e\rangle\right] S\hat{n}_e$$

$$+ \left[\mathfrak{L} - 2\langle R_1\rangle\langle n_e\rangle^2 - \langle R_1\rangle\langle \cdot\rangle\langle n_e\rangle^2\right] S\hat{n}_e$$

Overall conservation equation:

$$\left\{i\omega\langle n_e\rangle + 2\langle R_1\rangle\langle n_e\rangle^2 + \langle R_1\rangle\langle \cdot\rangle\langle n_e\rangle^2\right\} S\hat{n}_e$$

$$- \left\{\mathfrak{D}\left(\mathfrak{A} - \frac{11}{2}\right) + \mathfrak{A}\langle R_1\rangle\langle n_e\rangle^2\right\} S\hat{n}_e = 0 \qquad (4.22)$$

Putting the governing equations into matrix form, we get,

$$A(i,j) \begin{Bmatrix} \delta\hat{\phi}_e \\ \delta\hat{n}_e \end{Bmatrix} = 0 \qquad \text{(4.22 b)}$$

where

$$A(1,1) = i\omega\, eV_i \langle n_e \rangle \tau_e + eV_i (1+\tau_e) \left[\mathcal{D}\left(\mathcal{S} - \frac{\mathcal{S}}{L}\right) + \mathcal{S} \langle R_i \rangle \langle n_e \rangle \right] + eV_i \tau_e \mathcal{D} + i k \tau_e \frac{eV_i \langle \phi \rangle}{e} \cos\theta + \frac{137\,983 \left(\langle T_e \rangle \times 10^{-5}\right)^{5/2} \langle T_e \rangle}{1 - \langle \beta \rangle^2} k^2 + \frac{3}{2} \frac{\langle \phi \rangle}{\tau_{en}} \cos^2\theta - \frac{1}{2} \langle E_e \rangle \qquad \text{(4.22 c)}$$

$$A(1,2) = eV_i (1+\tau_e) \left[\frac{\mathcal{S}}{L} - \langle R_i \rangle \langle n_e \rangle \langle S \rangle - 2 \langle R_i \rangle \langle n_e \rangle^2 \right] + \frac{3}{2} \frac{k^2}{\tau_{en}} \langle \beta \rangle \sin\theta \cos\theta + 2 \langle E_R \rangle \qquad \text{(4.22 d)}$$

$$A(2,1) = -\mathcal{D}\left(\mathcal{S} - \frac{\mathcal{S}}{L}\right) - \mathcal{S} \langle R_i \rangle \langle n_e \rangle^2 \qquad \text{(4.22 e)}$$

$$A(2,2) = i\omega \langle n_e \rangle + 2 \langle R_i \rangle \langle n_e \rangle^2 + \langle R_i \rangle \langle S \rangle \langle n_e \rangle^2 \qquad \text{(4.22 f)}$$

ω, the variable of interest, can be solved for by setting the determinant to zero.

Other parameters such as the electron density, current, etc., are calculated as follow: From the zeroth order continuity equation,

$$\langle R_i \rangle \langle n_e \rangle \langle n_n \rangle \langle S \rangle - \langle R_i \rangle \langle n_e \rangle^3 = \frac{\langle D_a \rangle \langle n_e \rangle}{R^2} \tag{4.23}$$

Rearranging it and we find,

$$\langle n_e \rangle = \frac{\langle S \rangle}{-} \left\{ \sqrt{1 + 4 \left[\frac{n_H}{\langle S \rangle} - \frac{\langle D_a \rangle}{\langle R_i \rangle R^2 \langle S \rangle^2} \right]} - 1 \right\} \tag{4.24}$$

where n_H and R^2 are input parameters. The rest just shows electron temperature dependence. Figure (4.1) shows the relationship between electron density and temperature for a particular density. Other parameters such as pressure and input current will be shown in Table (4.1).

Then, the energy loss by means of collisions between electrons and ions can be calculated as,

$$\langle E_a \rangle = 3 \frac{m_e}{m_i} \langle n_e \nu_{ei} \rangle k \langle T_e \rangle$$

$$= 3 \frac{e^2 K}{m_i \omega_0} \frac{\langle n_e \rangle^2}{\langle \sigma \rangle} \langle T_e \rangle \tag{4.25}$$

From the zeroth order energy equation, we find the input current to be,

$$\frac{\langle I \rangle^2}{\langle \sigma \rangle} = \langle E_p \rangle + \frac{\langle i_0 \rangle \langle n_e \rangle}{R^2} \left(e V_i + \frac{3}{2} K \langle T_e \rangle \right) \qquad (4.26)$$

Then, ω can be calculated from the full matrix, and will be presented in the next section.

4.3 RESULTS

Solving the full determinant equation (4.22 b), we find in general two roots for ($\omega_r + i\,\omega_i$) for each set of $\mathcal{K}$, β, α, etc. This means that there are two distinct modes of plasma fluctuation (and possibly growth). In order to understant these two modes, we first examine the limiting conditions where one or the other will predominate.

First, very near full ionization (for $\alpha \gtrsim 0.99$, as we will see), electron density variation becomes negligible, and the energy equation controls the growth. With reference to equation (4.22 c), we see that $\theta = 90^\circ$ is the worst orientation, and that, since at $\theta = 90^\circ$ all terms in equation (4.22 c) are real, ω will turn out purely imaginary (i.e., the growth or decay will be purely local). Also the Saha factor $< S >$ will be very large, implying very fast electron kinetics, so that Saha equilibrium will be maintained and the perturbation continuity equation becomes.

$$\frac{\delta \hat{n}_e}{\delta \hat{t}_e} \approx \frac{\langle R_i \rangle \langle n_e \rangle^3 \not{\beta}}{\langle R_i \rangle \langle S \rangle \langle n_e \rangle^2} \qquad (4.27)$$

The energy equation becomes,

$$\left[-\omega_i \langle n_e \rangle \tau_e e V_i + \text{Heat Conduction} - \frac{3}{2}\frac{\langle p^2 \rangle}{\langle n_e \rangle} - \frac{1}{2}\langle E_e \rangle + e V_i \beta \langle R_i \rangle \langle n_e \rangle^3 (1+\tau_e) \right] \delta n_e$$

$$- e V_i (1+\tau_e) \langle R_i \rangle \langle n_e \rangle^2 \langle \quad \rangle \delta n_e^2 = 0 \qquad (4.28)$$

Combining the two expressions above we get,

$$-\omega_i \langle n_e \rangle \tau_e e V_i + \text{Heat Conduction} - \frac{3}{2}\frac{\langle p^2 \rangle}{\langle n_e \rangle} - \frac{1}{2}\langle E_e \rangle + e V_i (1+\tau_e) \beta \langle R_i \rangle \langle n_e \rangle^3$$

$$- e V_i (1+\tau_e) \frac{\langle R_i \rangle \langle n_e \rangle^2 \langle S \rangle \alpha_i \quad \frac{3}{2}\frac{\langle p^2 \rangle}{\langle n_e \rangle}}{\langle R_i \rangle \langle \quad \rangle \quad \langle n_e \rangle^2} \qquad (4.29)$$

and so, $e V_i \tau_e \langle n_e \rangle \omega_i =$ [illegible] $- \frac{3}{2}\frac{\langle p^2 \rangle}{\langle n_e \rangle}$

$$- \frac{1}{2}\langle E_e \rangle$$

The plasma is unstable without heat conduction and this is a static instability, in the sense that no wave propagation is involved. To look for the Hall

parameter under which condition the plasma with heat conduction is at the neutral stability point, we set ω_i equal to zero for the above equation.

$$\text{Heat Conduction} = \frac{137\ 5.23\times10^{5}\ (\langle T_e\rangle\times10^{-3})^{7/2}\ (\omega\tau)^2}{\lambda^2\ (1+\langle\beta\rangle^2)} \tag{4.30}$$

$$= \frac{3}{2}\frac{\langle j\rangle^2}{\langle\sigma\rangle} + \frac{1}{2}\langle E_e\rangle$$

More accurately, we set $\theta = 90^\circ$ and $\omega_i = 0$ for the full matrix to solve for the neutral Hall parameter. This is plotted in figure (4.2) for various values of electron temperature. It shows that there is a stabilizing effect of heat conduction within the plasma, since at wavelengths greater than about 3 cm. the plasma will be unstable at $\alpha \geq 99\%$, whereas it will not for shorter waves.

In the opposite limit, where electron density variation is the dominant effect (low degree of ionization), we combine the two governing equations with $\delta\hat{\epsilon}_e = 0$.

$$\langle\cdots\rangle\langle\cdots\rangle + 2\langle\cdots\rangle\langle\cdots\rangle^3 + \langle\cdots\rangle\langle\cdots\rangle\langle\cdots\rangle^2 = 0$$

and

$$\frac{\langle j\rangle^2}{\langle\sigma\rangle^2}\langle\beta\rangle\langle\cdots\rangle + \cdots\langle\cdots\rangle = eN_e(1+2\langle\cdots\rangle)^2\langle\cdots\rangle\langle\cdots\rangle\langle\cdots\rangle^2$$
$$+ 2\langle\cdots\rangle\langle\cdots\rangle^3 - \cdots$$

Since in this limit electron kinetics must be irrelevant, we eliminate < Ri > between the two equations. The damping part of ω is then

$$\omega_i = \frac{1}{eV(\quad)\langle n_e\rangle}\left\{\quad\right\} + \frac{\alpha}{\langle n_e\rangle} \tag{4.31}$$

The worst orientation returns to $\theta = 135^\circ$, and the stability factor is once again the Hall parameter. The plasma behavior returns to the same picture discussed in the previous chapters, except that the critical Hall parameter is smaller in order to account for the increased Joule dissipation due to the ambipolar diffusion effect. (Note that in the regime where the plasma is near full ionization, this limit will not be observed, and the critical Hall parameter has to be found by solving the full matrix.)

By solving the determinant above, we achieve two solutions of the damping part of ω, which correspond to the two modes of stability described above. Then, by concentrating on the worst angles, we can map the behavior of ω_i as the degree of ionization changes. As expected, the electron temperature variation mode shows up near the full ionization regime (Figure (4.3)), while the density variation mode dominates the rest (Figure (4.4)).

Stressing our interest in the situation where the plasma is in neutral stability for the worst orientation, we examine the ratio between $\delta\hat{t}e$ and $\delta\hat{n}_e$:

For the solution corresponding to the temperature variation mode, $\delta\hat{t}e$ is the dominant factor for stability analysis. It only appears in the region where the degree of ionization is very close to unity, and it agrees with the description stated previously. The neutral Hall parameter vs. degree of ionization is plotted in figure (4.5) (Same as the λ = 0.02 m curve in figure (4.2)).

For the other solution, corresponding to the density variation mode, $\delta\hat{n}_e$ is the dominant factor where the plasma is partially ionized and its contribution weakens as the degree of ionization rises (Figure 4.6). At the regime where both variations are comparable as one mode begins to diminish and the other to rise, the coupling effects between the two variation modes become important: the critical Hall parameter appears to be the lowest (Figure 4.7), and wave propagation (as measured by the real part of ω) is diminishing as the frequency approaches zero (Figure 4.8). As the plasma is further ionized, $\delta\hat{n}_e$ variation becomes insignificant. The critical Hall parameter rises again, and wave propagation resumes.

The overall boundary of the Hall parameter for stability regardless of the mode of variation is plotted in figure (4.9), for a 2 cm wavelength. It shows a smooth transition between the two modes.

4.4 CONCLUSION

We have explored the effects of heat conduction, which indeed is a stabilizing agent to the plasma. Since the direction for the conduction is assumed to be transversal to the magnetic field, the thermal conductivity depends on the Hall parameter inversely. So at high Hall parameter, this effect diminishes and can no longer provide the stabilizing force. The associated wavelength, must be in the order of 0.01 meter for this stabilization to be visible. Also, this mechanism affects the temperature variation mode only. For the other mode, the models from previous chapters remains the proper descriptions.

Electron temperature variation leads to the regime of static instability. It only happens at the regime where density variation can no longer be achieved, i.e. the plasma is almost fully ionized. At lower ionization fractions, this instability does not appear, and the density variation becomes the dominant factor for stability concern. The coupling effect between the two modes makes the transition between the regimes smoothly, but the stability of the $\delta\hat{n}_e$ mode deteriorates markedly in the region where both modes interact, i.e., between of 0.9 and 0.99. This is a regime of interest for MPD thrusters, and more study should be devoted to it.

CHAPTER V SUMMARY AND CONCLUSIONS

We have, throughout the course of this thesis, established some microscopic physical models for the plasma contained in a co-axial chamber with current passing through between the two end walls, so we can examine various effects, such as electron temperature, density and magnetic field variations, etc., that affect the overall local stability picture. The following conclusions have been drawn:

For a partially ionized plasma of constant induced magnetic field, instabilities occur whenever the direction of the wave vector of the propagating disturbances falls outside the direction of the current flow and electric field, since Joule heating in the originally low density region will decrease further, and thus it will increase the discrepancy of electron density between different regions. So the uniform background can no longer be attained.

The threshold value for the Hall parameter for which the disturbances are in neutral stability, i.e. no growth or damping (critical Hall parameter), is 2 in the worst wave vector orientation.

Even though the induced magnetic field exhabits space and time dependence associated with the presence of currents, the above threshold value of the Hall parameter is still valid for the wavelengths of spatial variation of the magnetic field from 1 mm to 1 cm. This variation has only little effects on the overall stability picture. The spatial variation of the magnetic field does provide some stablizing effects, where the growth rate of instabilities is less for a long wavelength. But this damping is insufficient for the typical MPD devices. The magnetic field variations

penetrate throughout the whole region quickly . And so it is viewed as constant inside the plasma, while the "skin-effect" which acts against the penetration is not effective enough. Constant magnetic field throughout the plasma is a valid assumption for those operations.

For a fixed magnetic field, two potentially unstable modes of wave propagation or growth exist. These are characterized by the predominance of electron density or electron temperature fluctuation in each of them. The mode with predominant density fluctuation tends to be the main instability at low ionization fraction, while the electron temperature mode becomes unstable near full ionization ($\alpha \simeq 0.99$). Of course, both modes occur throughout the range of ionization fraction. No wave propagation is invloved in this electron temperature mode instability. As the ionization fraction decreases, it diminishes very rapidly.

Heat conduction is a stabilizing agent to the undesirable situation described above. But as the direction for the heat conduction is transversal to the magnetic field, the corresponding thermal conductivity depends on the Hall parameter, and so this effect is insufficient to alter the stability picture at high Hall parameters. The corresponding wavelength for the heat conduction must be of the order of 0.01 meter or less in order for this stabilizing effect to be effective.

Because of the coupling effect, a smooth transition can occurs between the electron density and temperature variations in the region (α = 0.9 to 0.99) where both modes interact with each other. But this effect also courses the stability of the electron density variation mode to deteriorate to an undesirable level.

Finally, since the operating regime of the typical MPD thrusters falls into the region of the coupling between the two variations for the electrons, it will be necessary to devote more study into the coupling effect between the two modes. Other effect such as variations of plasma properties along the propagating wave front might affect the overall stability picture, and it is also worthwhile to investigate.

REFERENCES

1. Malliaris, A.C., John, R.R., Garrison, R.L., Libby, D.R., " *Performance of Quasi-Steady MPD Thrusters at High Powers*", AIAA Journal, V. 10, No. 2, Feb. 1972, pp 121-122

2. Rudolph, L.K., Jahn, R.G., Clark, K.E., von Jaskowsky, W.F., " *Performance Characteristics of Quasi-Steady MPD Discharge*", AIAA Paper No. 76-1000, Nov. 1976, Key Biscayne, FL.

3. Rudolph, L.K., Pawlik, E.V., "*The MPD Thruster Development Program*", AIAA Paper No. 79-20500, Nov. 1979, Princeton, N.J.

4. Jones, R.M. "*A Comparion of Potential Electric Propulsion Systems for Orbit Tannsfer*", AIAA Paper 82-1871, Nov. 1982.

5. Gabriel, S.B., King, D.Q., "*Thrust for Interorbital Propulsion: A Question of Lifetime* AIAA Paper, pending publication.

6. Burton, R.L., Clark, K.E., Jahn, R.G., "*Thrust and Efficiency of a Self-Field MPD Thruster*", AIAA Paper 81-0684, Apr. 1981.

7. King, D.Q., Smith, W.W., Jahn, R.G., Clark, K.E. "*Effect of Thrust Chamber Configuration on MPD Arcjet Performance*", AIAA Paper 79-2051, Oct. 1979.

8. Gabriel, S., AFOSR contract with JPL on plasma acceleration efficiencies with electrode heat loss mechanisms and anode sputtered ion heating of cathode, FY83.

9. King, D.Q., "*Magnetogasdynamic Channel Flow for Design of Coaxial MPD Thrusters*", PhD Dissertation, Princeton University, Dec. 1981.

10. Rudolph, L.K., Jahn, R.G., von Jaskowsky, W.F., "*Onset Phenomena in Self-Field MPD Arcs*", AIAA Paper 78-653, Apr. 1978.

11. Kuriki, K., Suzuki, H., "*Quasisteady MPD Arcjet with Anode Gas Injection*", AIAA Paper 79-2058, Oct. 1979.

12. Tanaka, M., Kimura, I., Arakawa, Y., "*Current Distribution in MPD Arcjets with Applied Magnetic Fields*", AIAA Paper 82-1918, Nov. 1982.

13. Baksht, F. G., Moizhes, B. Ya., Rybakov, A. V., "*Critical Regime of a Plasma Accelerator*", Zhurnal Tekhnicheskoi Fiziki, Vol. 43, pp. 2568-2573, Dec. 1973.

14. Turchi, P.J., Jahn, R.G., "*Cathode Region of a Quasisteady MPD Arc*", AIAA Journal, Vol. 9, No. 7, pp. 1372-1379, Jul, 1971.

15. Schottky, W., "*Zeitschrift fur Physik*", Vol. 25, pp. 635, 1925.

Figure 1.1

Self-field coaxial type accelerator

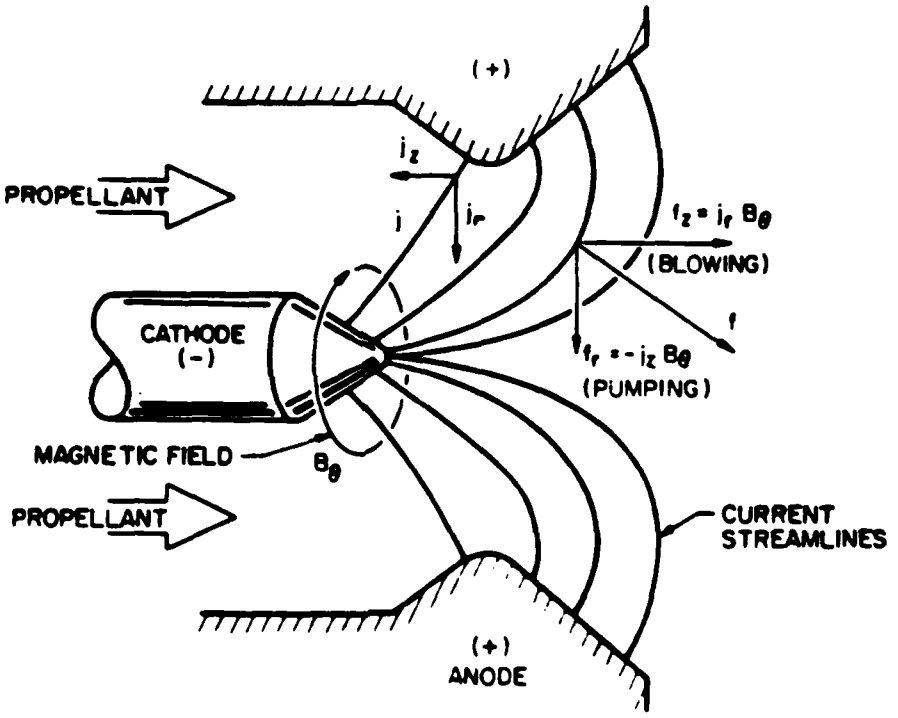

Figure 1.2

Self-field coaxial type accelerator

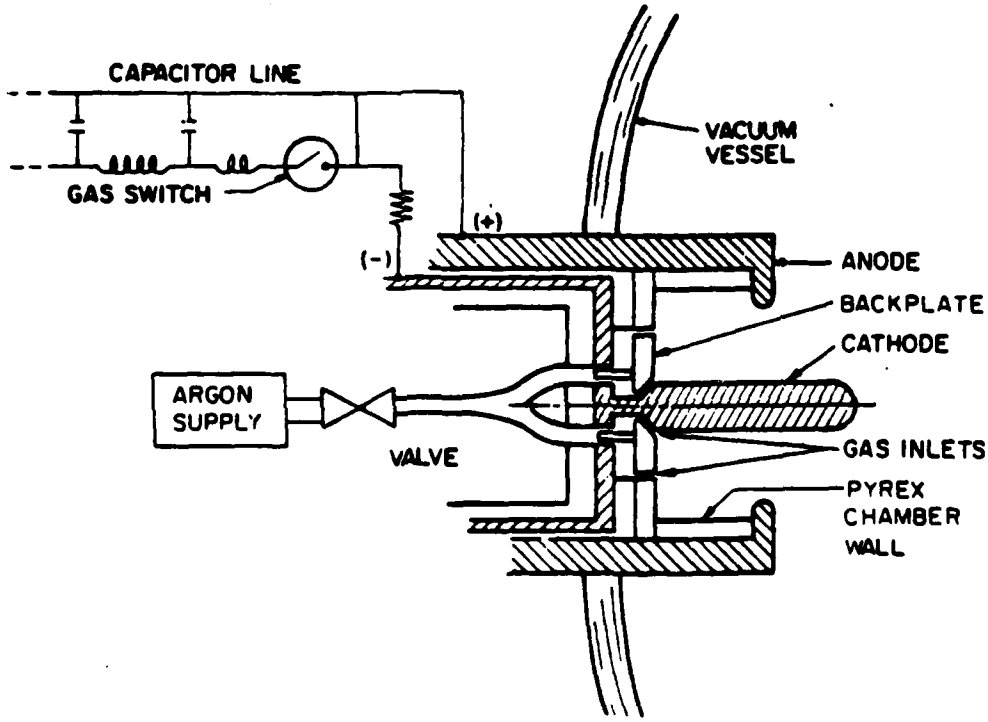

Figure 1.3

Self-field coaxial type accelerator

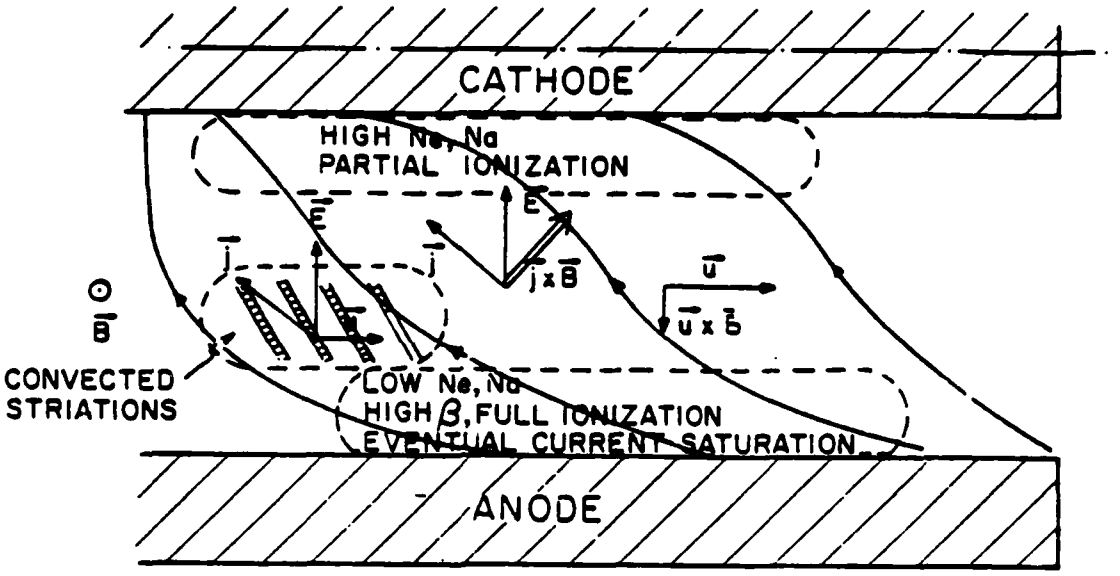

Figure 2.1

Coordinate system for the analysis

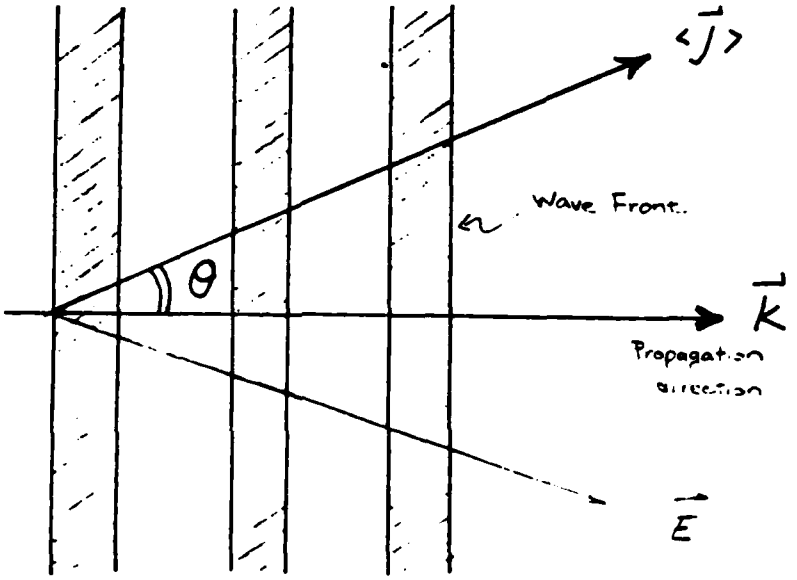

Figure 2.2

Damping factor vs. averaged value of

current angle for Hall parameter being 1 and 2

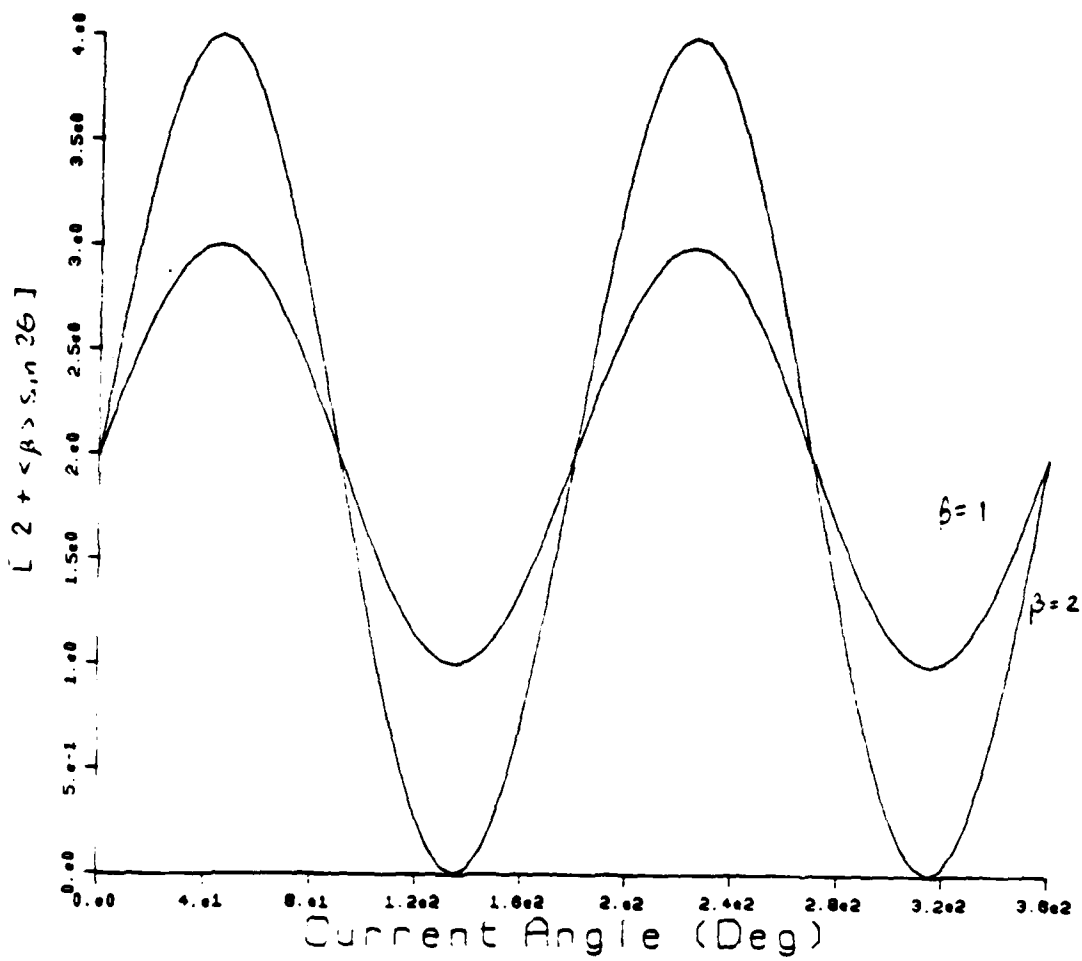

Figure 2.3

Damping factor vs. averaged value of

current angle for Hall parameter being 5 and 10

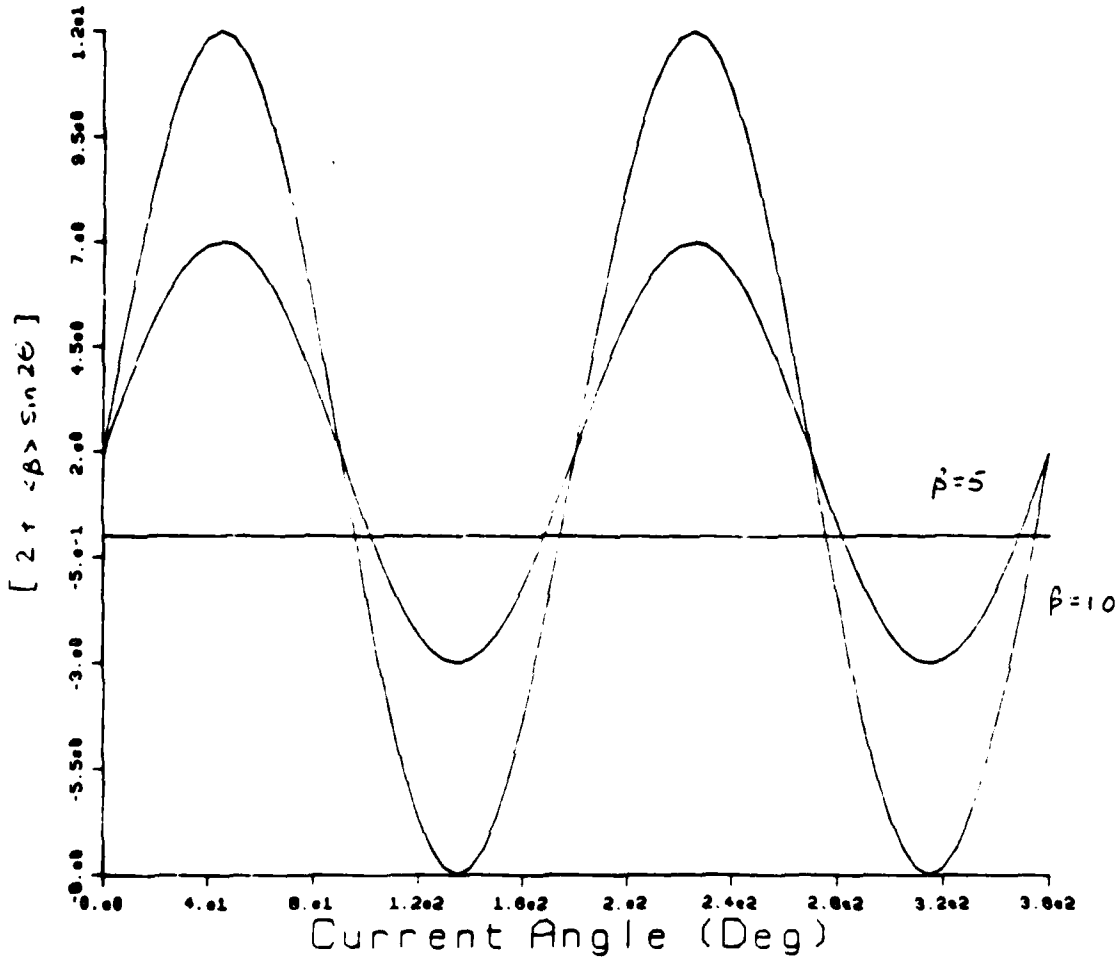

Figure 2.4

Diagram of averaged current direction in stable regime

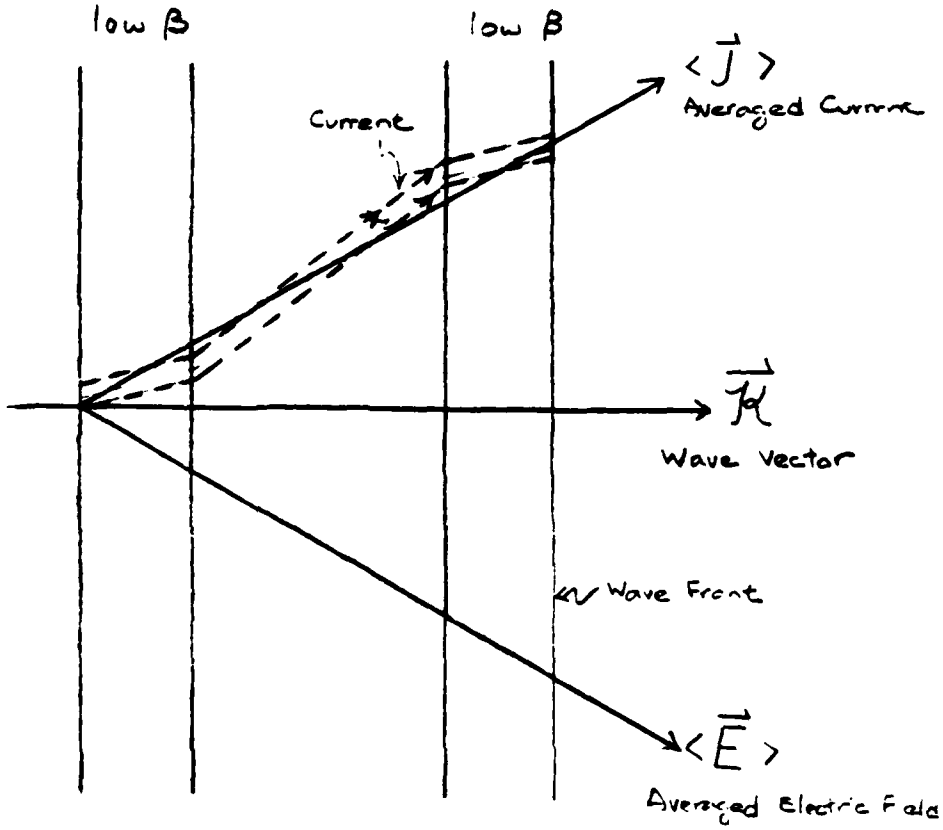

Figure 2.5

Diagram of averaged current direction in unstable regime

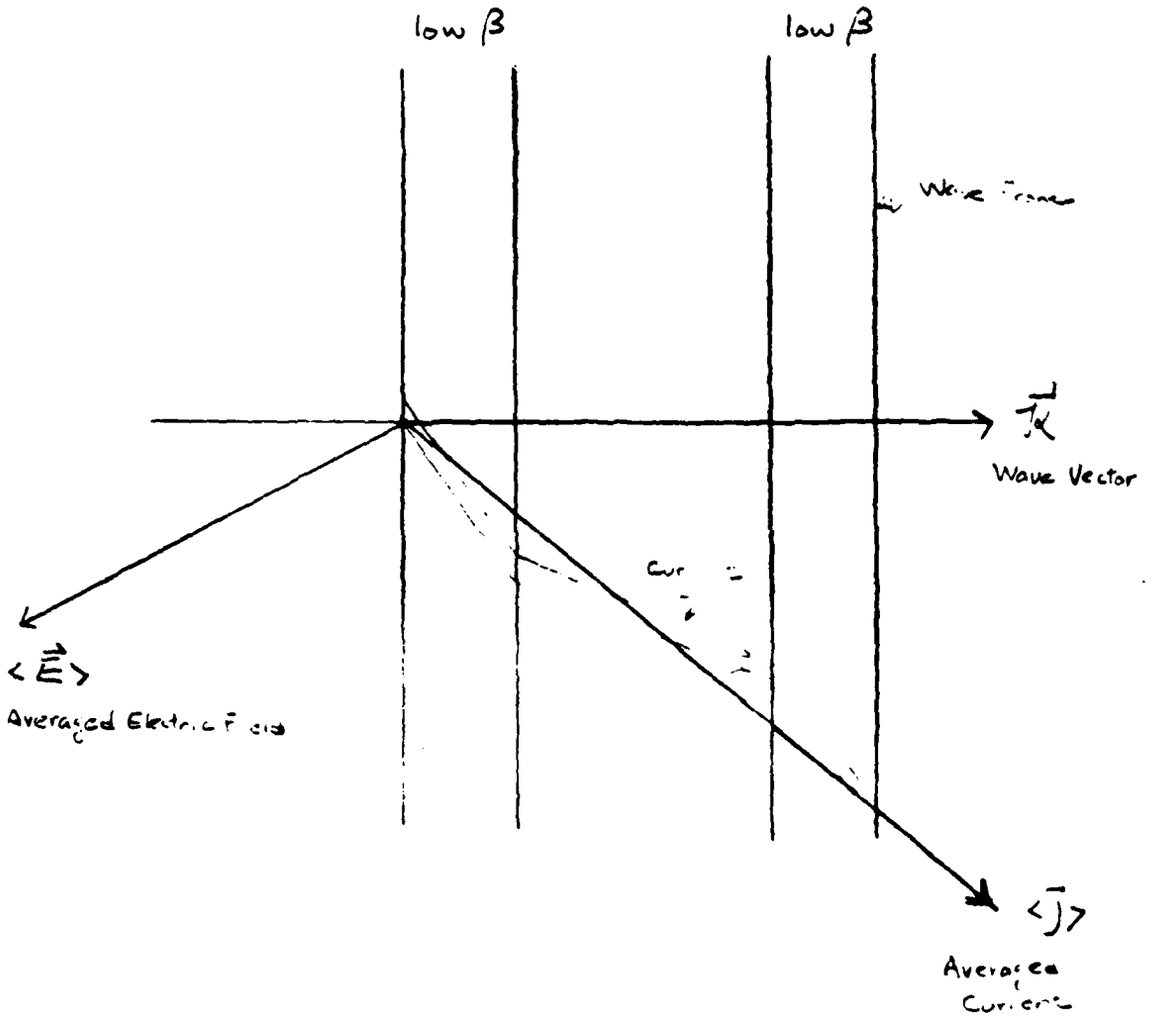

Figure 3.1

Variation of the worst current angle vs. wavelength ranging from 6.28 mm to 0.628 m

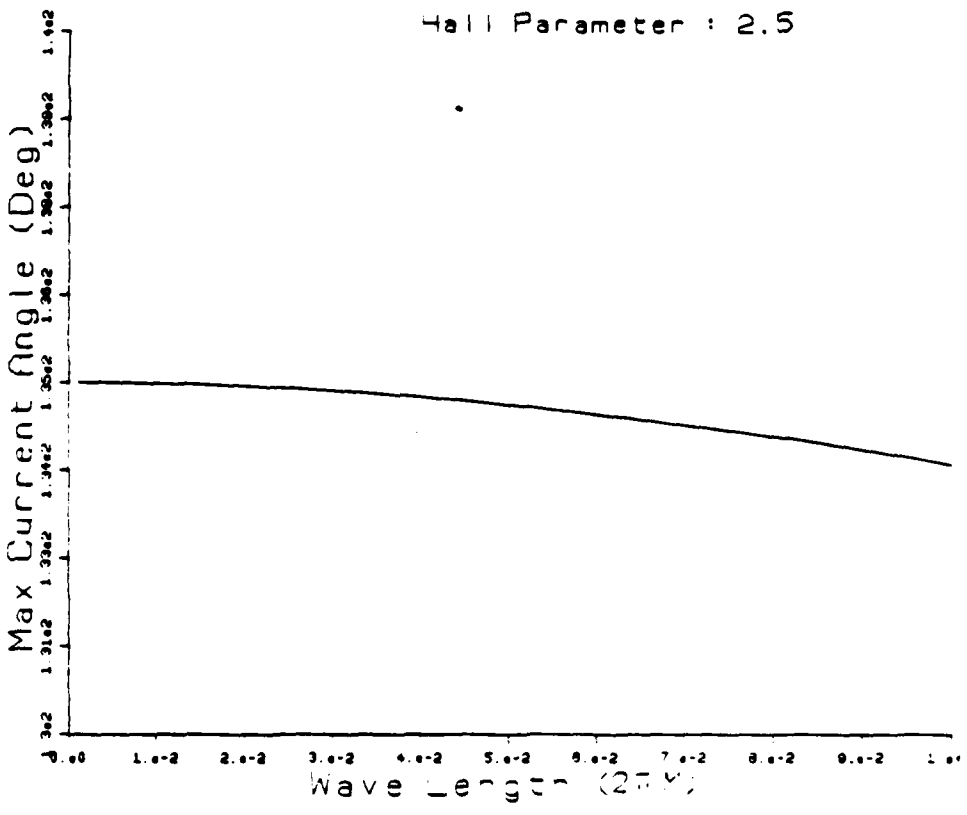

Figure 3.2

Critical Hall parameter vs. wave number

for spatial magnetic field variation

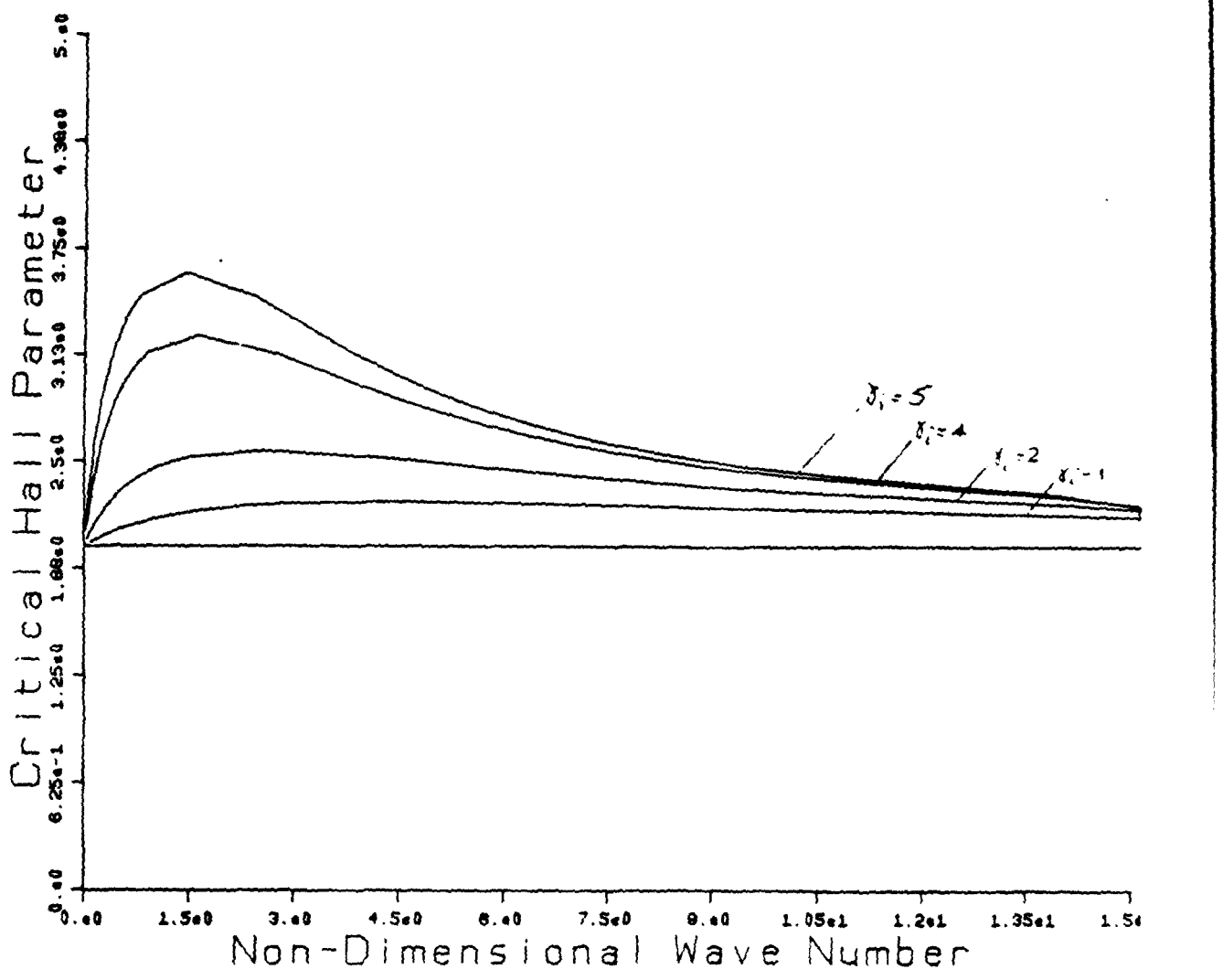

Figure 3.3

Variation of wavelength vs. the damping part of Ω

with various values of $< \beta >$

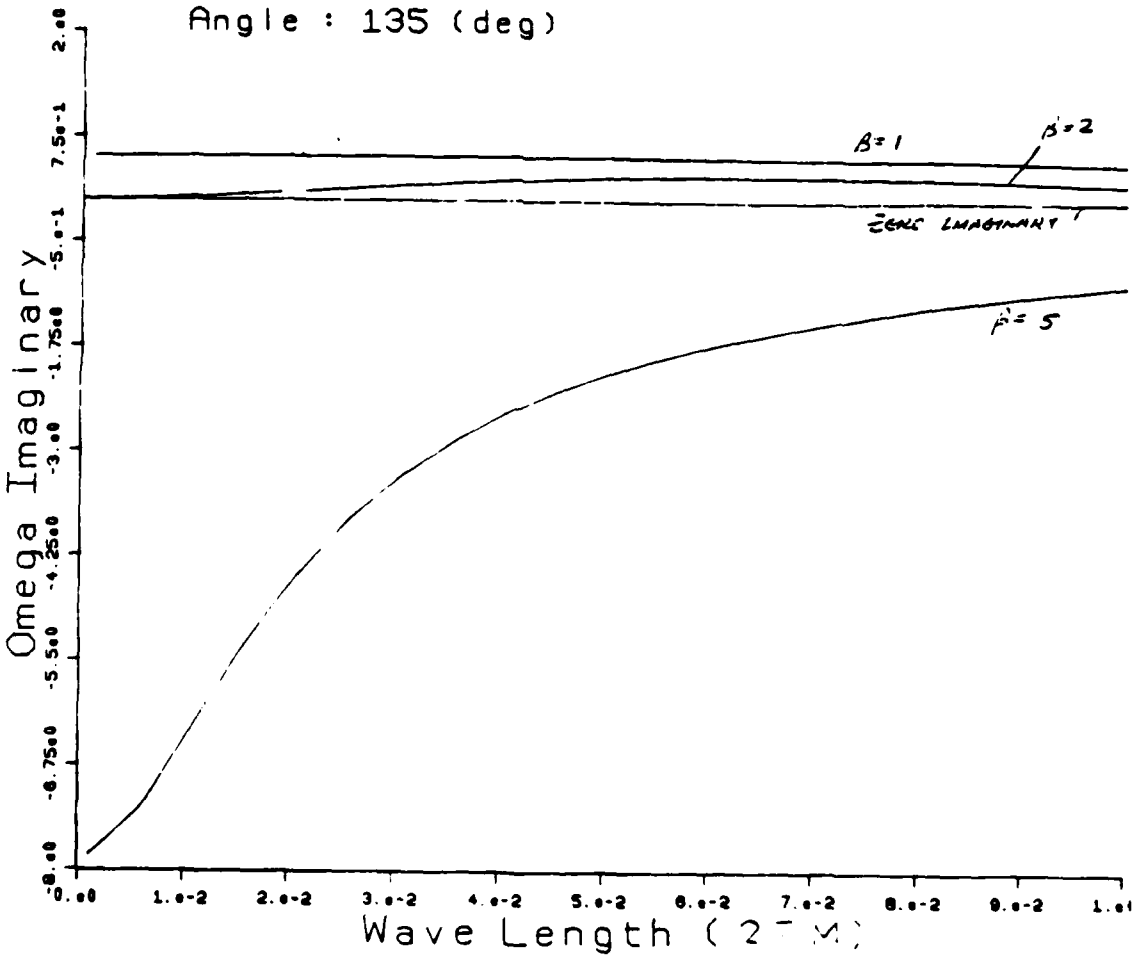

Figure 3.4

Oscillating part of Ω vs. wavelength

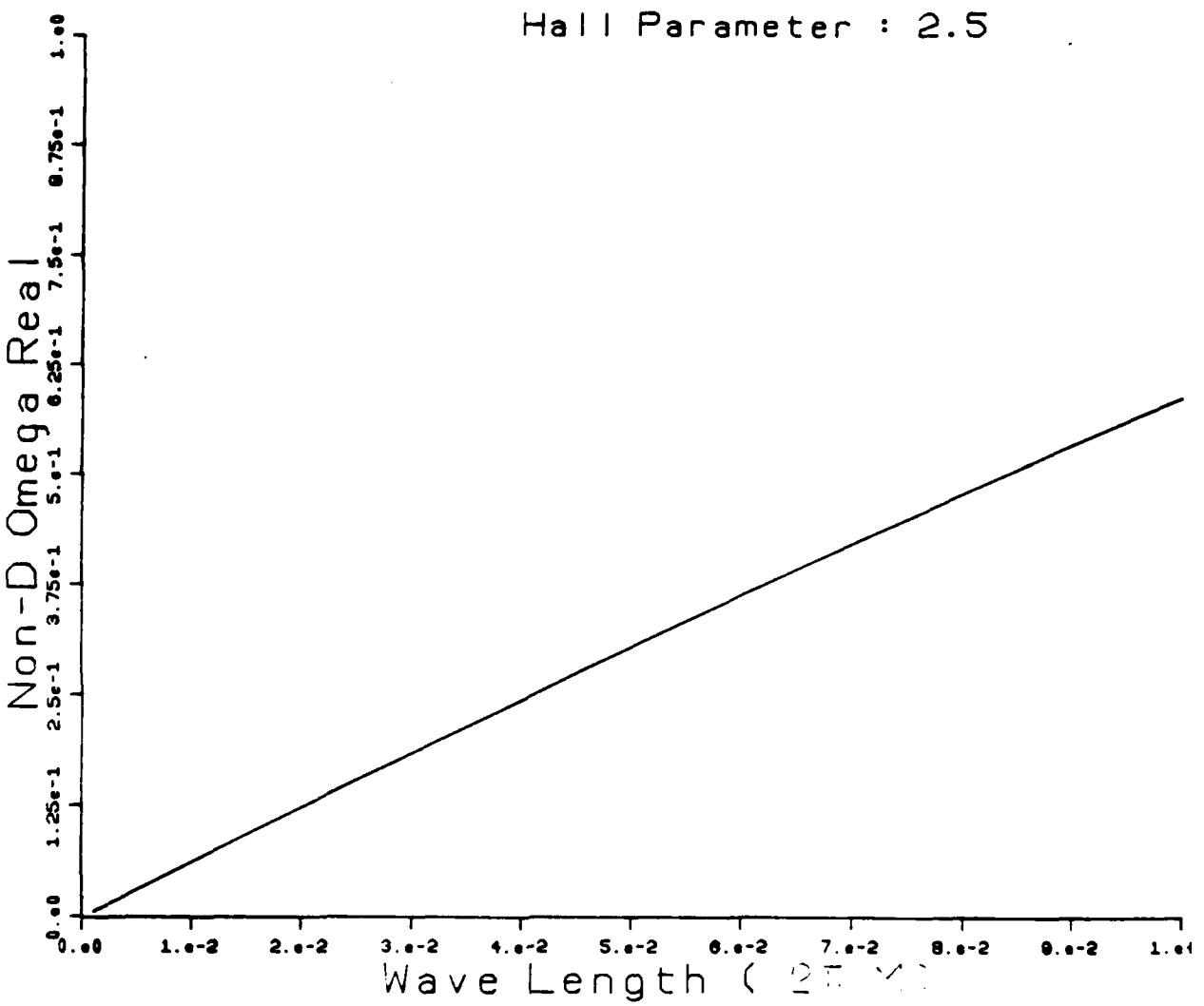

Figure 3.5

Damping part of Ω vs. current angle

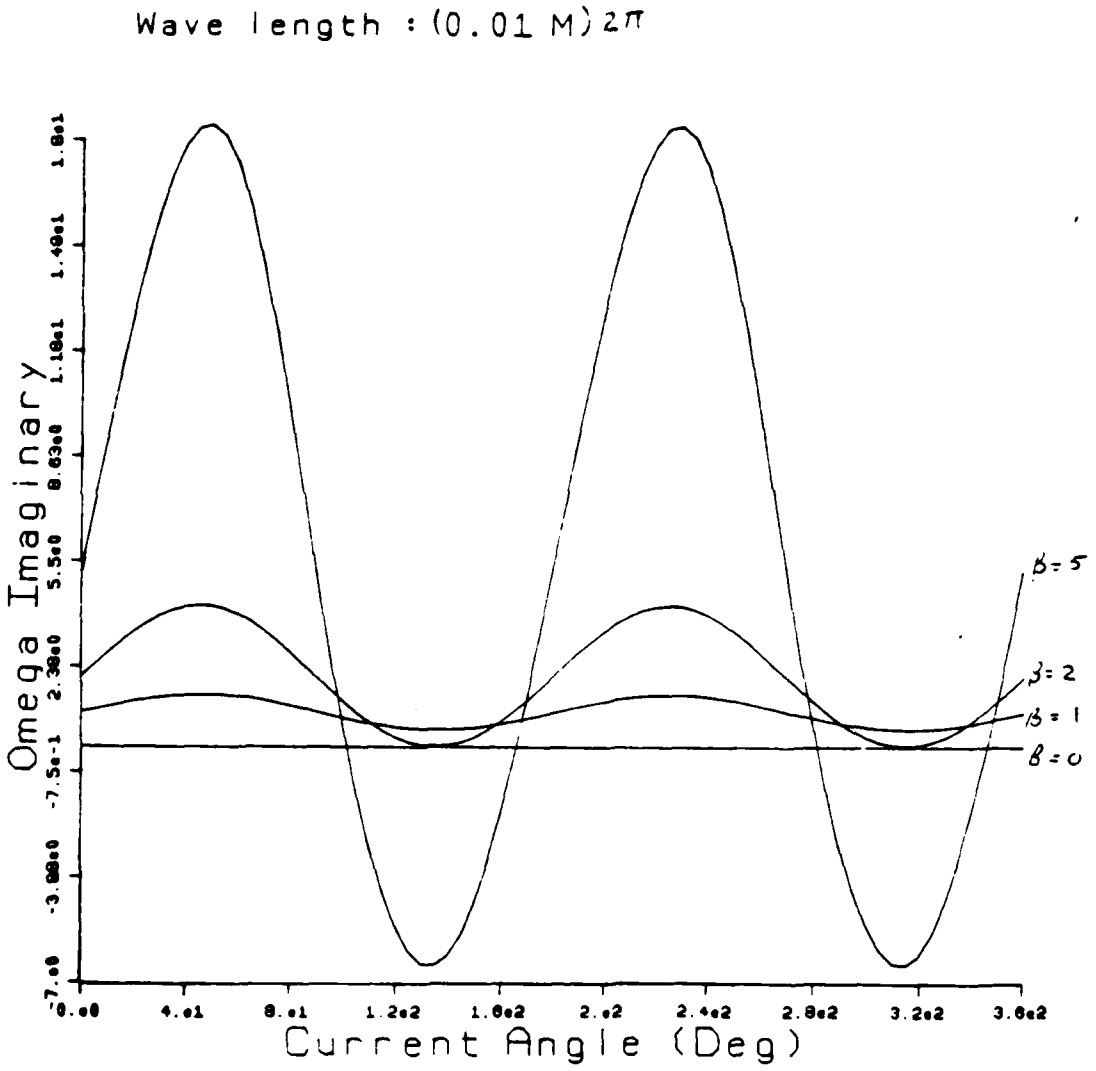

Figure 4.1

Degree of ionization vs. electron temperature

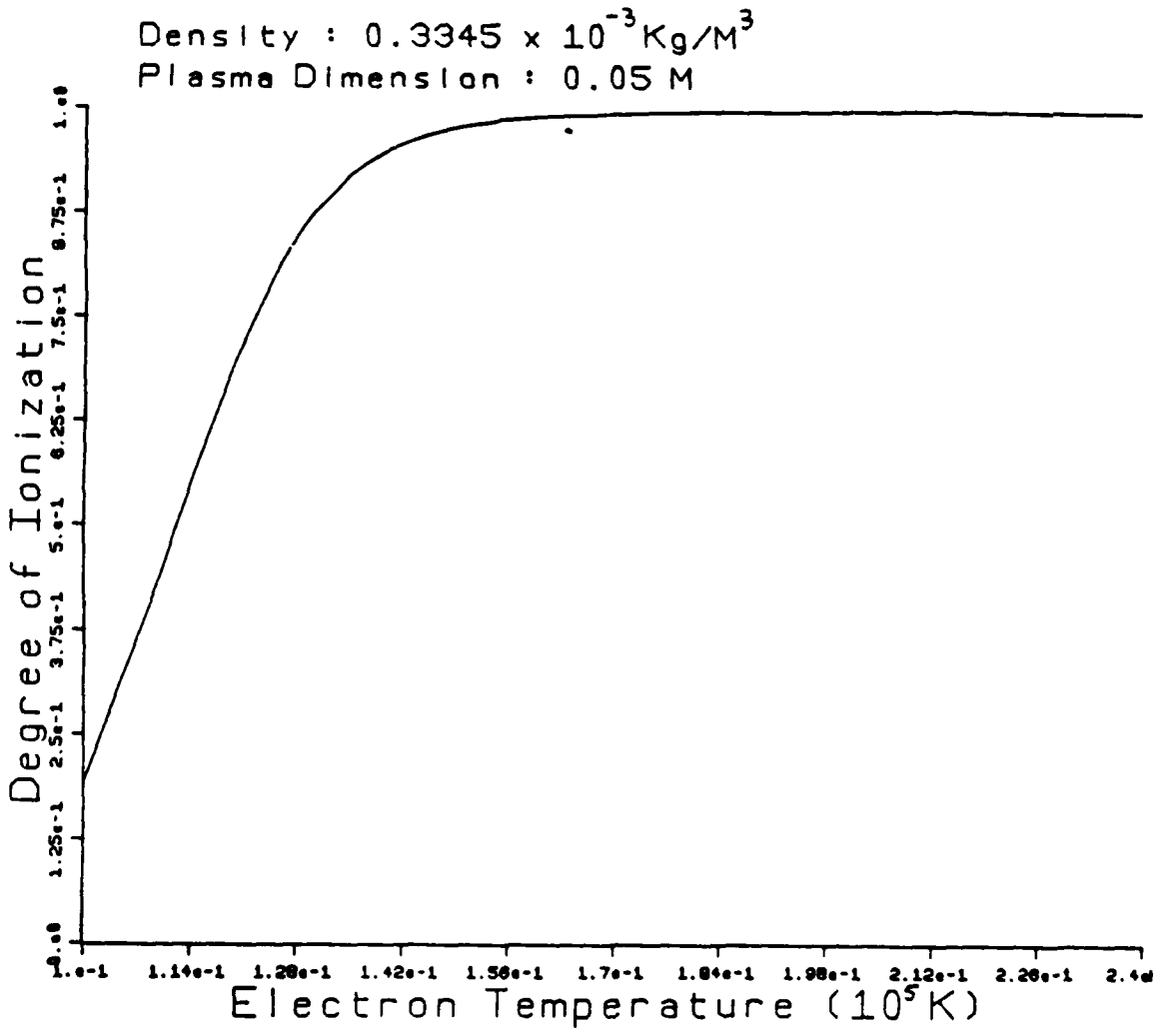

Figure 4.2

Neutral Hall parameter vs. degree of ionization

for various values of wavelength

($\delta\hat{t}_e$ mode)

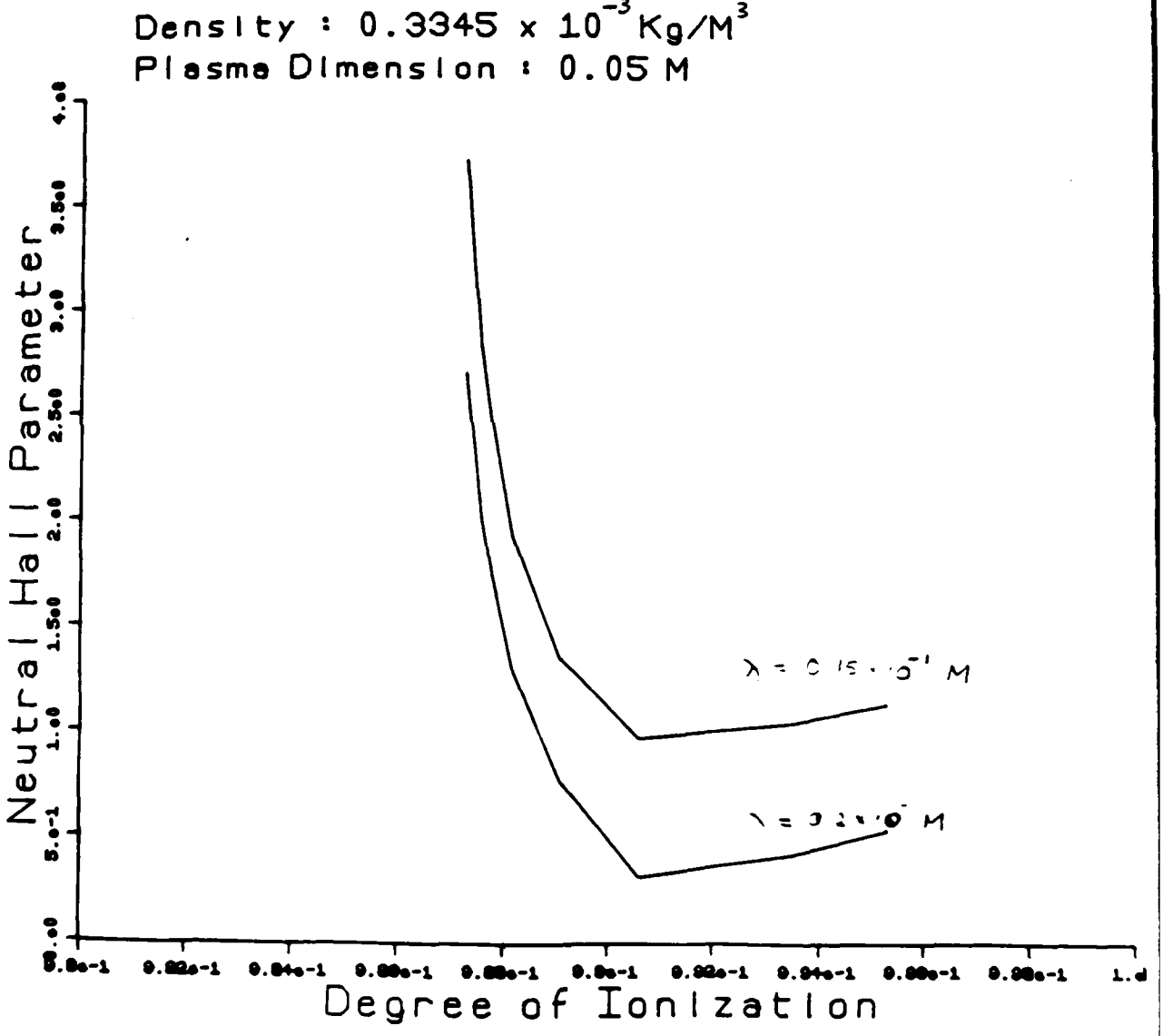

Figure 4.3

Damping part of ω vs. degree of ionization

($\delta\hat{t}_e$ mode)

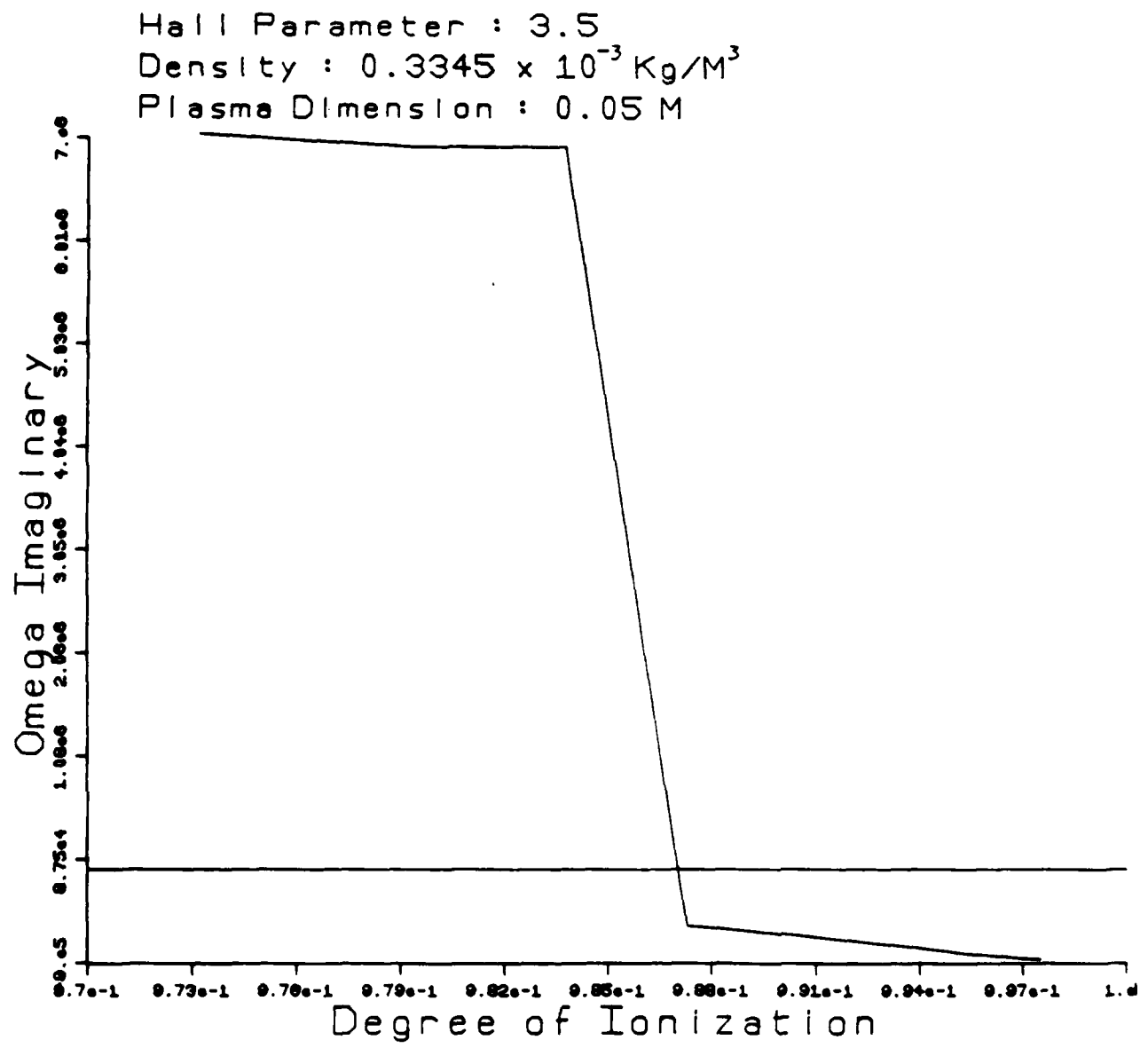

Figure 4.4

Damping part of ω vs. degree of ionization

($\delta\hat{n}_e$ mode)

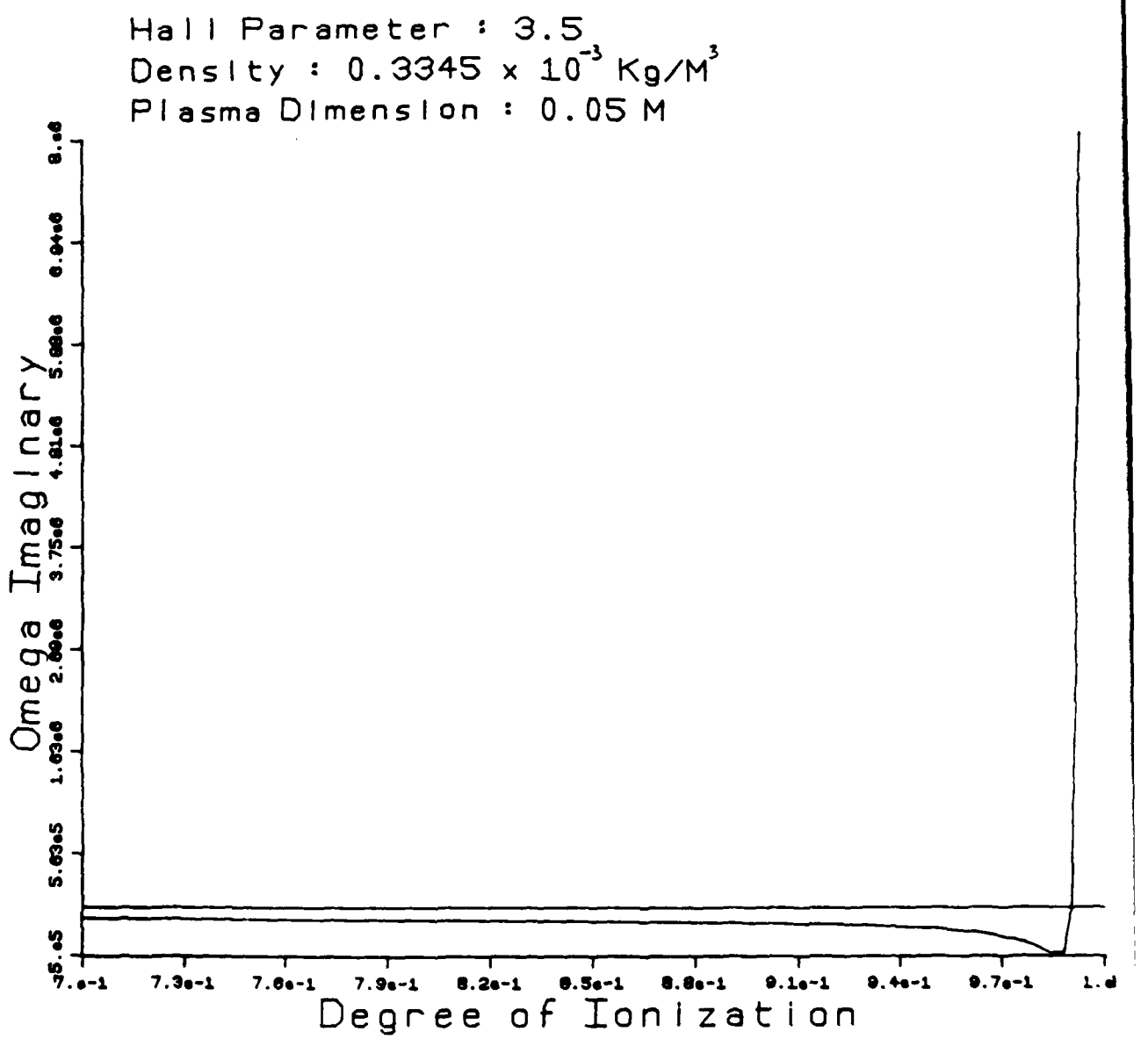

Figure 4.5

Neutral Hall parameter vs. degree of ionization

($\delta\ell_e$ mode)

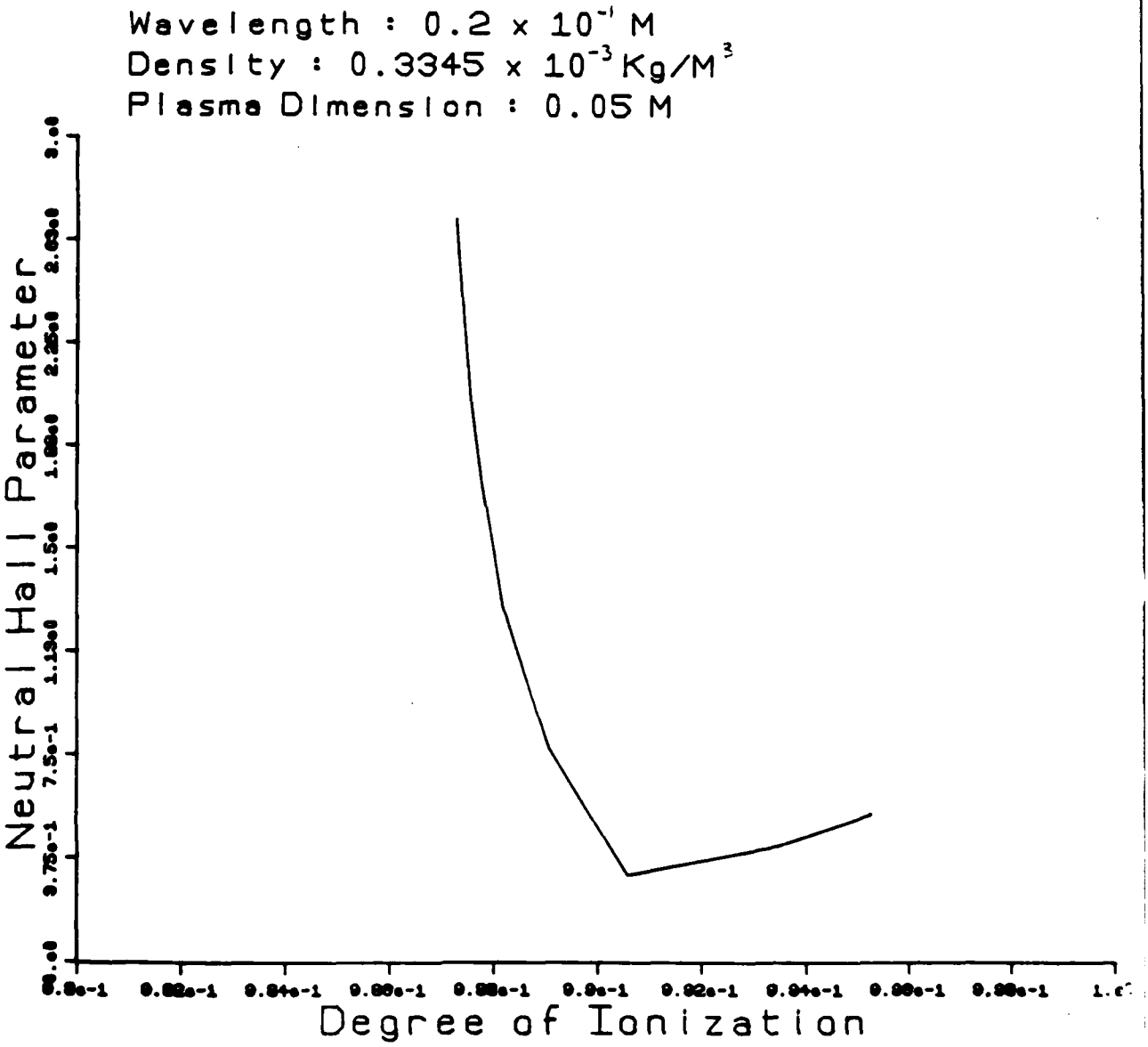

Figure 4.6

Ratio of $\delta\hat{n}_e$ variation vs.

degree of ionization

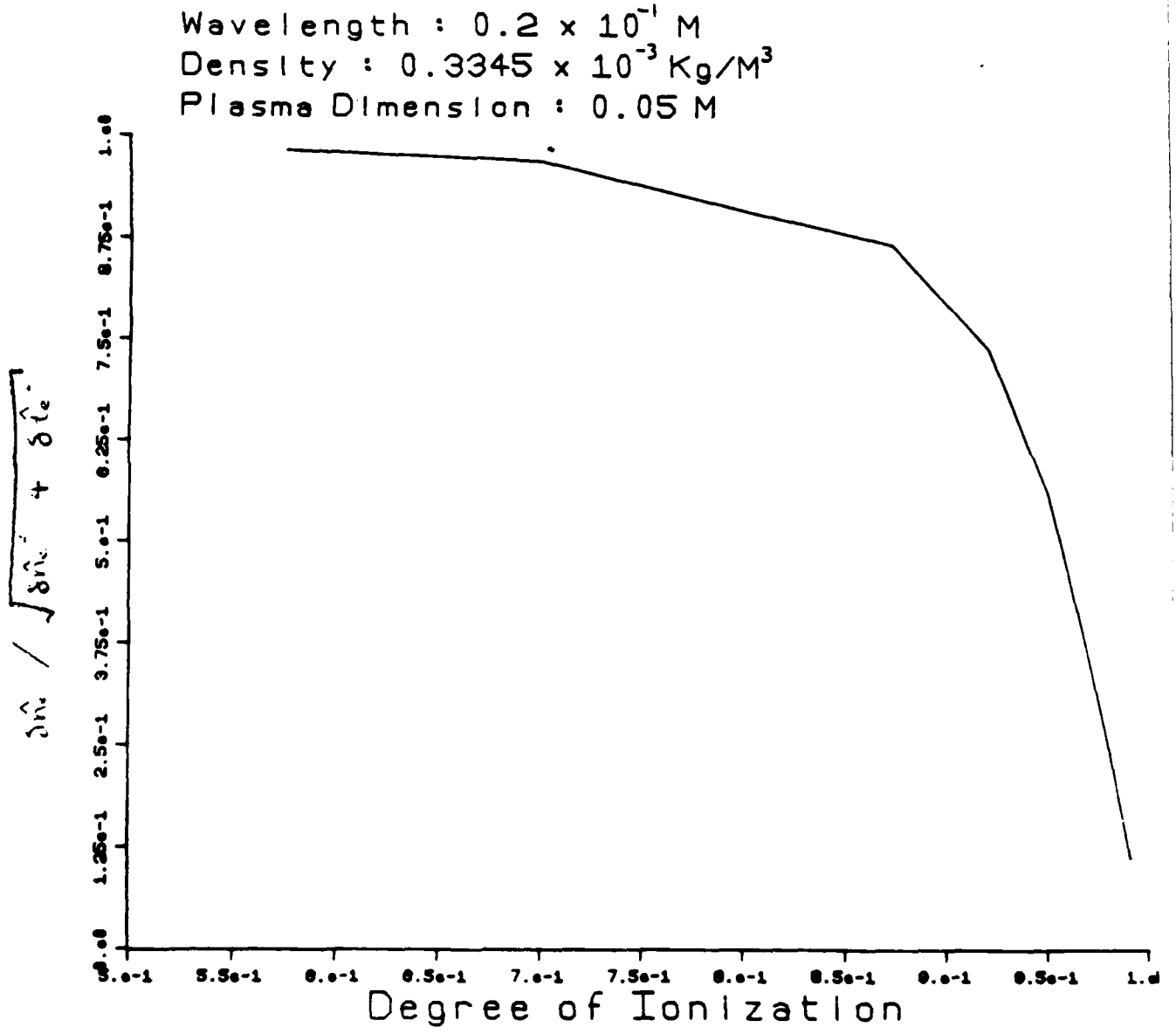

Figure 4.7

Critical Hall parameter vs. degree of ionization

($\delta\hat{n}_e$ mode)

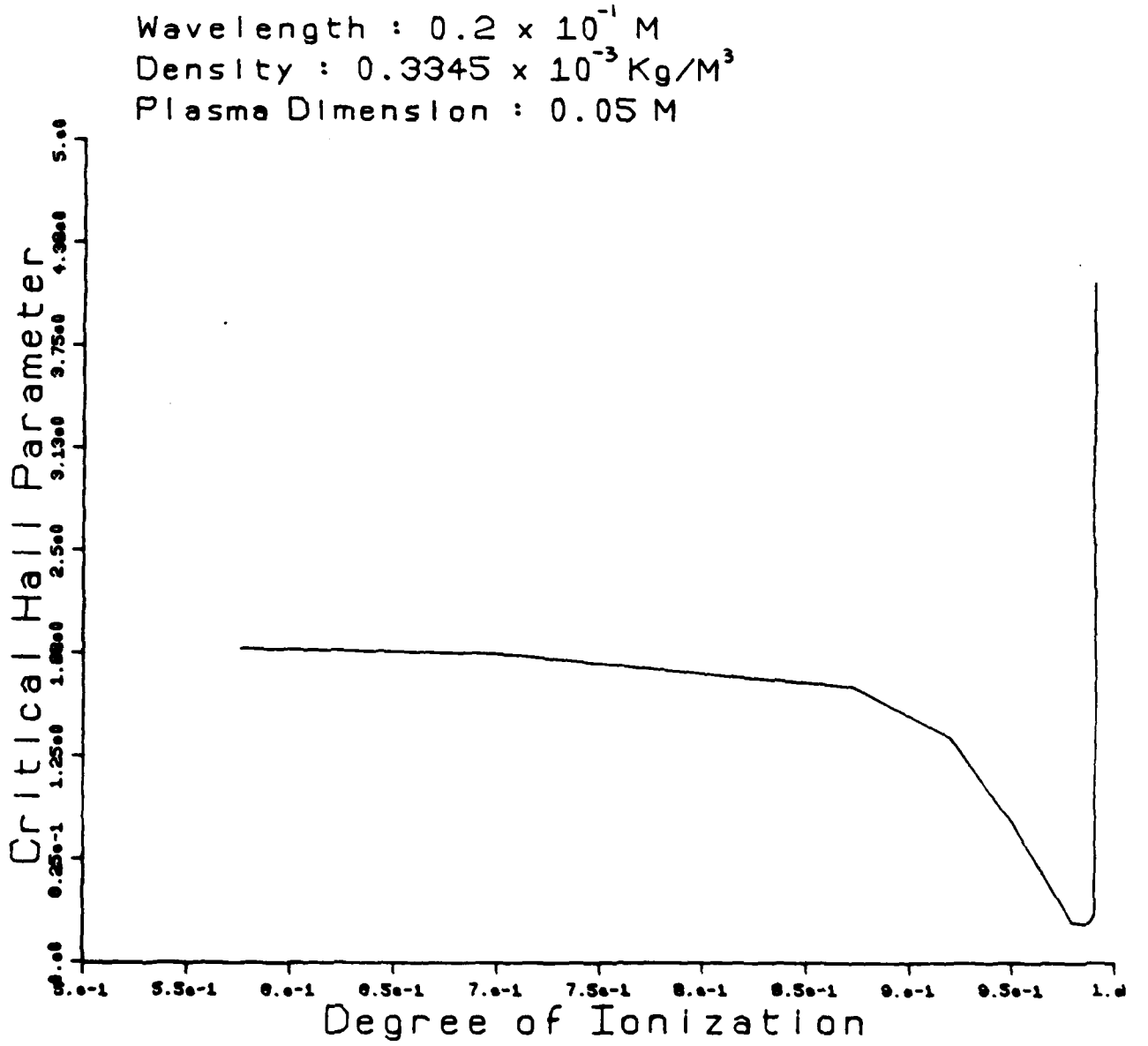

Figure 4.8

Wave frequency vs. degree of ionization

($\delta\hat{n}_e$ mode)

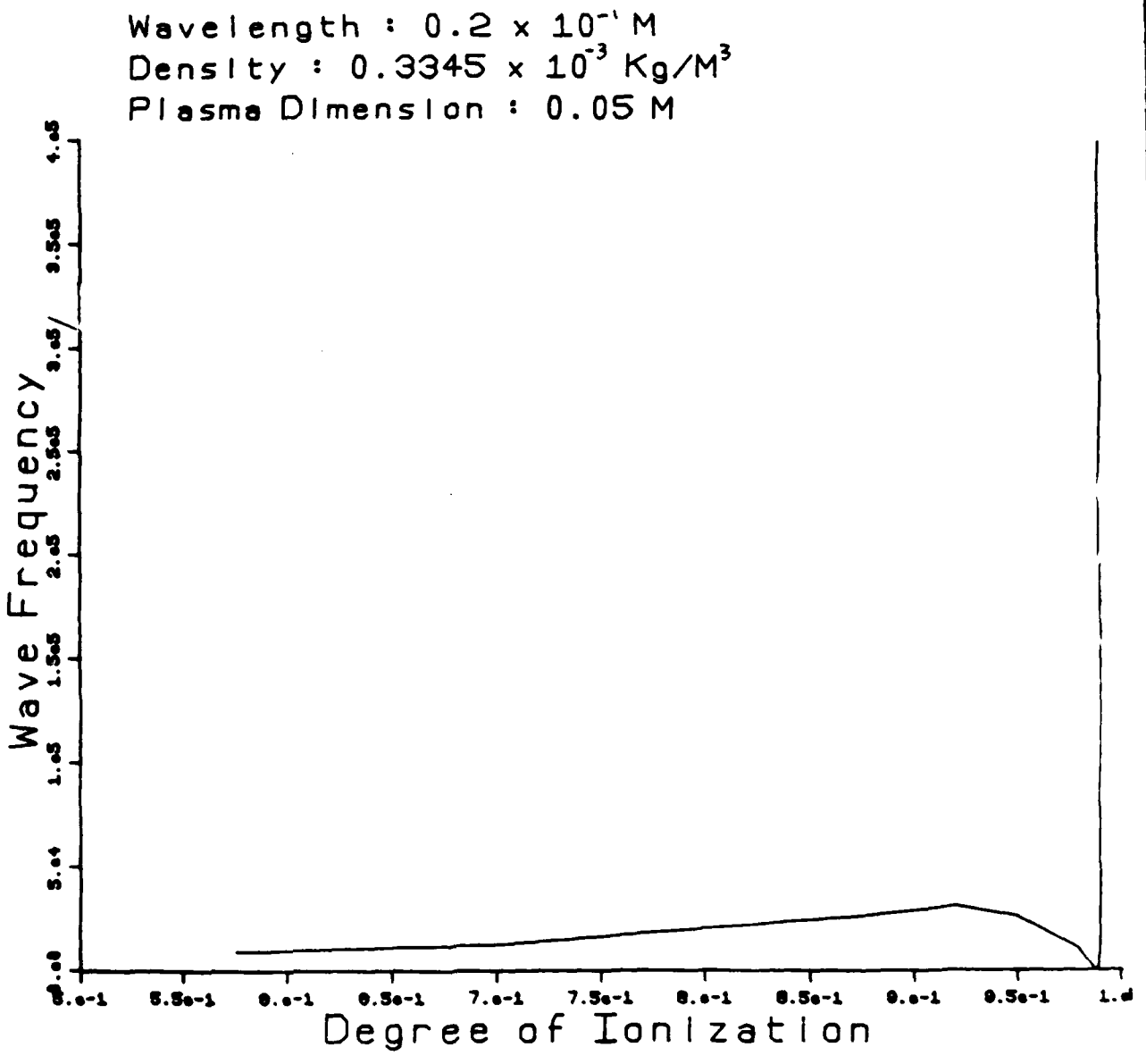

Figure 4.9

Hall parameter vs. degree of ionization

($\delta\hat{n}_e$ and $\delta\hat{\alpha}_e$ modes)

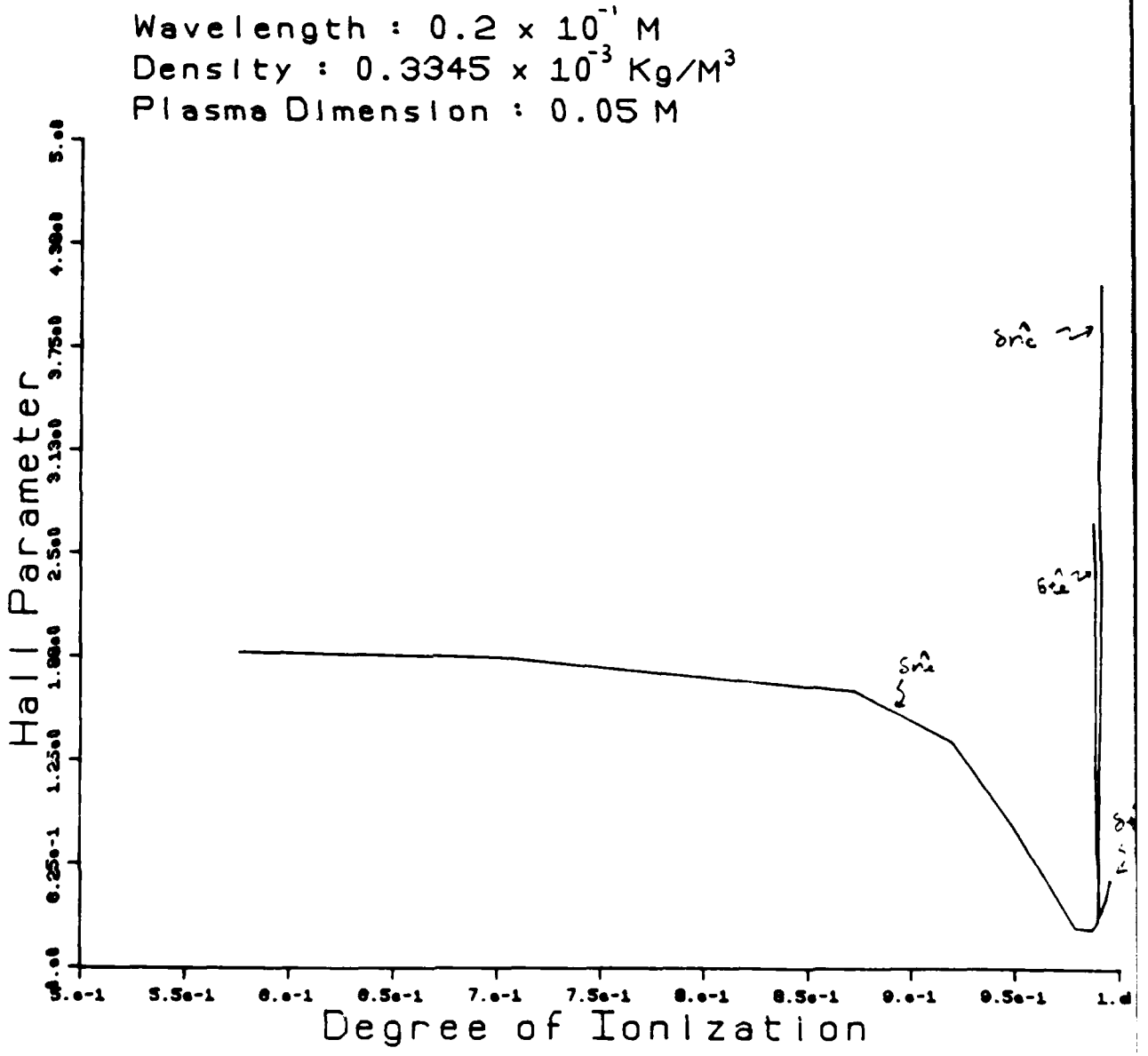

Table 4.1

Pressure and input current for various

degrees of ionization

Gas temperature : 1000 $^{\circ}K$
Heavy species number density : 5 x 10^{21}
Plasma dimension : 0.05 Meter

Electron temperature ($x10^5$ K)	Degree of ionization	Pressure (N / M^2)	Current ($x\ 10^7\ J/M^2$)
.1000	.1928	202.1	0.3978E-01
.1100	.4394	402.7	0.9168E-01
.1150	.5758	526.2	.1221
.1200	.7006	649.4	.1513
.1250	.8009	760.1	.1765
.1300	.8728	852.3	.1963
.1350	.9202	926.6	.2112
.1400	.9499	987.1	.2225
.1500	.9793	1083.	.2386
.1600	.9906	1163.	.2505
.1800	.9975	1309.	.2702

APPENDIX I

SAHA'S EQUATION AND EQUATION FOR IONIZATION AND RECOMBINATION RATE

For an ionization process,

$$Ze + i \rightleftharpoons n \qquad \text{(app 1.1)}$$

where z is the number of electron released if one positive ion is produced. e,i,n represent the electron, ion and neutral respectively.

From the law of Mass Action, we can write

$$\frac{(N_e)^z (N_i)}{(N_n)} = \frac{(Q_e)^z Q_i}{Q_n} \qquad \text{(app 1.2)}$$

N_e : number of electron

Q_e : partition function for electron

N_i, N_n, Q_i , Q_n are corresponding functions for ion and neutral(atom).

(z = 1 for Agron plasma, which is assumed to be used in our study.)

The partition functions for all three species are,

$$Q = \sum_i g_i \, e^{-\bar{\beta}\varepsilon_i}$$

$$\bar{\beta} = \frac{1}{kT}$$

$\varepsilon_i = 0$ for electron and ion since they don't possess any energy at rest.

$\varepsilon_a = -eV_i$ for neutrals at rest. (It is also called the energy for ionization)

V_i is the ionization potential(voltage).

so,

$$Q_e = g_e Q_e^{tr}$$

$$= 2\left(\frac{2\pi m_e kT_e}{h^2}\right)^{3/2} (\text{Volume})$$

$$Q_i = g_i^{int} \left(\frac{2\pi m_i kT}{h^2}\right)^{3/2} (\text{Volume})$$

$$Q_n = Q_n^{int} \left(\frac{2\pi m_n kT_n}{h^2}\right)^{3/2} (\text{Volume})$$

$(m_n = M_i)$

Q_n^{int} is the internal partition function.

Then, equation (app 1.1) becomes,

$$\frac{N_e N_i}{N_n} = 2\left(\frac{2\pi m_e k T_e}{h^2}\right)^{3/2} V_{ol} \frac{Q_i^{int}}{Q_n^{int}} e^{-\frac{eV_i}{kT_e}}$$

Since the number density is $n_e = N_e$ / Vol., equation can be arranged to the form,

$$\frac{n_e n_i}{n_n} = 2 \frac{Q_i^{int}}{Q_n^{int}} \left(\frac{2\pi m_e k T_e}{h^2}\right)^{3/2} e^{-\frac{eV_i}{kT_e}} \qquad \text{(app 1.3)}$$

which is the Saha's Equation.

Because the electron number density should be equal to the ion number density, we have,

$$\frac{n_e^2}{n_n} = 2 \frac{Q_i^{int}}{Q_n^{int}} \left(\frac{2\pi m_e k T_e}{h^2}\right)^{3/2} e^{-\frac{eV_i}{kT_e}}$$

(app 1.4)

$$\left(\frac{Q_i^{int}}{Q_n^{int}} = 6 \quad \text{for Argon}\right)$$

The ratio between the number density of electron and neutral is determined only by temperature.

Now, if a net ionization rate does exist, then we can write,

$$(\dot{n}_e) = (\dot{n}_e)_{\text{ionization}} - (\dot{n}_e)_{\text{recombination}}$$

Assuming ionization is by electron-neutral impact, and recombination is by a three-body e-e-i process.

$$(\dot{n}_e) = \gamma n_e n_n - \alpha n_e^2 n_i \qquad \text{(app 1.5)}$$

(γ , α are function of electron temperature only.)

In equilibrium, $\dot{n}_e = 0$ (Let us denote n_e as the electron density at equilibrium)

$$\gamma = \alpha \frac{n_e^2}{n_n}$$

where (n_e^2/n_n) is the Saha equilibrium constant depends on temperature only.

Return to (app 1.5), we find

$$\dot{n}_e = \alpha n_e \left\{ n_n \frac{n_e^2}{n_n} - n_e \right\} \qquad \text{(app 1.6)}$$

where α is expressed by the Bates' law.

$$\alpha = 1.09 \times 10^{-20} T_e^{-4.5}$$

If the Saha equilibrium density (n_e^2 / n_n) is much greater than the electron density(plasma density), then

$$n_n \frac{n_e^2}{n_n} - n_e^2 \cong n_n \frac{n_e^2}{n_n}$$

in other words, the bulk recombination process is negligible. In a steady state this is usually due to ambipolar diffusion to walls, followed by recombination there. In a transient state, it may occur at the start of a strong discharge, before the electron density has had time to build up.

END

8-87

DTIC